Final Report

Project Title: A Computational and Biochemical Drug Discovery Targeting Protein Kinase C as Anti-Latency Agents towards the Eradication of HIV-1 Reservoirs

By Dr. Nuttee Suree

May 2015

Contract No. MRG5680003

Final Report

Project Title: A Computational and Biochemical Drug Discovery Targeting Protein Kinase C as Anti-Latency Agents towards the Eradication of HIV-1 Reservoirs

Researcher	Institute
Dr. Nuttee Suree	Chiang Mai University

This project granted by the Thailand Research Fund

Abstract

Project Code: MRG5680003

Project Title: A Computational and Biochemical Drug Discovery Targeting Protein Kinase C Anti-Latency Agents towards the Eradication of HIV-1 Reservoirs

Investigator: Dr. Nuttee Suree

Email Address: nuttee.suree@cmu.ac.th

Project Period: 3 June 2013 – 2 June 2015

Protein kinase C (PKC) isozymes are important regulatory enzymes that have been implicated in many diseases, including cancer, Alzheimer's disease, and in the eradication of HIV/AIDS. Given its potential clinical ramifications, PKC modulators, e.g. phorbol esters and bryostatin, are also of great interest in the drug development. However, structural detail on the binding between PKC and its modulators, especially bryostatin—the highly potent and non-tumor promoting activator for PKCs, is still lacking. Here we report the first comparative molecular dynamics (MD) study aimed at gaining structural insight into the mechanisms by which the PKC delta activator domain is used in its binding to phorbol ester and bryostatin. Potential energy analysis revealed that PKC-bryostatin complex is energetically more favorable than either free PKC protein or the PKC-phorbol ester complex. The indole Nε1 of the highly homologous Trp252 also forms an H-bond to the C20 ester group on bryostatin. Backbone fluctuations also suggest that this H-bond formation may abrogate the transient interaction between Trp252 and His269, thus dampening the fluctuations observed on the nearby Zn^{2+}-coordinating residues.

Moreover, we have also applied the structural knowledge onto the development of computational methods for screening of 896 small molecules from the US NIH Clinical Collection against PKC. Virtual screening and affirmative re-docking, combined with Partial Least Squares (PLS) or Self-Organizing Maps (SOMs) were employed. As a result, we have identified various ligands that were predicted as effective PKC activators. The PLS model anticipated rolitetracycline and pancuronium dibromide with a predicted fold activation of 1.79 and 1.69, respectively, while the SOMs model predicted mecillinam and ketorolac with fold activation values of ca. 1.18. Virtual screening yielded telmisartan and irinotecan with binding affinity values of -8.6 and -8.2 kcal/mol, respectively. Reliability and accuracy of the predicted results from the computational models will ultimately be confirmed using our direct *in vitro* PKC biochemical assay, as well as a cell-based anti-latency assay that we have successfully demonstrated in the case of bryostatin. This research could potentially identify small chemical candidates for reactivating cells that have been latently infected with HIV-1 and could lead to a functional cure for HIV-AIDS.

Keywords: protein kinase C; molecular dynamics simulation; phorbol ester; bryostatin; binding mechanism

บทคัดย่อ

รหัสโครงการ: MRG5680003

ชื่อโครงการ: การค้นคว้าหาตัวยาด้วยวิธีการคำนวณด้วยคอมพิวเตอร์และวิธีการทางชีวเคมีโดยมีเป้าหมายที่โปรตีนไคเนสซี เพื่อนำไปสู่การกำจัดการติดเชื้อเอชไอวี-1 แบบแฝงและการรักษาหายขาด

ผู้วิจัย: อาจารย์ ดร.นัทธี สุรีย์

อีเมล์: nuttee.suree@cmu.ac.th

ระยะเวลา: 3 มิถุนายน 2556 – 2 มิถุนายน 2558

โปรตีนไคเนสซี (PKC) เป็นกลุ่มเอนไซม์ที่มีความสำคัญต่อการสื่อสัญญาณในเซลล์และเกี่ยวข้องกับโรคร้ายแรงหลายชนิด อาทิ มะเร็ง โรคอัลไซเมอร์ หรือในการกำจัดการติดเชื้อเอชไอวี-1 แบบแฝง ดังนั้นสารที่มีฤทธิ์ในการกระตุ้นการทำงานของโปรตีนไคเนสซี อาทิ กลุ่มสารฟอร์บอลเอสเทอร์ หรือไบรโอสแตติน จึงได้รับความสนใจเป็นอย่างมาก อย่างไรก็ดี ข้อมูลเกี่ยวกับการจับเกาะของสารกลุ่มนี้กับโปรตีนไคเนสซียังมีจำกัด โดยเฉพาะอย่างยิ่งสำหรับไบรโอสแตตินนั้น ยังไม่เคยมีรายงานก่อนหน้าใดที่เกี่ยวข้องกับกลไกการจับเกาะ ดังนั้นผู้วิจัยจึงทำการศึกษาด้วยการเปรียบเทียบพลศาสตร์โมเลกุลจำลอง (molecular dynamics simulations) ของโครงสร้างโปรตีนไคเนสซีที่จับเกาะด้วยฟอร์บอลเอสเทอร์ หรือไบรโอสแตติน ณ ตำแหน่งบริเวณจับกับตัวเร่งของโปรตีน ค่าพลังงานศักย์ของการเกิดโครงสร้างเชิงซ้อนระบุว่า เมื่อโปรตีนไคเนสซีจับกับไบรโอสแตตินนั้น จะมีเสถียรภาพมากกว่าขณะจับกับฟอร์บอลเอสเทอร์หรือแม้กระทั่งโปรตีนเปล่า เสถียรภาพนี้เกิดจากการสร้างพันธะไฮโดรเจนระหว่างอะตอม Nε1 ของวงอินโดล (indole) ในกรดอะมิโนทริปโตฟาน 252 ของโปรตีนไคเนสซี กับหมูเอสเทอร์ ณ ตำแหน่ง C20 ของไบรโอสแตติน ค่าการแปรปรวนเชิงพลศาสตร์ (dynamics fluctuation) ชี้ว่า เดิมกรดอะมิโนทริปโตฟาน 252 นั้นมีอันตรกิริยากับกรดอะมิโนฮิสติดีน 269 ซึ่งเป็นหนึ่งในศูนย์กลางจับกับโคแฟกเตอร์ Zn^{2+} และการแปรผันทิศทางของทริปโตฟานนั้นทำให้เกิดความไม่เสถียรของโครงสร้าง เมื่อทริปโตฟานจับกับตัวยาไบรโอสแตตินแล้วนั้น การแปรผันทิศทางจึงถูกจำกัด และก่อให้เกิดเสถียรภาพขึ้นในโครงสร้างใกล้เคียงโดยรวมขึ้นได้

ผู้วิจัยยังได้นำความรู้ในด้านโครงสร้างโมเลกุลโปรตีนไคเนสซีมาช่วยในกระบวนการค้นหาตัวยาใหม่ที่มีฤทธิ์กระตุ้นการทำงานของโปรตีนโดยทำการคัดเลือกในฐานข้อมูลสารคล้ายยาของสถาบันสุขภาพสหรัฐอเมริกาจำนวน 896 สาร เมื่อศึกษาการจับเกาะด้วย molecular docking และการทำการทดลองเชิงชีวเคมีแล้วจึงได้วิเคราะห์ต่อด้วยแบบจำลองคณิตศาสตร์สองชนิดคือ Partial Least Squares (PLS) และ Self-Organizing Maps (SOMs) ผลของ virtual screening และ molecular docking ทำให้ค้นพบสารคล้ายยาบางตัวที่อาจมีฤทธิ์กระตุ้นการทำงานของโปรตีนไคเนสซี อาทิ rolitetracycline, pancuronium dibromide, mecillinam, ketorolac, telmisartan และ irinotecan นอกจากนี้ผู้วิจัยยังได้นำเอาวิธีการทดสอบฤทธิ์ของสารคล้ายยาในการกระตุ้นออกจากการติดเชื้อเอชไอวี-1 แบบแฝงโดยอาศัยเซลล์ทดลองจำเพาะ มาทดลองใช้กับสารไบรโอสแตติน และพบว่าประสบผลสำเร็จเป็นอย่างดี ซึ่งจะสามารถนำไปใช้ต่อในการศึกษาผลของยาตัวนำที่ค้นพบได้เหล่านี้ในระดับเซลล์ดังกล่าวต่อไป ดังนั้น งานวิจัยนี้เป็นวิธีการใหม่ที่บูรณาการการค้นคว้าหาตัวยาโดยวิธีการคำนวณด้วยคอมพิวเตอร์และทางชีวเคมีเข้าด้วยกัน เพื่อนำไปสู่การกำจัดการติดเชื้อเอชไอวี-1 แบบแฝงและรักษาหายขาดได้

Executive Summary

เชื้อเอชไอวี-1 (HIV-1, Human Immunodeficiency Virus-1) เป็นไวรัสที่ทำให้เกิดโรคเอดส์ (AIDS, Acquired Immune Deficiency Syndrome) ถึงแม้ว่าสาเหตุของการเกิดโรคนี้จะได้รับการค้นพบเมื่อกว่า 35 ปีก่อน (1) และมีการพัฒนายาเพื่อนำมารักษาบำบัดอย่างต่อเนื่องเรื่อยมา แต่ก็ยังไม่มีวิธีการที่จะรักษาให้หายขาดได้ และยังไม่มีวัคซีนที่ช่วยป้องกันการติดเชื้อ โรคเอดส์จึงยังเป็นปัญหาสำคัญในระดับโลก โดยสถานการณ์เอดส์ล่าสุดในปี 2555 มีจำนวนผู้ติดเชื้อทั่วโลกประมาณ 35 ล้านคน และจำนวนผู้ติดเชื้อรายใหม่ถึงกว่า 2.1 ล้านคนภายในปี พ.ศ. 2555

ในประเทศไทยนั้น จากการจัดอันดับการสูญเสียปีสุขภาวะของประชากรไทยระหว่าง พ.ศ. 2554 พบว่าโรคเอดส์เป็นสาเหตุอันดับหกในประชากรชาย และอันดับเก้าในประชากรหญิง ซึ่งอาจเป็นผลมาจากการใช้ยาต้านไวรัสที่มีประสิทธิภาพสูง (highly active antiretroviral therapy–HAART) อย่างไรก็ดี กระทรวงสาธารณสุขและสำนักงานคณะกรรมการพัฒนาการเศรษฐกิจและสังคมแห่งชาติยังได้คาดการณ์ไว้ว่าภายในปี พ.ศ. 2563 จะยังคงมีจำนวนผู้ติดเชื้อเอชไอวีสะสมในประเทศไทยประมาณ 1,250,000 คน ยิ่งไปกว่านั้น สำนักนโยบายสำนักยุทธศาสตร์ กระทรวงสาธารณสุขยังได้กล่าวว่า นอกจากประเทศไทยจะเผชิญกับปัญหาการควบคุมป้องกันการแพร่ระบาดของโรคแล้ว ยังมีปัญหาการเข้าถึงยาต้านไวรัสที่มีราคาแพงที่ทำให้ต้องเสียค่าใช้จ่าย โดยเฉพาะยาต้านไวรัสขั้นพื้นฐาน และการรักษาโรคฉวยโอกาสต่างๆ ถึง 85,000 บาทต่อคนต่อปี และมีการประมาณการว่าหากเยาวชนติดเชื้อเอดส์ตั้งแต่อายุ 20 ปี อาจต้องดูแลรักษานานกว่า 20 ปี ทำให้มีค่าใช้จ่ายราวคนละ 2 ล้านบาท ซึ่งในกรณีที่เชื้อดื้อยาก็จะต้องเสียค่าใช้จ่ายเพิ่มเป็นถึง 4 ล้านบาทต่อคน จึงนับได้ว่าปัญหาการติดเชื้อไวรัสเอชไอวีและการเกิดโรคเอดส์ยังคงเป็นปัญหาที่รุนแรง เรื้อรัง และต้องได้รับการจัดการที่ดีอย่างเร่งด่วน (2)

ในปัจจุบันองค์การอาหารและยาแห่งประเทศสหรัฐอเมริกา (The U.S. Food and Drug Administration, U.S. FDA) ได้อนุมัติการใช้ยาต้านไวรัสเอชไอวีจำนวนทั้งสิ้น 23 ตัวยา และ 7 สูตรยาผสมผสาน การบำบัดต้านไวรัสประสิทธิภาพสูงหรือ highly active antiretroviral therapy (HAART) นั้นสามารถลดปริมาณเชื้อไวรัสที่ตรวจพบในกระแสเลือด (viral load) ได้ถึงระดับที่ไม่สามารถตรวจพบได้ด้วยเทคนิคการตรวจสอบ (undetectable level) (3) อย่างไรก็ตาม ผลที่ตามมาอีกรูปแบบหนึ่งของการบำบัดนี้คือการดื้อยาของเชื้อไวรัสที่มีอัตราการเปลี่ยนแปลงพันธุกรรมสูงมาก ดังนั้น การพัฒนายาตัวใหม่ๆ ที่สามารถนำมาช่วยบำบัดรักษาการติดเชื้อไวรัสจึงยังคงมีความจำเป็นอย่างยิ่งยวดในการจัดการกับโรคติดเชื้อชนิดนี้ (4) ยิ่งไปกว่านั้น ในปัจจุบันก็ยังมีความต้องการเป็นอย่างยิ่งสำหรับยาต้านเชื้อเอชไอวีที่มีผลข้างเคียงน้อย สะดวกในการใช้งาน และราคาไม่แพงจนเกินไป เพราะเป็นไปได้ว่า หากเรายังไม่มียาหรือวิธีการที่จะรักษาโรคนี้ให้หายขาดได้ การติดเชื้อเอชไอวีก็จะยังคงเป็นโรคเรื้อรังที่ต้องได้รับการบำบัดต่อเนื่องที่สำคัญที่สุดของโลก ผลักดันทำให้ต้องมีการบำบัดด้วยยาไปตลอดอีก 20 กว่าปีข้างหน้า (4) ดังนั้น งานวิจัยด้านการพัฒนายานี้ หากประสบความสำเร็จ จะทำให้เกิดวิธีการบำบัดใหม่ที่เป็นตัวเลือกอีกตัวหนึ่งสำหรับผู้ติดเชื้อเอชไอวีและผู้ป่วยโรคเอดส์ วิธีการที่พัฒนาได้ก็จะสามารถกลายเป็นนวัตกรรมใหม่ที่ช่วยในศาสตร์การพัฒนายาอื่นๆ ต่อไป ทั้งนี้ทั้งนั้น ความรู้ที่จะได้จากการทำวิจัยนี้ จะได้ช่วยทำให้ประเทศไทยก้าวเข้าสู่ความเป็นเลิศทางงานวิจัยเชิงเวชเคมี และมีความเข้าใจการติดเชื้อเอชไอวีมากยิ่งขึ้น ซึ่งในอนาคตเราอาจจะสามารถค้นพบวิธีการรักษาโรคติดเชื้อชนิดนี้ให้หายขาดก็เป็นได้

สาเหตุที่การติดเชื้อไวรัสเอชไอวียังไม่มีวิธีการที่สามารถรักษาให้หายขาดได้ และการที่ผู้ป่วยต้องรับการบำบัดรักษาด้วยยาไปตลอดชีวิตนี้ ส่วนหนึ่งก็เนื่องมาจากการติดเชื้อในเซลล์เม็ดเลือดขาวชนิดจดจำ

memory CD4+ T cells หรือเซลล์ยั่งยืนอื่นๆ ที่เข้าสู่ในสภาวะแฝง (resting latency) (5) ในสภาวะนี้เซลล์จะไม่มีการแสดงออกของยีนไวรัสที่ได้ถูกแทรกลงไปในดีเอ็นเอของเซลล์มนุษย์ที่ถูกติดเชื้อ จึงไม่สามารถถูกตรวจพบหรือแยกแยะได้เลยจากระบบภูมิคุ้มกันของร่างกาย และเมื่อใดที่ถูกกระตุ้นออกมา เซลล์เหล่านี้ก็จะทำการแสดงออกของยีนไวรัสออกมาได้อีก จึงเป็นสาเหตุที่ทำให้ผู้ป่วยต้องรับการบำบัดรักษาด้วยยาไปตลอด ในทางทฤษฎีแล้ว ยาที่สามารถย้อนคืนสภาวะการแฝง อาจทำให้ยีนของไวรัสที่ได้ฝังตัวอยู่เหล่านั้นแสดงออกมา กลายเป็นอาร์เอ็นเอและโปรตีนของไวรัส และเป็นเชื้อไวรัสตัวใหม่ อันเป็นกระบวนการที่เราสามารถจะกำจัดได้ด้วยตัวยาแบบ HAART เซลล์ที่ถูกกระตุ้นออกมาก็อาจจะตายไปเองจากกระบวนการการสร้างไวรัส หรือถูกทำลายได้ด้วยระบบภูมิคุ้มกันของร่างกาย (6) ดังนั้นการรักษาให้หายขาดอาจเป็นไปได้ หากมียาที่สามารถกระตุ้นเซลล์ติดเชื้อแบบแฝงเหล่านี้ออกมาถูกทำลายจนหมดไป (7,8)

โครงการวิจัยฉบับนี้ จึงมีวัตถุประสงค์หลักเพื่อทำการค้นคว้ายาเพื่อรักษาการติดเชื้อเอชไอวีแบบแฝง โดยมีเป้าหมายยาเป็นโปรตีนไคเนสซี (protein kinase C - PKC) อาศัยวิธีการบูรณาการเอาศาสตร์และเทคโนโลยีทางการคำนวณด้วยคอมพิวเตอร์ มาผสมผสานกับการทดลองทางชีวเคมีและเซลล์ทดลอง เพื่อให้เกิดเป็นกระบวนการพัฒนายาแบบใหม่ที่มีประสิทธิผลสูง และอาจนำไปสู่วิธีการรักษาโรคติดเชื้อเอชไอวีแบบหายขาดได้ในอนาคต นอกจากนี้โปรตีนไคเนสซี ยังเป็นกลุ่มเอนไซม์ที่มีความสำคัญต่อการสื่อสัญญาณในเซลล์และเกี่ยวข้องกับโรคร้ายแรงหลายชนิด อาทิ มะเร็ง โรคอัลไซเมอร์ หรือในการกำจัดการติดเชื้อเอชไอวี-1 แบบแฝง ดังนั้นสารที่มีฤทธิ์ในการกระตุ้นการทำงานของโปรตีนไคเนสซี อาทิ กลุ่มสารฟอร์บอลเอสเทอร์ หรือไบรโอสแตติน จึงได้รับความสนใจเป็นอย่างมากในวงการวิทยาศาสตร์การแพทย์แผนใหม่ อย่างไรก็ดี ข้อมูลเกี่ยวกับการจับเกาะของสารกลุ่มนี้กับโปรตีนไคเนสซียังมีจำกัด โดยเฉพาะอย่างยิ่งสำหรับไบรโอสแตตินนั้นยังไม่มีรายงานก่อนหน้าใดที่เกี่ยวข้องกับกลไกการจับเกาะเลย ดังนั้นผู้วิจัยจึงทำการศึกษาด้วยการเปรียบเทียบพลศาสตร์โมเลกุลจำลอง (molecular dynamics simulations) ด้วยคอมพิวเตอร์ของโครงสร้างโปรตีนไคเนสซีที่จับเกาะด้วยฟอร์บอลเอสเทอร์ หรือไบรโอสแตติน ณ ตำแหน่งบริเวณจับกับตัวเร่งของโปรตีน ค่าพลังงานของการเกิดโครงสร้างเชิงซ้อนระบุว่า เมื่อโปรตีนไคเนสซีจับกับไบรโอสแตตินนั้น จะมีเสถียรภาพมากกว่าตอนจับกับฟอร์บอลเอสเทอร์หรือแม้กระทั่งโปรตีนเปล่า เสถียรภาพนี้เกิดจากการสร้างพันธะไฮโดรเจนระหว่างอะตอมบนกรดอะมิโนทริปโตฟาน 252 ของโปรตีนไคเนสซี กับหมูเอสเทอร์ ณ ตำแหน่ง C20 ของไบรโอสแตติน ค่าการแปรปรวนเชิงพลศาสตร์ (dynamics fluctuation) ชี้ว่า เดิมการแปรผันทิศทางของทริปโตฟานนั้นทำให้เกิดความไม่เสถียรของโครงสร้าง แต่เมื่อทริปโตฟานหันเข้ามาจับกับตัวยาไบรโอสแตตินแล้วนั้น การแปรผันทิศทางดังกล่าวจึงถูกจำกัดและก่อให้เกิดเสถียรภาพขึ้นในโครงสร้างใกล้เคียงโดยรวมขึ้นได้

ในขั้นประยุกต์ใช้งานนั้น ผู้วิจัยยังได้นำความรู้ในด้านโครงสร้างโมเลกุลโปรตีนไคเนสซีมาช่วยในกระบวนการค้นหาตัวยาใหม่ที่มีฤทธิ์กระตุ้นการทำงานของโปรตีน โดยทำการคัดเลือกในฐานข้อมูลสารคล้ายยาของสถาบันสุขภาพสหรัฐอเมริกาจำนวน 896 สาร เมื่อศึกษาการจับเกาะด้วยคอมพิวเตอร์และการทำการทดลองเชิงชีวเคมีแล้วจึงได้วิเคราะห์ต่อด้วยแบบจำลองคณิตศาสตร์สองชนิด ซึ่งมีความสัมพันธ์เชิงเส้นตรงและชี้ให้เห็นว่าสามารถนำแบบจำลองนี้มาใช้ในการทำนายฤทธิ์กระตุ้นการทำงานของโปรตีนไคเนสซีของสารคล้ายยาได้จริง ผลของการจำลองการจับเกาะด้วยคอมพิวเตอร์ทำให้ค้นพบสารคล้ายยาบางตัวที่อาจมีฤทธิ์กระตุ้นการทำงานของโปรตีนไคเนสซี อาทิ rolitetracycline, pancuronium dibromide, mecillinam, ketorolac, telmisartan และ irinotecan นอกจากนี้ผู้วิจัยยังได้นำเอาการทดสอบฤทธิ์ของสารคล้ายยาในการกระตุ้นออกจากการติดเชื้อเอชไอวี-1 แบบแฝงโดยวิธีเซลล์ทดลองจำเพาะ มาทดลองใช้กับสารไบรโอสแตติน

และพบว่าประสบผลสำเร็จเป็นอย่างดี ซึ่งจะสามารถนำไปใช้ต่อในการศึกษาผลของยาตัวนำที่ค้นพบได้เหล่านี้ในระดับเซลล์ดังกล่าวต่อไป

ดังนั้นงานวิจัยนี้ นอกจากจะเป็นการศึกษาความรู้พื้นฐาน (basic science) เชิงโครงสร้างของการจับเกาะตัวยาของโปรตีนเป้าหมายยาที่มีความสำคัญมากแล้ว ยังเป็นการประยุกต์สร้างวิธีการใหม่ที่บูรณาการการค้นคว้าหาตัวยาด้วยวิธีการคำนวณด้วยคอมพิวเตอร์และทางชีวเคมีเข้าด้วยกันอย่างผสมผสาน เพื่อเป็นการประหยัดเวลาและงบประมาณที่ใช้ในการพัฒนายาโดยทั่วไปที่อาจทำได้ยากในประเทศไทยหรือในวงการการศึกษา และอาจจะสามารถนำไปประยุกต์ใช้กับการพัฒนายาสำหรับโรคร้ายแรงหรือโรคอุบัติใหม่อื่นๆ ได้อีกด้วย ผลการทดสอบยาที่ระบุได้นั้น ยังจะสามารถนำไปสู่การกำจัดการติดเชื้อเอชไอวี-1 แบบแฝง และสู่การรักษาโรคติดเชื้อแบบหายขาดได้ในอนาคต

Table of Contents

Table of Figures

Abbreviations

AIDS	Acquired Immunodeficiency Syndrom
DHCA	Dehydrocholic acid
DMSO	Dimethylsulfoxide
EC_{50}	Half-maximal response (effectiveness) concentration
FDA (US FDA)	U.S. Food and Drug Administration
GFP	Green fluorescence protein
HAART	Highly Active Antiretroviral Therapy
HIV	Human Immunodeficiency Virus
HRP	Horseradish peroxidase
IC_{50}	Half-maximal inhibitory concentration
µL	Microlitre
µM	Micro molar
MD	Molecular Dynamics
mL	Millilitre
MM	Molecular Mechanics
NIH (US NIH)	U.S. National Institutes of Health
nM	Nano molar
PBS	Phosphate buffered saline
pIC_{50}	-log (IC_{50})
PKC	Protein Kinase C
PKCδ	Protein Kinase C Delta
PLS	Partial Least Squares
QM	Quantum Mechanics
RMSD	Root Mean Square Deviation
RMSE	Root Mean Square Error
RMSF	Root Mean Square Fluctuation
SOMs	Self-Organizing Maps

Introduction to the Research Problem and Its Significance

Human immunodeficiency virus-1 (HIV-1) is the causative agent of the acquired immunodeficiency syndrome (AIDS). The development of drugs for HIV infection began soon after the virus was discovered 34 years ago (1), but there is still no cure or vaccine to protect against HIV infection. Thirty-five million people were living with HIV in 2012 (9) and facing numerous uncertainties about the best way to manage the disease. So far, the U.S. Food and Drug Administration (U.S. FDA) has approved 23 drugs and 7 drug combinations, which are mainly either reverse transcriptase (RT) or protease (PR) inhibitors. There are only 3 recently approved drugs those are targeting other steps of the HIV-1 life cycle: Maraviroc (an entry inhibitor targeting human co-receptor CCR5); Enfuvirtide (a peptide-mimic fusion inhibitor); and Raltegravir (targeting HIV-1 integrase, IN) (10). Currently, highly active antiretroviral therapy (HAART) composed of an HIV RT with PR or IN inhibitors successfully suppresses HIV viral load to an undetectable level (3). However, the effect of this therapy is compromised by emergence of resistant HIV strains. Therefore, there are great demands in continuing developing new agents for the treatment of HIV/AIDS.

For the past 30 years, the focus of drug discovery for HIV has been almost entirely on developing drugs targeting active viral replication. Although this development has unquestionably yielded tremendous benefits to the patients and prolongs their life expectancy considerably, this strategy also has its limitations. Most notably, it is not a cure, as the patients must take the anti-viral drugs every day for the rest of their lives. Subtle toxicities associated with the drugs also accumulate over decades, causing inflammation and immune dysfunction that have detrimental consequences. Moreover, although the viraemia is reduced, low levels of viral replication still persist, causing the exhaustion of immune system from battling with persistent infection (6,11,12).

Furthermore, it is likely that HIV will be one of the most common chronic infectious diseases in the world, forcing the drive for HIV pharmacotherapy for the next 20 years (4). Undoubtedly, the global resources necessary to provide complex drug regimens for those who need them, for many decades, are limited. Hence, it is imperative for us to develop a new therapeutic strategy to completely eradicate the virus from the body after a limited intervention. In other words, we need an effective cure for HIV infection (6,7,13).

Although HAART has been highly effective in suppressing HIV-1 infection and reduce the viraemia to undetectable level (<50 copies of viral RNA in 1 mL of the plasma, as detected

by PCR), this is far from an eventual eradication or a complete cure. The persistence of quiescent HIV infection within a small population of long-lived CD4+ T cells is currently a major obstacle to this goal (14,15). These latently infected cell reservoirs do not express viral proteins; thereby remain invisible to the immune surveillance. However, if activated, these cells can restart new rounds of viral replication, giving rise to new infection in other bystander cells, and hence forcing the patients to remain on the drugs indefinitely. In theory, drugs that can reverse viral latency within the quiescent cells should lead to viral expression, producing HIV RNA and proteins, as well as newly assembled viral particles. This process should result in killing of these cells or they may be eliminated naturally by the patient's immune system. Therefore, a cure might be possible if the latent virus in all infected cells can be forced out of its latent state, leading ultimately to the death of the cells and to the elimination of the viral reservoir (5,15-22). Such a potential therapeutic approach is known as 'shock and kill'.

To this end, we aimed to develop an initial drug discovery scheme by targeting a physiological mechanism that can reverse HIV-1 latency in quiescent cells, namely the human protein kinase C (PKC) enzymes. We have applied our knowledge and expertise in computational biochemistry, biochemical screening and assays, virology, as well as in vitro cell immunology to help propel this drug development. Focus was placed on commercially available compounds and/or approved drugs in order to shorten the length of time spent during the lead optimization steps. If successful, this drug discovery scheme can become a prototypical pipeline for accelerated drug development under limited resources and for many emerging diseases. Ultimately, the discovered compounds will be optimized further and tested in vivo for their efficacy in reversing the viral latency. Nonetheless, this work will lay a novel foundation for future discoveries and knowledge in finding a cure for HIV diseases.

Literature Review

In the past 25 years, an unprecedented success has been achieved in the drug discovery for HIV/AIDS, as evidenced by many highly active antiretroviral therapeutic drugs approved and available to the patients, even more so than those for other viral infections combined (23). The currently available drugs, approved by the U.S. FDA, can be divided into seven categories: nucleoside reverse transcriptase inhibitors (NRTIs), nucleotide reverse transcriptase inhibitors (NtRTIs), non-nucleoside reverse transcriptase inhibitors (NNRTIs), protease inhibitors (PIs), fusion inhibitors (FIs), co-receptor inhibitors (CRIs), and integrase inhibitors (INIs). However, the use of these drugs can be limited due to their toxicity (24), development of drug resistance (25), and more importantly the fact that some of the newly infected patients are carrying the virus strains that are already resistant to the approved AIDS treatments (26). Some approved drugs also possess serious side effects that could shorten lifespan of a patient dramatically. Hence, both new therapeutic agents and novel mechanisms of inhibition are urgently needed (23,27).

In an ongoing effort to help develop novel anti-HIV molecules for complete eradication of HIV-1, we aimed to establish a drug discovery campaign targeting the latency mechanism of the virus. The purpose of such strategy was to reactivate the latently infected cells from quiescent state to become susceptible and destroyed by HAART. The background information and rationale for the project are described below.

HIV Latency and Protein Kinase C (PKC) Enzyme

In an activated CD4+ T cell, once the cell has been infected and the viral DNA has been integrated into the host's genome, transcription of the integrated viral DNA can be facilitated by both cellular transcription factors or the viral transcription activator-Tat. This gives rise to the production of the viral proteins, which will be assembled with the newly transcribed viral RNA, and subsequently formed into a new HIV particle; then the infected T cells generally undergo apoptosis (4,24,28-30). In contrast, in latently infected T cells the viral life cycle is arrested after integration, and these quiescent T cells with HIV-integrated genome possess a very long half-life equivalently to some normal uninfected cells. These latently infected cells become a replication competent reservoir for HIV that cannot be reached by HAART. Once HAART regimen is interrupted, the latent cells can be activated and the viral production resumes, causing a rebound in HIV viraemia that can be observed in nearly all patients (30,31).

Several clinical trials were attempted to completely eradicate HIV-1 infection by activating these quiescent and long-lasting infection using cellular activators such as Muromonab-CD3 (trade name Orthoclone OKT3, marketed by Janssen-Cilag) or interleukin (IL)-2 (32-37). Though genotypic alterations of the viral reservoir were observed, the overall effect in complete activation and eradication was not achieved. Since then, the list of candidates includes small hydrophobic agents such as phorbol ester compounds (38), as well as bryostatin-1, a macrolide lactone (39). This family of compounds was found to modulate the protein kinase C (PKC) pathway, which ultimately induces latent HIV-1 expression (38,39). This discovery gave rise to the concept of 'shock and kill' strategy to eradicate the infection by specifically activating the latently infected cells, upregulating the latent HIV-1 genes in the quiescent reservoir, and can be combined with HAART drugs to get rid of the virus completely.

To reverse the latency, PKC is a logical target due to its regulation of HIV-1 transcription via multiple mechanisms. First, PKC activates the transcription factor NF-κB, which binds to several enhancer sites of the HIV-1 long terminal repeat (LTR) in the integrated genome (40). Second, PKC activates AP-1 (c-Jun) transcription factor that binds to both HIV-1 enhancer and to its downstream sequence elements (41-43). Finally, PKC also phosphorylates the viral transcription activator—Tat (a virally encoded accessory protein required for transcription elongation to produce full-length HIV-1 RNAs), as well as cellular TAR-binding factors, which directly activate the viral transcription (44,45).

Normally, PKC is activated by mitogens, antigens or other extracellular ligands through the lipid second messenger called 1,2-diacylglyceral or DAG, which binds to the C1 regulatory domain of PKC. This process thereby exposes the catalytic domain of PKC by displacing a restrictive pseudosubstrate region and induces its translocation to the plasma membrane. PKC are categorized into at least 12 different serine/threonine kinase isozymes, each with different cellular localizations, responses to inducers, and substrate specificity. Calcium-dependent classical PKC isoforms (cPKCs), which include PKCs α, βI, βII, and γ, require calcium for their activity. Calcium-independent isoforms or novel PKC (nPKC) (δ, ε, η, and θ) are independent to calcium but still DAG-responsive. A third class of PKCs are atypical isoforms, which include PKCs ξ, and λ/I, are not responsive to either calcium or DAG (46-48).

PKC Modulator Compounds

Potent and long-lasting PKC activation can be achieved by many naturally occurring compounds such as phorbol esters (fig. 1), teleocidins, and some macrocyclic lactones such as the bryostatins or aplysiatoxins. Nonetheless, most of these compounds have serious side effects such as tumor promotion, local irritation, platelet aggregation and activation of inflammatory cytokines, rendering tremendous problem in applying them as human therapeutics (38,46-49). Moreover, their highly complex structures also hinder the organic modification process by chemical synthesis. Therefore, recent studies have been focusing on the use of pharmacophore- and receptor-guided approaches to design DAG analogues that can bind tightly to the C1 domain of PKC (50). DAG lactones (Figure 1) are a group of compounds that have been found to mediate specific activation of PKC isotypes and their translocation to cellular compartments (51). However, chemotherapeutic treatments that can markedly accelerate the process of reservoir decay and yield minimal side effects have yet to be discovered, in order to advance toward the goal of curing HIV-1 infection.

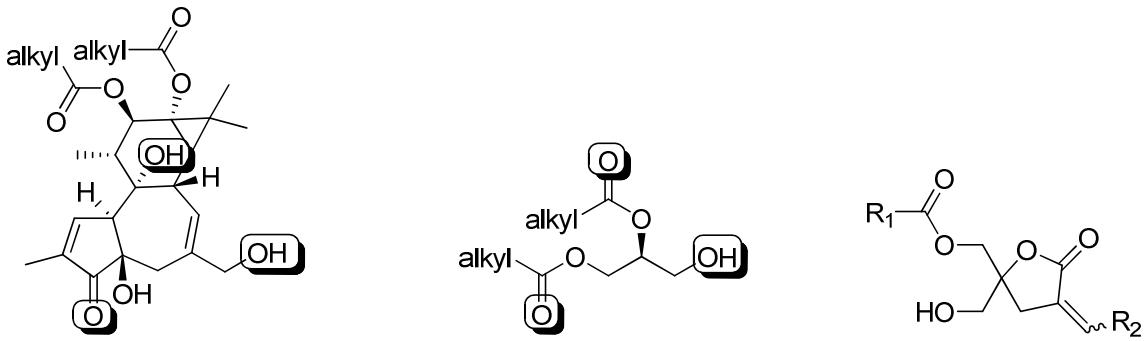

Phorbol Ester DAG DAG Lactone

Figure 1. Chemical structures and corresponding pharmacophores on phorbol ester, DAG, and DAG lactones.

Drug Discovery: Bottlenecks and Modern Techniques

The development of a new drug is a lengthy, complicated, costly and highly risky process (Figure 2). Moreover, it is estimated that only approximately 1 in 15-25 drug candidates survives the detailed safety and efficacy testing, both in animals and in humans (52,53). Some drugs that have been brought to market may never recover their costs of development in the competitive marketplace (53). Undoubtedly, this is a high-stakes, long-term, risky process, but the potential outcomes that could benefit millions of patients with serious diseases provide a great motivation to medicinal chemists, both in the pharmaceutical industry and in academia.

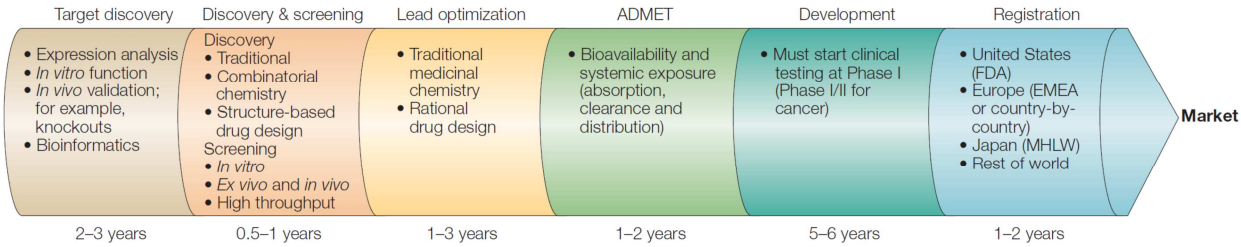

Figure 2. A General Pipeline of a Drug Discovery. De novo drug discovery and development is a ~10–17 year process from idea to marketed drug. The probability of success is generally lower than 10%. ADMET, absorption, distribution, metabolism, excretion and toxicity; EMEA, European Medicines Agency; FDA, Food and Drug Administration. (Figure adapted from Ref. (20))

One of the big problems in the drug development pipeline that causes a 'bottleneck' and impedes the progress occurs between the lead optimization and the evaluation of the absorption, distribution, metabolism, excretion and toxicity (ADMET) (52-55). This issue stems from having too much emphasis on in vitro screening of compounds against molecularly defined targets (53). The in vivo animal models for pharmacokinetic and pharmacodynamic studies, though necessary, are very expensive and, sometimes, do not represent human metabolism. Modern drug development concepts have addressed these issues by incorporating the in vitro and in silico screens that are predictive of human pharmacokinetic performance. Permeability and transporter assays have also been developed to characterize drug uptake into organs (52-55). Nonetheless, further in vivo testing is then required to show that the compound attains levels at the target organ commensurate with achieving the desired biological effect that is proposed to result from the in vitro activity.

Computational techniques have become more advanced and essential components for many drug discovery campaigns, from hit identification (virtual screening), to lead design and optimization (de novo design), ADMET prediction, and beyond (56-58). Docking of small molecules into the drug target binding sites remains a highly effective method in the in silico application (54,59). Once the simulated version of the mode of action has been verified, a high-throughput search—a virtual screening—can then be used to identify 'hit' compounds. Similar calculations can also be adapted during the lead optimization and/or novel designs, where modifications to known pharmacophores can quickly be tested in computer models before the actual in vitro testing. Incorporating of reliable computational techniques should help accelerate the drug discovery pipeline dramatically.

Objectives

The main objective of this project was to develop a novel and efficient chemotherapeutic treatment for HIV/AIDS by focusing on tackling the latency mechanism of the viral infection that can be reversed via protein kinase C pathway. Ultimately, we aimed to identify a few drug candidates that can be advanced toward pre-clinical (animal) testing. The structural knowledge gained from the structure-activity relationship and molecular dynamics studies would also provide basic understanding of the target proteins. This study mainly concentrated on the initial discovery steps, using an innovative multifaceted drug development approach, which attacked several technical problems in parallel to ensure the chance of success. We have established a multi-pronged strategy to overcome multiple issues commonly found in a drug discovery campaign. Specifically, there were two main aspects of the proposed strategy, which coincided with two objectives of this work.

Objective 1) To investigate structural detail of the binding and to optimize virtual docking protocols for anti-HIV-1 latency, targeting PKC, and for a practical virtual screening platform.

To maximize productivity and reduce costs associated with traditional drug discovery, we have implemented computational methods to aid the initial drug screening. The optimized molecular docking and virtual screening platforms were expected to yield multiple 'hit' compounds that can be readily purchased and subsequently tested biochemically. To further optimize the leads identified from this approach, we also used advanced computational techniques such as molecular dynamics (MD) simulations to gain structural insights into the binding of known potent ligands, namely bryostatin. Based on the structural dynamics information, we hoped to implement an automated ligand assembly to yield new candidates. Only outstanding candidates with high predicted potency will be further biochemically tested in the future.

Objective 2) To develop *in vitro* biochemical and cell-based assays for evaluating efficacy of the drug candidates.

To validate the virtual screening and molecular docking, we used previously established biochemical assay to guide the prediction, and cell-based assays to evaluate the small chemical compounds identified from objectives 1. These assays will be further improved during the next phase of discovery to gain molecular insights into the mode of action of the candidate compounds.

Research Methodology

Equipment

- Three personal computers (PCs, Intel Core i7)
- Two refrigerators, 4 Celsius, non-automatic defrosting (for chemicals and for media/ antibodies)
- Two freezers, -20 Celsius, (for chemicals and for media)
- One deep freezer, -80 Celsius (for cells, viruses, cytokines, sera, plasma samples etc.)
- One microcentrifuge with plate spinning
- Micropipettes, single- and multi-channel
- Multi-well dropper
- Ultrasensitive balance
- Vortex mixer
- Temperature controlled waterbath
- Magnetic stirrer

Molecular Docking

Preparation of protein structure

The co-crystal structure of the cys2 activator binding domain of PKCδ with phorbol 13-acetate (PRB) (PDB ID: 1PTR)(60) was retrieved from the RCSB Protein Data Bank. The PRB structure at the binding site of the complex was isolated from the protein structure using Accelrys Discovery Studio 4.0. The protein structure was then converted from 'pdb' into a 'pdbqt' format using AutoDockTools (ADT). Resolution of the three-dimensional grid box (x, y and z) was set as 30×30×30 with a grid spacing of 0.375 Å. The grid center, which is based on the original ligand, was set to 10.903 Å, 26.391 Å and 24.495 Å for x, y and z dimensions, respectively.

Preparation of ligand structures

The PKC activator, bryostatin 1, structure was sketched as a 'mol2' file using Accelrys Discover Studio 4.0. Phorbol 13-acetate (PRB) structure that was initially separated from the starting complex, and the bryostatin 1 structure were then assigned for atom type and energy minimized using Tripos force field in SYBYL 7.3 suite. The ligands were then converted from 'mol2' into a 'pdbqt' format using ADT.

Molecular docking for preparing ligand coordination in complexes

All docking calculations were performed using AutoDock Vina (61) on a Linux platform. From output files, the best docking conformation for each complex was chosen based on position and non-bonding interactions of the ester group of each ligand with the five key amino acid residues (Ser240, Pro241, Thr242, Leu251 and Gly253) at the binding site on the PKCδ structure. Partial atomic charges were optimized for their geometry and were calculated for ESP charges with Gaussian 09W software (G09) through the ground state using Restricted Hartree-Fock method with a split valence basis set 6−31G(d).

MD Simulations

MD simulations for all experiments were performed using GROMACS 4.6.3 package, incorporated with Amber99SB force field (62,63). Three simulating systems, consisting of free PKCδ, PKCδ-phorbol 13-acetate and PKCδ-bryostatin 1, were neutralized by adding counter ions (sodium and chloride ions) and solvated by a cubic box with diameter of 2.0 Å with TIP3P water model (64). Energy minimization was completed for three systems through steepest descent method for 5,000 steps, followed by 80-ps of MD simulations in all ensembles using the Berendsen coupling method (65) with a pressure (P) of 1 bar, at a reference temperature (T) of 300 K. The LINCS algorithm (66) was performed to keep all the bonds containing rigid hydrogen atoms. The long range electrostatic interactions were investigated by using the particle-mesh Ewald (PME) algorithm (67,68) with a 2-fs time step. The MD production run for all of simulating system was set as 80 ns of constant-pressure and was carried out at 300 K. The atomic coordinates of the simulated structures were saved every 2 ps for the data analysis.

Data analysis

The data from all experiments were collected and analyzed by GROMACS analysis tools. GROMACS utilities such as g_energy (potential, kinetic, and total energy), g_rms (RMSD), g_rmsf (RMSF) and g_hbond (number of hydrogen bond), g_dist (hydrogen bond distance) were employed at various points in the process of performing molecular dynamics simulations. Trajectories and structures were visualized using Visual Molecular Dynamics (VMD) (69), Accelrys Discovery Studio Visualizer 4.0 (Accelrys Software Inc.) and PyMol v.1.3 (Schrödinger, LLC.). GraphPad Prism 5 software was used for generating all the plots.

Mathematical models for post-docking analysis

Because our initial analysis for the correlation between theestimated free energy of binding from the dockings and the actual (experimental) activation effectiveness of the sets of

compounds did not yield a linear correlation (R^2 = 0.39), we decided to employ mathematical models for predicting the post-docking parameters in order to gain a linear correlation. Normally, a docking run from AutoDock 4 would result in 8 highly variable parameters, which include 1) Estimated Free Energy of Binding; 2) Estimated Inhibition Constant, K_i; 3) Final Intermolecular Energy; 4) van der Waal + Hydrogen Bond + Desolvation Energy; 5) Electrostatic Energy; 6) Final Total Internal Energy; 7) Torsional Free Energy; and 8) Unbound System's Energy. Closer inspection of these parameters revealed that the trends of each parameter were not always in the same incremental direction, indicating a non-linear correlation among the parameters. Therefore, a non-linear analysis from this post-docking result was possible. We used two statistical methods: Partial Least Squares (PLS) and Self-Organizing Maps (SOMs) for building a model and finding the proper usage of each parameter in order to more accurately predict the compound activity (Figure 4). From the docking of each compound, 30 conformations with various values of parameters were obtained. PLS and SOMs were used to selectively decide which conformation would be used based on the closest correlation with the actual experimental result. All of parameter values from that conformation were then picked and subjected to the weighted calculation to predict a 'predicted fold-activation' for that particular compound. A linear plot was then generated to obtain a linear correlation between the 'predicted fold-activation' values and the 'actual fold-activation' values.

Virtual screening

A modern cost-effective and time-efficient technology to access a significantly larger portion of chemical space is to use computational techniques to virtually screen the commercial catalogues of chemical vendors, from which a selected number of molecules is ultimately purchased for experimental testing. Virtual screening was performed on the optimized docking structures from objective 1, and made use of similarity-based search as described previously (70). Because the structure-activity relationship (SAR) studies are generally impeded by the long process of organic synthesis of new compounds, we delayed this lengthy, though necessary, procedure toward the end of the initial discovery. We thus performed an initial virtual screening based on the commercially available library from ChemBridge Corp. first, using Autodock Vina.

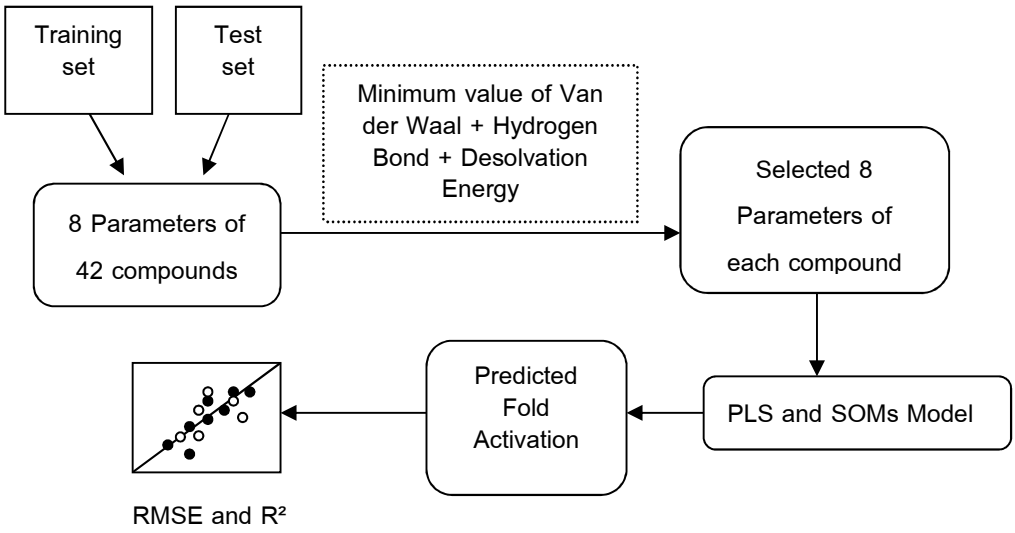

Figure 3. Schematic showing the generation of predictive models using Partial Least Squares (PLS) or Self-Organizing Maps (SOMs)

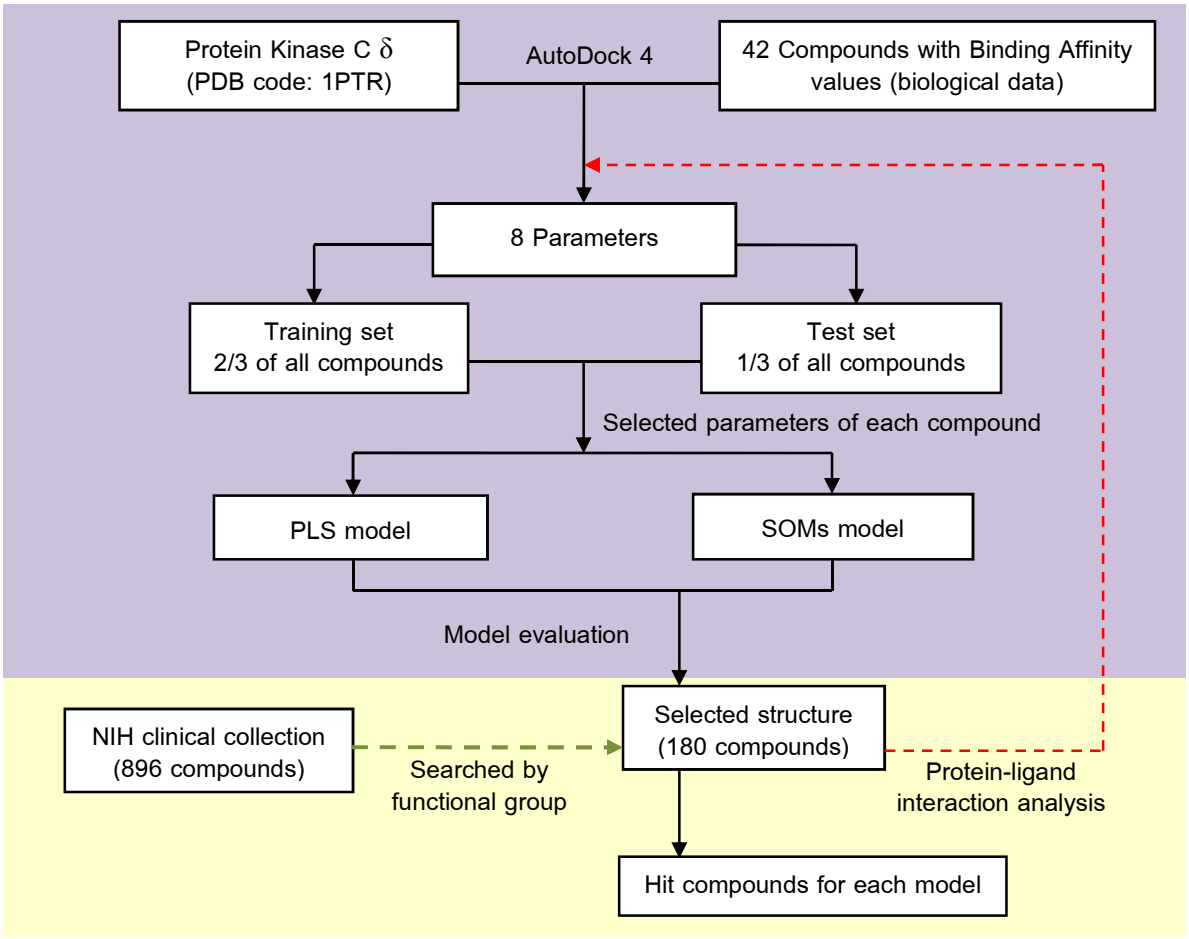

Figure 4. Schematic showing overall process for the molecular docking combined with the mathematical models (top part), as well as the pharmacophore similarity search (bottom part) for selecting candidates for PKCδ

The subsequent SAR study will also be performed on commercially available compounds, which is the most time efficient strategy. Initially, in this report, the predicted hit compounds and their analogues with distinct substituents within the chemical scaffold were purchased directly from ChemBridge (~500-3,000 Baht/compound). As needed, we also sought within the ZINC database (71-73) for additional commercially available analogues that are sold by vendors other than ChemBridge. Biochemical assay on PKC activation was performed on these compounds to obtain the fold-activation values.

Direct *in vitro* Biochemical Assay for Evaluating Modulatory Effects on PKC

The modulatory effects on the activity of PKC were measured by solid phase enzyme-linked immuno-absorbent assay (ELISA) kit from Enzo Life Sciences International, Inc. Assay protocols were optimized based on the manufacturer's instructions. The assay has been designed for the analysis of PKC activity in the solution phase. Briefly, microplates pre-coated with PKC substrate were used. The microplate wells were soaked with dilution buffer and emptied after 10 minutes. An equal volume of the enzyme solution was then added to the wells, followed by the addition of ATP to initiate the reaction. After incubation for 90 minutes at 30°C, the kinase reaction was terminated by emptying the contents of each well. The phosphopeptide substrate thus obtained could be immunodetected by using phospho-substrate specific primary antibody and peroxidase-conjugated secondary antibody as per manufacturer's instructions. The mean absorbance ($x10^3$) of samples was divided by the quantity of total protein (μg) used per assay, and the data are represented as relative PKC activity for each modulator compound.

Cell-based Assays for Anti-Latency Effects

For the cell-based latency evaluation, latently HIV-1 infected T-cell line, J-Lat 10.6, was obtained from the US National Institutes of Health (NIH) AIDS Research and Reagent Reference Program and maintained in RPMI 1640 medium containing 2 mM glutamine, 10% fetal bovine serum, and antibiotics. One hundred thousand cells were incubated with various concentrations of modulator compounds. Bryostatin-1 (Sigma) was used as positive activator control. After 24 hours of incubation at 37 °C under 5% CO_2, each reaction was spun at 180×*g* to separate the supernatant and the cell pellet. Cells were resuspended and fixed with 4% paraformaldehyde in PBS solution. Antigen capture enzyme-linked immunosorbent assay (ELISA) kits were used to measure the HIV-1 p24 antigen (XpressBio) produced in the supernatant. Flow cytometry was used to monitor the expression of the GFP gene encoded in the full-length (env-) HIV-1 provirus. Percentage of GFP expression is correlated to the

reactivation efficacy of the cell line and thus representing the indirect in vivo PKC modulation. Flow cytometric graphs were analyzed via FlowJo version 10.0.7 (TreeStar).

Results and Discussion

Structural Analysis of PKCδ Protein

In the present study, comparative MD simulations were performed on the free cys2 activator binding domain of PKCδ (henceforth 'PKCδ'), phobol 13-acetate (henceforth 'phorbol ester') complexed with PKCδ, and bryostatin 1 (henceforth 'bryostatin') complexed with PKCδ, in order to gain insights into the binding mode as well as to explain differences in the activation mechanisms among the free and the activator-bound proteins. Focus was put also on the binding of bryostatin, which is one of the most potent activators for PKCs identified to date, in order to gain insight into how it functions. This is because, despite decades of effort focused on structural explanation of the mechanism, this information does not yet exist (74,75).

The free cys2 activator binding domain, as known as the C1 domain, is a part of five-domain conventional and novel PKCs (Figure 5A). It comprises three canonical long beta sheets (β1, β4, and β5), two short beta sheets (β2, and β3), and a C-terminal α-helix. The activator binding region is between the β1/β2 loop (Met239, Pro241, Thr242) and the β3/β4 loop (Leu251, Trp252, Gly253, and Leu254) (Figure 5B). The structure of this domain, as determined by X-ray crystallography (60) (PBD ID's: 1PTQ for free protein, and 1PTR for phorbol ester-bound protein) revealed that its overall topology developed a global fold with two Zn^{2+} binding sites distal and proximal to the activator binding region. In good agreement with previous studies (60,76), the activator binding patch located at the tip of the molecule appears generally polar on the outer surface while a few hydrophobic residues covers parts of the inner wall of the binding pocket. However, most of the surface of the protein is hydrophilic, making this globular protein highly soluble in the cytosol (60).

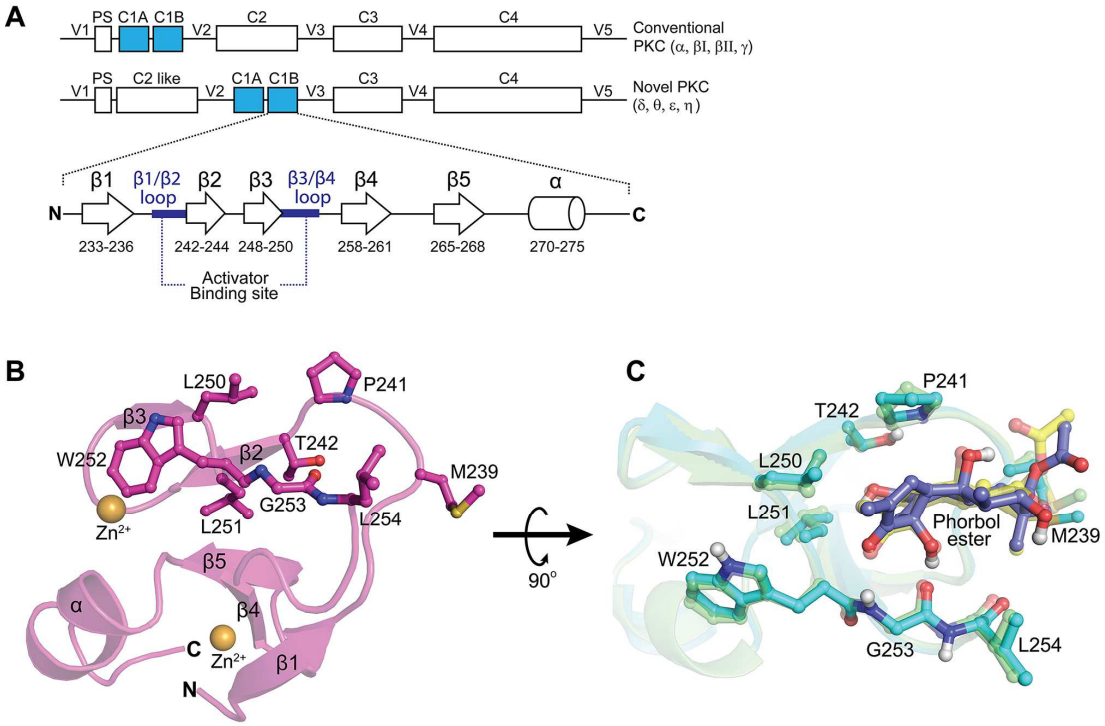

Figure 5. Structure of the cys2 activator-binding domain of protein kinase C. (A) Schematic representation of C1 (cys2) domain located within PKC proteins. For both conventional (α, βI, βII, γ) and novel (δ, θ, ε, η) PKCs, four distinct domains (C1–C4) and five variable regions (V1–V5) are present, along with the amino-terminal pseudosubstrate (PS) domain. The secondary structure topology of the C1A or cys2 domain is highlighted, showing the activator binding site located between the β1-β2 and the β3-β4 loops. (B) Crystal structure of the cys2 activator-binding domain of PKCδ (PDB ID: 1PTR)(60) with the activator binding site (residues 239–242 and 250–254) highlighted in stick representation. Phorbol ester molecule was removed from the original crystal structure. (C) Comparison between the crystal structure of PKCδ (PDB ID: 1PTR, shown in yellow and pale yellow) and the 80-ns MD simulated complex of phorbol ester molecule docked onto the original activator binding site of PKC (this study, shown in cyan and purple). Backbone and ligand RMSD between the two structures is 0.353 Å.

MD Simulations

In order to gain insight into the modes of activator-binding mechanism, MD simulations were performed for free PKCδ and activator-bound PKCδ complexes. Initially, the crystal structure of phorbol ester-bound protein (PDB ID: 1PTR)(60) was used as a template protein for this present study. The phorbol ester (phorbol 13-acetate) molecule was removed manually from the protein structure to create a free PKCδ protein. Subsequently, the ligand molecule, either phorbol ester or bryostatin, was docked onto the activator binding region of PKCδ, and the MD simulations were performed for 80 ns. To confirm the validity of the docking and the MD simulations, an 80-ns snapshot of stable structure of PKCδ-phorbol ester complex was

overlaid onto the original crystal structure complex of PKCδ-phorbol ester (Figure 5C). The comparison yielded a good alignment with an RMSD value between the two complexes (backbone and ligand) of 0.353 Å, indicating that the docking and the MD simulation are reliable.

When comparing the parameters resulting from the MD simulations of the free protein and the protein-activator complexes, several interesting discrepancies can be found. First, the potential energy plots (Figure 6A) showed a quick stabilization of all molecular systems and they remained stable for the entire 80 ns of the MD runs. However, the potential energy from the PKCδ-bryostatin complex stabilized at a significantly lower level (approximately -1.67×10^5 kcal/mol) than those of the free protein or the PKCδ-phorbol ester (approximately -1.51×10^5 kcal/mol). Second, during the MD simulations, the RMSDs of heavy atoms, side chains, and Cα-atoms of all molecular systems also showed different trends (Figure 6B). For both PKCδ-activator complexes, the monitored RMSDs fluctuated during the first 30 ns, and then became more stable afterwards. This is different in the case of the free protein where the RMSDs fluctuated throughout the 80 ns of MD. This indicated that, in the absence of activator, the PKCδ protein was constantly moving and was more away from the initial structure. On the other hand, when bound with either activator, the monitored structures initially moved slightly (within ca. 0.2 nm of backbone coordinates, or approximately an average of a single bond distance), and subsequently became stabilized after 30 ns and throughout the rest of the MD runs. Nonetheless, both the RMSD and potential energy trends of the complexes monitored during the MD simulations support the timeframe of 80 ns as adequate for analyzing the dynamics of both molecular systems.

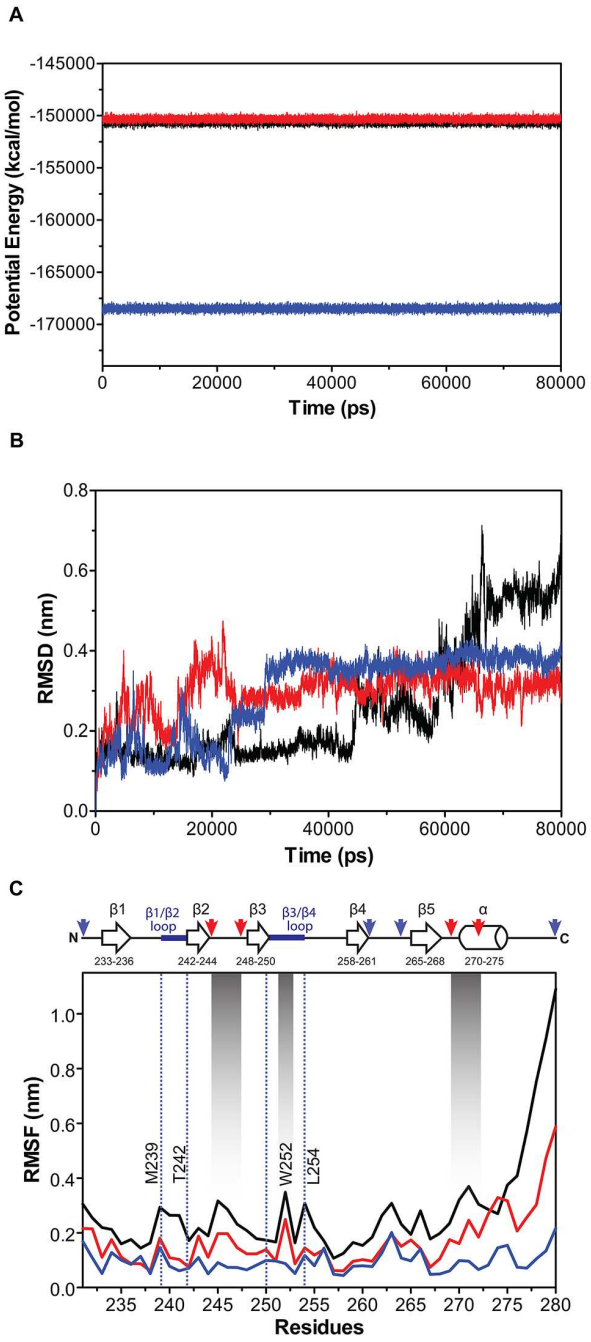

Figure 6. Comparison of parameters resulted from the MD simulations of free PKCδ protein (black), PKC-phorbol ester complex (red), and PKC-bryostatin complex (blue). (A) Plot of the potential energy (kcal/mol) during 80 ns MD of the free protein and complexes. (B) The backbone RMSD vs. MD simulation time. (C) RMSF of the free protein and complexes during 80 ns MD showing fluctuations among the protein amino acids. Activator binding regions are highlighted in the dotted lines with some key binding residues indicated. Downward arrows on the topology schematic line indicate the locations of two sets (red or blue) of Zn^{2+}-coordinating residues. The three gradient columns highlighted the regions that have the most prominent differences of the RMSF values from all molecular systems, which coincide with Trp252 and one set of the Zn^{2+}-binding residues.

Root mean-square fluctuations (RMSF) of backbone atoms (N, Cα and C atoms) during the molecular dynamics (MD) simulations are shown in Figure 6C. It is apparent that the PKCδ-bryostatin complex has the lowest values throughout the entire protein sequence, suggesting that lower average atomic mobility can be observed when the protein is bound to bryostatin. Free PKCδ protein had the highest fluctuation, and, as expected, showed the most prominent fluctuation towards the C-terminal loop. Interestingly, the areas with the fluctuation are also located in the activator binding regions (Met239–Thr242 and Trp252–Leu254), and on the two sets of Zn^{2+}-binding residues (His231, Cys261, Cys264, Cys280; and Cys244, Cys247, His269, and Cys272). However, when comparing the trends among all three molecular systems, it can be observed that three particular regions showed a dramatic drop in atomic mobility when a free protein is bound to bryostatin (Figure 6C, gradient columns). These include Trp252 and one set of the Zn^{2+}-binding residues (Cys244, Cys247, His269, Cys272). Notably, these two regions are in close proximity in the three-dimensional space, as the distances between His269 imidazole ring and the Trp252 benzene and indole rings are approximately 3.7 Å and 5.4 Å, respectively. This could imply a plausible π-π interaction or cation-π interaction between His269 and Trp252, as previously suggested (75), and possibly a role of Trp252 in the binding mechanism of bryostatin (vide infra). Taken together, it can be concluded from all the MD simulation throughout the monitored period, especially from the potential energy and the RMSFs, that the PKCδ-bryostatin complex is the most stable and shows the least fluctuation among the three molecular systems.

Hydrogen Bonding Networks in the PKCδ-Activator Complexes

Figure 7 summarizes the hydrogen bonding networks that can be observed during the 80-ns simulations. Phorbol ester forms four distinct hydrogen bonds with the activator binding groove of PKCδ (Figure 7A) while bryostatin forms only two (Figure 7B). As shown in Figures 7C and 7E, phorbol ester forms one hydrogen bond with the backbone amide of Thr242, one bond with the backbone carbonyl of Leu251, and two bonds with the backbone carbonyl and amide of Gly253. Bryostatin forms one hydrogen bond with Nε1 of the Trp252 indole ring and one bond with the backbone amide of Gly253. The evolution of bond formation between these two complexes is rather different. In the case of the phorbol ester binding, the numbers of H-bond varied greatly throughout the MD run. For bryostatin binding, on the other hand, the bond formation becomes much more consistent after the 30 ns time point, possibly when the H-bond to the Trp252 has been formed (vide infra).

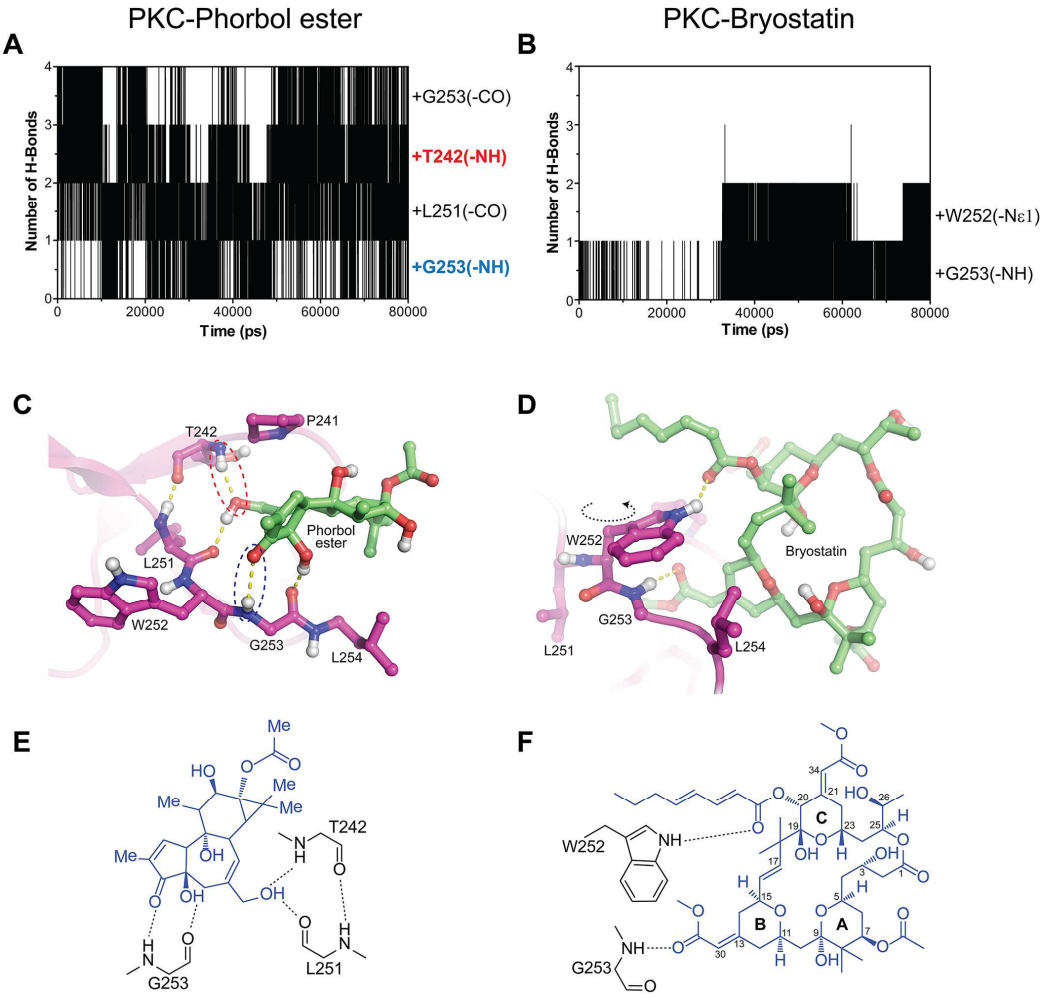

Figure 7. Hydrogen bond formations found in the complexes between the PKC protein and phorbol ester (A, C, E) or bryostatin (B, D, F). (A, B) Number of H-bonds between PKC and the ligands during total course of 80 ns of MD simulations. (C, D) Three dimensional structures of the binding site of the protein focusing on the H-bond formations (dotted yellow lines). Key binding residues are indicated. The dotted elliptical lines highlight H-bond formations to Gly253(-NH) and Thr242(-NH) as color-coded in figure 7A. (E, F) Schematics summarizing hydrogen-bonding interactions (dotted lines) in the phorbol ester binding or in the bryostatin binding.

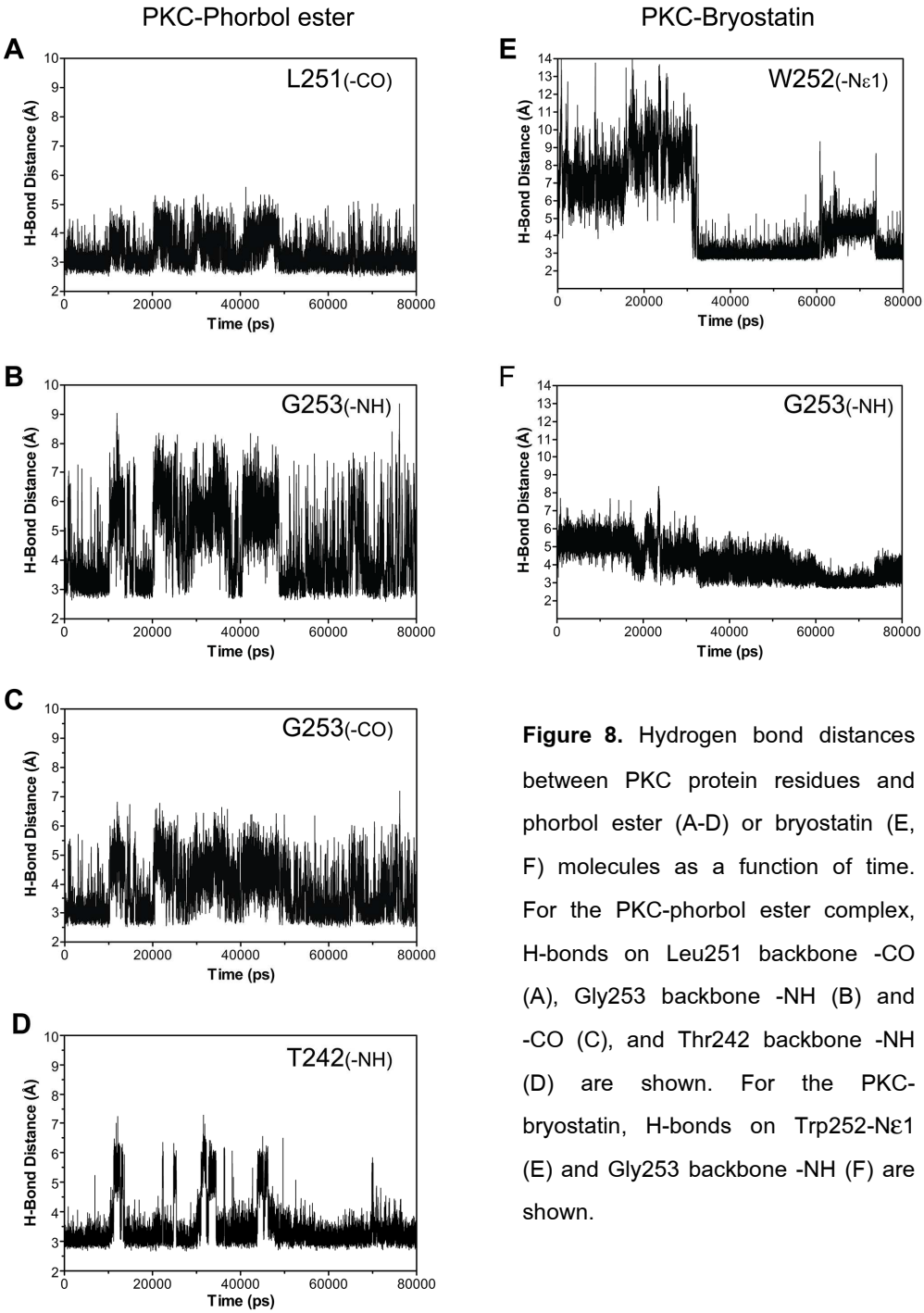

Figure 8. Hydrogen bond distances between PKC protein residues and phorbol ester (A-D) or bryostatin (E, F) molecules as a function of time. For the PKC-phorbol ester complex, H-bonds on Leu251 backbone -CO (A), Gly253 backbone -NH (B) and -CO (C), and Thr242 backbone -NH (D) are shown. For the PKC-bryostatin, H-bonds on Trp252-Nε1 (E) and Gly253 backbone -NH (F) are shown.

When considering the H-bond formations, as indicated in Figures 7A–B, together with the bond distance of each (Figure 8), the identity of each H-bond could be specified roughly which key partner atom on the protein activator binding site is contributing to the H-bond formation (Figures 7A–B, side labels). Interestingly, in the case of PKCδ-phorbol ester complex, H-bonds of Gly253(-NH) and Thr242(-NH) exhibited almost exactly opposite bond formation behaviors over time (i.e. when one is present, the other is absent, and vice versa). The location of these two H-bonds are also on the opposite sides of the phorbol ester

molecule (Figure 7C, dotted elliptical lines). This could imply that these two bonds are pulling against each other by having the phorbol ester molecule in the middle. This 'tug-of-war' H-bond network may potentially cause the binding to phorbol ester to become less energetically favorable when compared to the bryostatin binding (Figure 6), even though it has more H-bonds.

H-bond formation profile in the PKCδ-bryostatin complex (Figure 7B) can also be correlated with the H-bond distance (Figure 8). The evolution of H-bond formation on Gly253 (-NH) appears more gradual than that of the one on Trp252(-Nε1). Moreover, when comparing all the H-bond formations in the PKCδ-phorbol ester complex, the bond formation on Gly253 (-NH) to bryostatin exhibited much more consistent stability after 30-ns time period. The H-bond on Trp252(-Nε1), on the other hand, was not present before this time point. This may suggest a cooperative behavior of these two H-bond formations to bryostatin. It is possible that the Z-enoate of the B-ring on bryostatin (C13) may thread into the binding pocket first. Once the Gly253(-NH) of the protein starts to form a hydrogen bond to it, the side chain of Trp252 swings its indole ring coincidentally towards the binding pocket and forms a hydrogen bond to the ester group on the C-ring, thus helping to stabilize the ligand in place. The movement of this Trp252 side chain and its possible relevance to the structural fluctuation will be discussed further in the next section.

Notably, it is possible that in both complexes, Gly253(-NH) may form a hydrogen bond to the activator molecule first, leading to the other H-bond formations to the ligand. If this initial bond is not then stabilized by the other bonds (as in phorbol ester binding) the complex may not be as energetically favorable as the one that helps stabilizing this initial bond (as in bryostatin binding).

The validity of these two H-bond formations on the PKCδ-bryostatin complex is bolstered by previous structure-activity relationship studies of bryostatin derivatives (77-82). For example, when the ester group on the C-ring C20, which potentially binds to Trp252, is absent in bryostatin 10 or in bryostatin 18, the K_i with the isozyme mixed PKCs increased from ca. 1 nM to 3.4-4.8 nM (80,83). Attempts by the Wender group (81,82) to replace the aliphatic chains after the ester group at C20 with multiple substituents also resulted in two-to-sixty-fold decreases in the binding affinity for the rat brain PKCs. However, on the bryopyran analogues (pyran scaffolds on the A and B rings), it has been discovered that various modifications after this ester group on the C20 of the C ring still yielded very high affinity for PKC (K_i with PKCα = 0.70–1.05 nM, when compared to 1.35 nM for bryostatin 1). Nonetheless, when the

functional effect of these bryopyran analogues was considered, they are more similar to that of the phorbol-12-myristate-13-acetate (PMA) as they are promoting proliferation of U937 leukemia cells, the effect that bryostatin 1 antagonizes and thus distinguishes itself from the phorbol ester activity (77). Therefore, it can be deduced that the ester group on the C20 may be important for the binding to PKC. On the other hand, the long aliphatic chain beyond this ester group may neither be critical for the binding nor for retaining the unique biological characteristic of bryostatin. The biological characteristic may, rather, depend on the original substituents on the A and B rings. Taken together, these lines of experimental evidence are consistent with the MD structure of the PKCδ-bryostatin complex presented in this study that the ester group at C20 is important, but the aliphatic chain beyond this ester group may be dispensable. For the binding of Gly(-NH) to the C30 carbomethoxy substituent on the B-ring of bryostatin, it has been reported that the Z-enoate analogues (as found in the bryostatin-1 structure) were slightly more potent in the binding than their corresponding *des*-enoate forms (79). Similar to the results from the PKC binding, *Z*-enoate analogues were also found to be more potent than the pyran form of the B-ring in their ability to reactivate latent HIV-1 expression in the model cell line J-Lat 10.6 (79). These results confirmed that the substitution on the C13 of bryostatin may be critical in the activation function of PKC.

Furthermore, the Keck group (78) also reported a poor contribution of the A-ring C7 acetate to the binding and the biological function of bryostatin. Biological evaluation of several bryopyran analogues revealed that any modifications of this location did not result in an enhanced binding affinity for PKC. Thus, it can be concluded that the A-ring acetate is not the important structural determinant for antagonizing phorbol ester-induced biological responses (78). These lines of experimental evidence also coincide with the MD structure of PKCδ-bryostatin complex reported in this study that bryostatin may initially binds to the activator binding pocket via its C20 and C30 groups, while orienting the C7 substituents away from the binding site.

The Role of Trp252 in the Activator Binding

The highly homologous Trp252 is also of particular interest in this study, largely due to its close proximity to one of the Zn^{2+} binding centers and to the activator site, and especially due to its vast side-chain movement during the MD simulations of both free protein and the protein-activator complexes (Figures 9A-C). Therefore, we have focused on delineating the role of this movement by correlating our MD structures to the backbone fluctuation data, in order to derive a possible model describing its relevance in the binding and activity.

Although the motions of this Trp252 side chain, observed by our 80-ns MD simulations, appear to be similar between the free protein and phorbol ester complex (Figures 9A, B), the motion in the bryostatin complex revealed a distinctive behavior (Figure 9C). It is apparent that, in the case of the free protein, Trp252 side chain samples various conformations, toggling randomly in and out of the activator binding site. When the phorbol ester molecule is bound, no apparent H-bond is formed between this residue and the ligand (Figures 7C, E), and the side chain is still rotating randomly, though orienting away from the binding pocket, suggesting its non-involvement in the recognition. In contrast, bryostatin binding causes the toggling behavior of the Trp252 side chain to become much more restricted, largely due to the H-bond formation between the indole Nε1 and the ester group on C20 of the ligand (Figures 7D, 7F, and 9C). Notably, during the MD run, the aromatic rings of Trp252 starts to flip at approximately 30 ns (Figure 9C), which coincides with the beginning of the H-bond formation observed (Figures 7B and 8E).

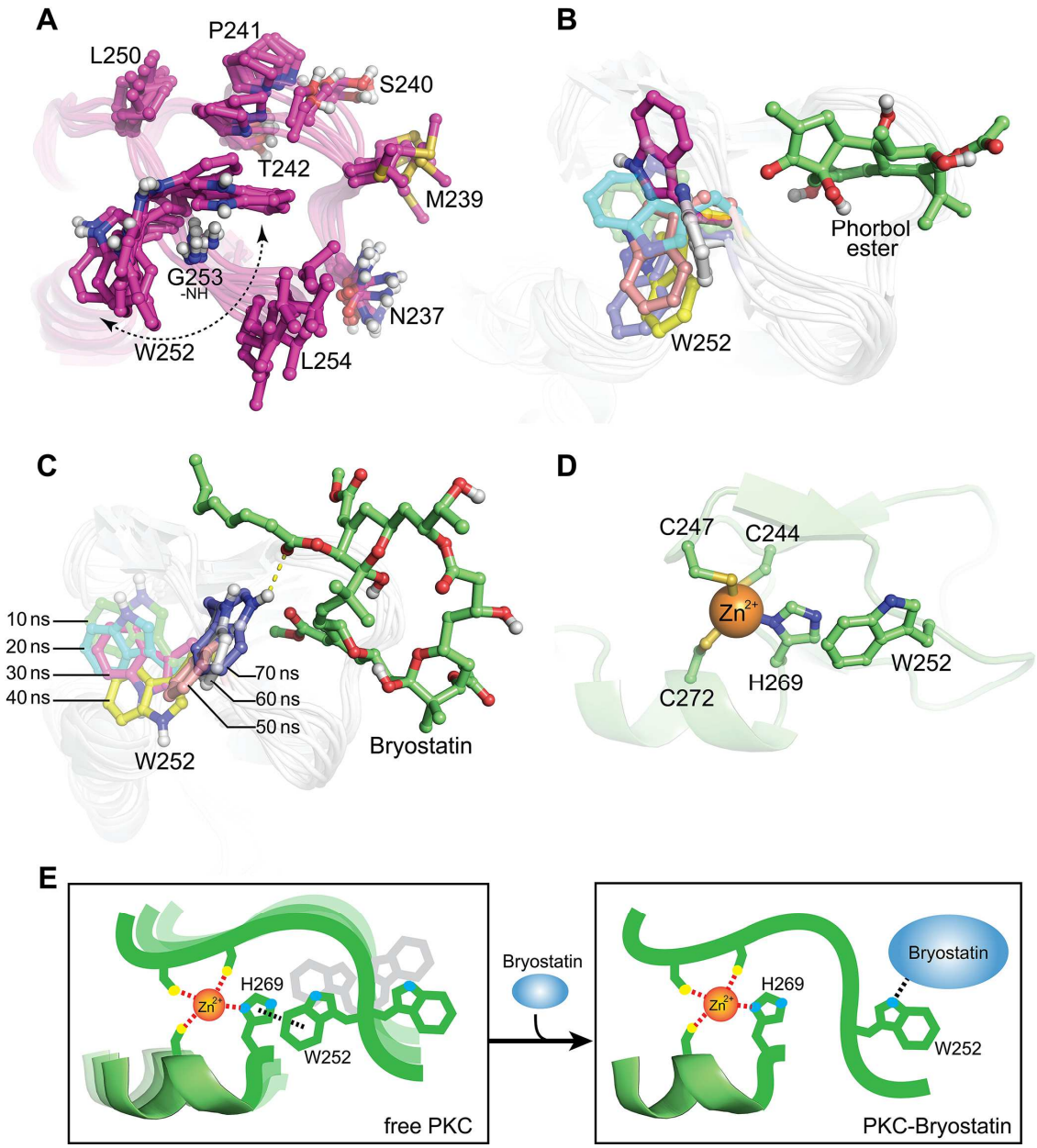

Figure 9. The role of Trp252 in activator binding. Cartoon views of the activator binding site of PKC highlighting the movements of the Trp252 side chain in the free PKC protein (A), PKC-phorbol ester complex (B), and the PKC-bryostatin complex (C) are shown. The vibrational motions on residues of PKC structures are represented by superimposing seven snapshots at different time points during the MD simulations. In the complexes (B, C), 10 ns: light green, 20 ns: cyan, 30 ns: magenta, 40 ns: yellow, 50 ns: pink, 60 ns: light gray, and 70 ns: purple. For (C), the ligand conformation and the H-bond of only the 70-ns structure is represented. (D) Cartoon representation of free PKC structure showing a close proximity (3.7–5.4 Å) between the side chain of Trp252 and the Zn^{2+}-coordinating His269. (E) Dynamic fluctuation dampening model describing how the binding of bryostatin may influence a reduction of the backbone fluctuation of Trp252 and the proximal Zn^{2+}-binding center. In the free protein, interaction between Trp252 and His269 modulates the fluctuation of this area due to the toggling movement of Trp252 side chain. Once

bound with bryostatin, this interaction diminishes and may result in the evident reduction in fluctuation of all involved residues.

At the farthest position away from the activator binding pocket, the Trp252 aromatic ring becomes in close contact and in parallel with the His269 imidazole ring (Figure 9D). Based solely upon this close proximity, it has also been proposed previously that these two side chains may interact with one another via cation-π or π-stacking interactions (75). As mentioned above, His269 also coordinates to a Zn^{2+} ion, along with Cys244, Cys247 and Cys272. Interestingly, Trp252 and these Zn^{2+}-binding residues are the only areas that have spiked backbone fluctuations observed in the free protein and in the phorbol ester complex, yet these fluctuations are quenched when bryostatin is bound (Figure 6C, gradient columns). Hence, although more complex models are possible, the available MD data from the free protein and from the bryostatin complex in this study, along with the previous combined NMR perturbation and relaxation study (84) on the homologous Y123W mutation of PKCα C1B domain, are consistent with the following dynamic fluctuation dampening model. Portions of the loops harboring the Zn^{2+}-binding residues are vibrationally influenced by the toggling movement (in a nanosecond timescale) of the Trp252 aromatic ring, which is mediated by the transient interaction between Trp252 and His269. Once the bryostatin molecule is bound and the Trp252 Nε1 H-bond has been formed, the Trp252-His269 interaction no longer exists, thus resulting in lower fluctuations among the Zn^{2+}-binding residues (Figure 9E). We assume that these conformers may be further stabilized once the PKC-bryostatin complex tethers into the cell membrane lipid bilayer, where His269 becomes in close contact with the acidic phospholipid surface. It is possible that the previous interaction between His269 and Trp252 may not be easily reconstituted at this stage, thereby creating a more pronounced effect than that from the binding to phorbol ester, which does not require Trp252. The confirmation of this latter hypothesis is being investigated in detail in our laboratory by both MD simulation and quantum mechanical studies of the PKC-bryostatin complex in the context of its membrane tethering process.

The role of bryostatin binding in PKC activation is still largely unknown and the structural information of the PKC-bryostatin-membrane still does not yet exist (74,75,85). Previous mutation and molecular dynamics studies indicated that Trp252 may have some importance in the binding of the activators (86,87). Recently, a combined mutagenesis, MD and NMR perturbation and relaxation study (84) also discovered that the homologous Y123W mutation of PKCα C1B domain (that resulted in a profound >100-fold increase in DAG binding affinity) did not alter the dynamics of the protein in the sub-nanosecond timescale, but rather

caused a dramatic change in microsecond-timescale conformational dynamics. This change in lower timescale dynamics generally suggests a “preequilibrium sampling” or “selected fit” behavior, that the ligand selects a high-affinity conformer among others (88). Some variations of the orientation of the Trp252 side chain and its analogues are also observed in multiple homologous C1 domain structures, either positioning toward or away from the activator binding pocket (89,90).

When considering our PKCδ-bryostatin complex structure, there still are several hydrophilic parts of the ligand being exposed to the solvent. This indicates that the binding mechanism might not be the same as the one proposed for the phorbol ester binding by which the ligand simply caps the activator cleft and switches the hydrophobicity of the protein head and making it suitable for the membrane penetration (60). It is possible that the PKCδ C1B-bryostatin may require another binding partner (or partners) to fulfill a complete activation. This hypothesis can be bolstered by the fact that the C1A and C1B domains both contribute to the PKC translocation induced by bryostatin (91,92), and the C1A and the catalytic (C4) domains may be involved in a protection from downregulation of PKCδ induced by bryostatin (75,92,93).

The mechanism by which the bryostatin-bound PKC triggers cellular localization is also unclear. It has been known that, in the case of hydrophobic ligands such as phorbol ester or 12-O-tetradecanoylphorbol-13-acetate (TPA), they tend to translocate PKCs to the cell membrane, while hydrophilic ligands such as bryostatin (at 10-1,000 nM concentration) translocate them to the nuclear membrane (94). Therefore, structural biology studies on the C1B domain and other potentially involved domains of the PKC protein, both in the presence and absence of bryostatin or phospholipid bilayer, are greatly needed. Though the analyses of the conformational activation pathway is more complex than anticipated, our MD data presented here has provided structural insight into the activator binding, as well as one of the possible models leading to a more complete description of the mechanism and to their function.

Mathematical Models for Post-Docking Parameters

Molecular docking using AutoDock 4 resulted in 8 energy parameters, which are 1) Estimated Free Energy of Binding; 2) Inhibition Constant; 3) Intermolecular Energy; 4) Van der Waal+Hydrogen Bond+Desolvation Energy; 5) Electrostatic energy; 6) Total Internal Energy; 7) Torsion Free Energy; and 8) Unbound System’s Energy. Ideally, these parameters should be weighted and optimized based on the target protein-ligand system to match the biological

binding values, and the estimated free energy of binding should be linearly correlated to the actual (experimental) binding between entities. However, this has not been the case due to the imperfection within the docking technology that lacks the optimization process and cannot adaptively input the experimental data to automatically calibrate. Therefore, the correlation between the predicted ligand activity (based on the docking energies) and the actual efficacy of the ligands has been either non-linear or has no correlation whatsoever. Moreover, a closer inspection of the trends from these parameters revealed a non-linear behavior among the docked ligands. To this end, we have applied mathematical models to calibrate the prediction process to match the actual efficacy data. A statistical analysis, 'Partial Least Squares' (PLS), and an adaptive neural network protocol, 'Self-Organizing Maps' (SOMs), were explored. Briefly, 30 conformations resulted from a docked ligand were selectively chosen for the best energy profile (8 parameters) that agrees well with the actual biological data as a whole. The prediction models were built based on two-third of the ligand population ('training set'), while one-third of the ligand population were used to test the predictive capability of the model ('test set').

Initially the models were built based on the dockings of 42 isophthalic acid derivatives onto the activator binding region of PKCδ (PDB code: 1PTR). Twenty-eight compounds were randomly selected and used to build the prediction models and fourteen compounds were assigned to test the model. The PLS parameter analysis indicated that the fourth parameter, van der Waal + Hydrogen Bond + Desolvation Energy, resulted the best final correlation of prediction. Therefore, both PLS and SOMs were built based on this selected parameter as the highest priority for our selection criteria. Linear correlations between the predicted and the actual fold-activation efficacies were plotted for each model (Figure 10). Root mean square errors (RMSE) from both models were calculated, and were found to fall within the acceptable error range (near zero). This indicates that both models can be effective enough to quickly screen the ligands and distinguish the potential candidates from the remainder ligands within the library.

PLS: Traning set RMSE = 0.2405, Test set RMSE = 0.2596 (in fold-activation unit)

SOMs: Traning set RMSE = 0.0011, Test set RMSE = 0.2319 (in fold-activation unit)

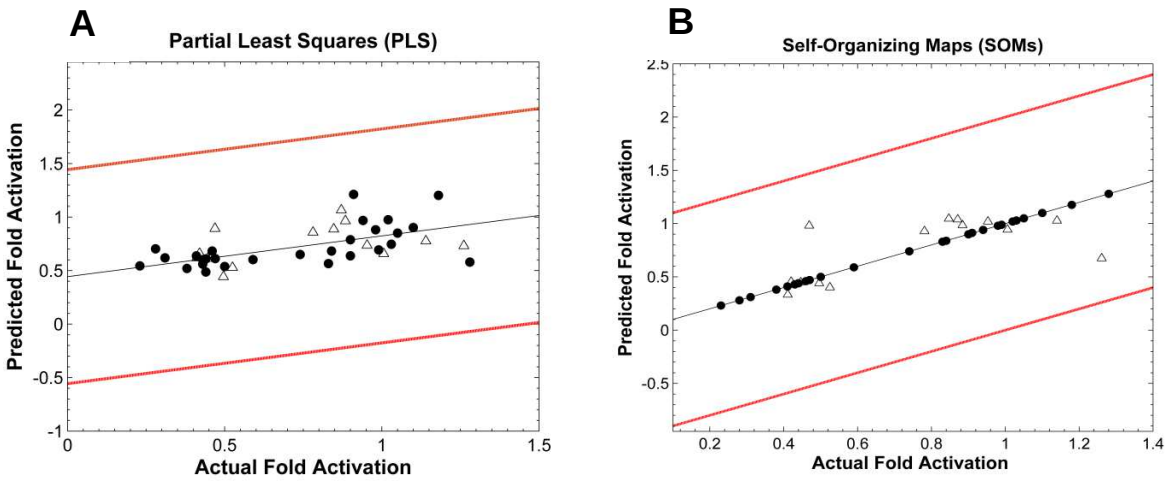

Figure 10. Correlation plots between the actual fold activation values (from PKC activation protein assay) and the predicted fold activations from either PLS model (A) or from SOMs model (B). Black dots are ligands within the training set, while white triangles are ligand within the test set.

Virtual Screening of PKC Modulators

The mathematical modeling results can also be further optimized by using multiple series of compound derivatives to imporve the predictive capability of the models for other unrelated ligand scaffolds. However, these proof-of-concept models were further employed for the ligands virtually screened, using AutoDock Vina, from the NIH Clinical Collection (896 compounds), which were also preliminarily screened based on pharmacophore similarity (down to 180 compounds) before being re-docked onto the active site of PKCδ via AutoDock 4. Parameters from AutoDock 4 were subjected to the the PLS and SOMs analyses to predict the fold activation values of these compound candidates. Top 8 compounds from the PLS model are shown in Table 1, while top 8 compounds from the SOMs model are shown in Table 2. Predicted fold activation of each compounds are also indicated. Compound with the highest predicted fold activation values from the PLS model is rolitetracycline (Figure 11, left) and compound with the highest fold activation predicted from the SOMs model is mecillinam (Figure 11, right). Interestingly, except for pidotimod (Figure 12), none of the top 8 compounds from both model overlapped, suggesting that a confirmative bioassay is necessary for validating the model prediction. Nonetheless, all top 20 compounds from both models will be subjected to the PKC protein assay to increase the chance of discovering novel PKC modulator scaffolds. Of note, rolitetracycline is a tetracycline antibiotic, where a N-Mannich base prodrug can be prepared from tetracycline by condensation with pyrrolidine and formaldehyde to produce rolitetracycline. Mecillinam or amdinocillin is an extended-spectrum

penicillin antibiotic that binds specifically to penicillin binding protein 2 (PBP2), and is only considered to be active against Gram-negative bacteria.

Table 1 Compounds within the US NIH Clinical Collection with the highest fold activation predicted by the Partial Least Squares (PLS) model.

Partial Least Squares (PLS)	
Compound Name	**Predicted Fold Activation**
Rolitetracycline	1.793
Pancuronium dibromide	1.689
Artarit	1.618
Topotican Hydrochloride	1.535
Pidotimod	1.520
Pefloxacin mesylate	1.428
D-NG-Monomethylarginine	1.408
Rufloxacin Hydrochloride	1.400

Table 2 Compounds within the US NIH Clinical Collection with the highest fold activation predicted by the Self-Organizing Maps (SOMs) model.

Self-Organizing Maps (SOMs)	
Compound Name	**Predicted Fold Activation**
Mecillinam	1.177
Ketorolac	1.177
Ozagrel hydrochloride	1.173
Pidotimod	1.171
Amiexanox	1.167
Picrotin	1.152
Loxoprofen	1.152
Flumazenil	1.122

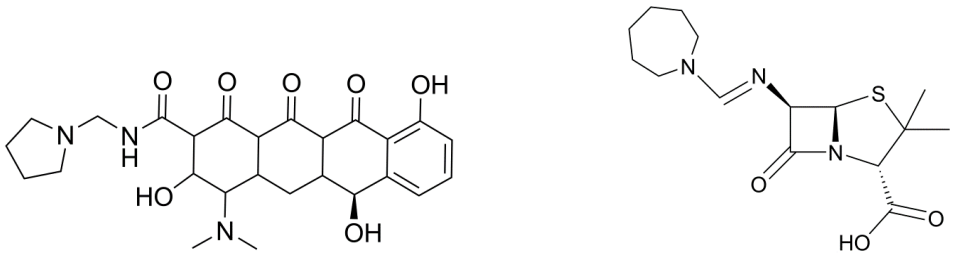

Figure 11. Chemical structures of rolitetracycline (left) and mecillinam (right), the top compounds predicted from the PLS and SOMs models, respectively.

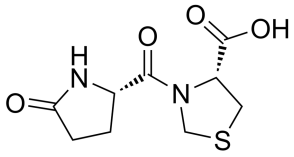

Figure 12. Pidotimod

Molecular Interactions between PKCδ and Candidate Ligands from PLS and SOMs

PLS and SOMs resulted in predicted fold activation values that can be ranked among the candidate ligands within the NIH Clinical Collection. Although all of top ligands (20-40 compounds from each method) are under biochemical investigation in our laboratory at the moment, some ligands were studied for their molecular interactions to the activator binding site of PKCδ via molecular docking.

1. Rolitetracycline (predicted by PLS)

Rolitetracycline (Figure 11) or (2Z,4S,4aS,5aS,6S,12aS)-4-(dimethylamino)-6,10,11, 12a-tetrahydroxy-2-{hydroxy[(pyrrolidin-1-ylmethyl)amino]methylene}-6-methyl-4a,5a,6,12a-tetrahydro tetracene-1,3,12(2H,4H,5H)-trione] is an antibiotic drug within the tetracycline family that has been used against bacterial infection. PLS model suggested that rolitetracycline may have the highest fold activation for PKCδ, with a predicted value of 1.79 folds. When considering the interaction of the docked rolitetracycline in the activator binding site of PKCδ (Figure 13), it was found that hydrogen bonds between the ligand and four of the key amino acids contributed to the binding. These include the backbone carbonyls of Met239, Gly253, Leu254, and a backbone amide of Gly253. Moreover, π-σ interaction between the phenol ring of the ligand and the side-chain aliphatic group of Leu250 is also found as a part of the hydrophobic interaction.

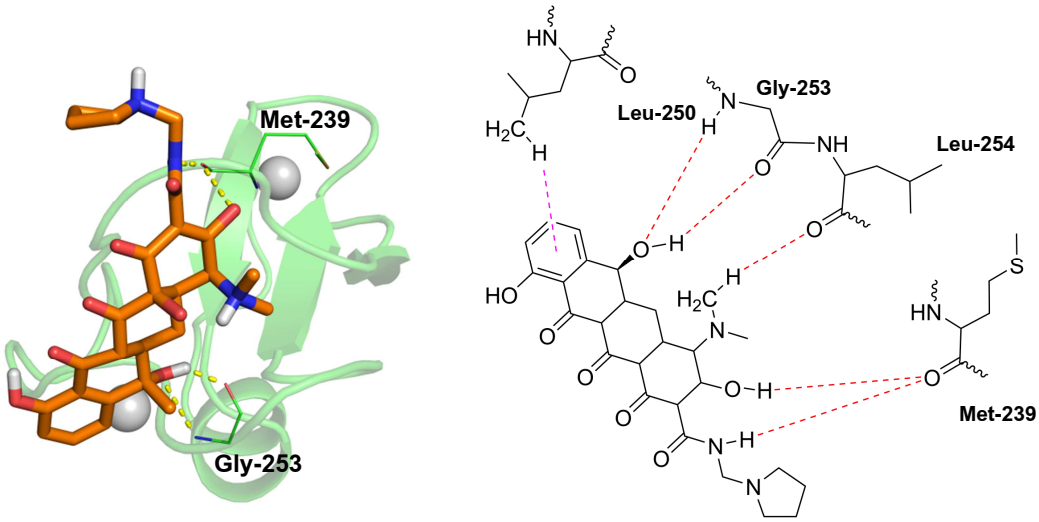

Figure 13. (Left) Best docked conformation of rolitetracycline in the activator binding cleft of PKCδ, highlighting the H-bonds with Gly253 backbone amide and carbonyl, and Met239 backbone carbonyl. (Right) Schematic showing interactions between the ligand and the protein activator binding cleft. Dotted purple line represents the π-σ interaction and dotted red lines represent the hydrogen bonding.

2. Pancuronium dibromide (predicted by PLS)

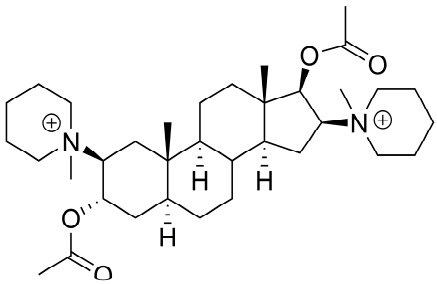

Figure 14. Pancuronium dibromide

Pancuronium dibromide (Figure 14) or [(2S,3S,5S,8R,9S,10S,13S,14S,16S,17R)- 17-acetyloxy-10,13-dimethyl-2,16-bis(1-methyl-3,4,5,6-tetrahydro-2H-pyridin-1-yl)2,3,4,5,6,7,8,9,11,12,14,15,16,17-tetradecahydro-1H-cyclopenta[a]phenanthren-3-yl] acetate with a commercial name as Pavulon® is a typical non-depolarizing curare-mimetic muscle relaxant generally used to relax muscles during surgery or other medical procedures (e.g. for intubation). It acts as a competitive acetylcholine antagonist on neuromuscular junctions against post-synaptic nicotinic acetylcholine receptors. PLS model also predicted that this coumpound should result in ca. 1.69 fold activation against PKCδ. Docking of the pancuronium moiety onto the activator binding cleft revealed an H-bond interaction between the O1 atom of the ligand and the backbone amide of Thr242 (Figure 15).

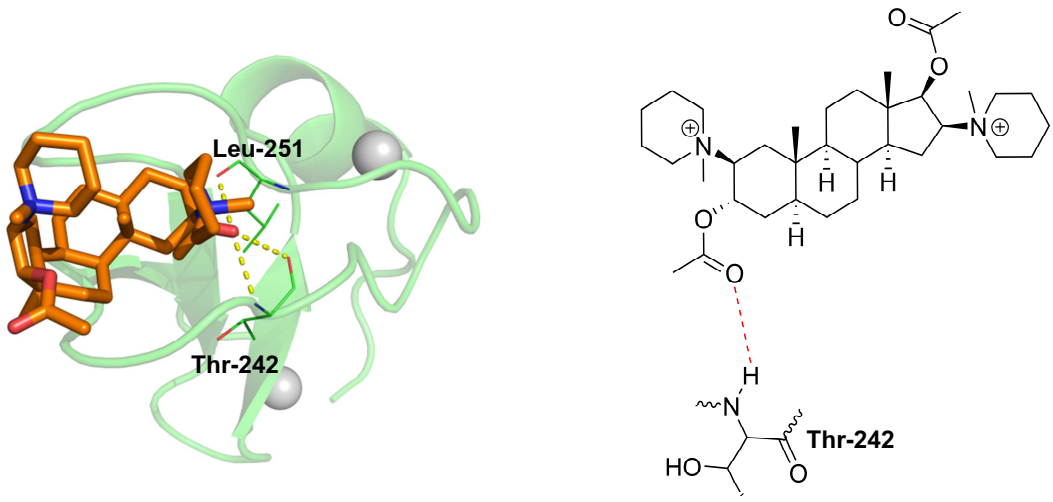

Figure 15. (Left) Best docked conformation of the pancuronium moiety in the activator binding cleft of PKCδ, highlighting the H-bond between the backbone amide of Thr242 and the ester O1 on the ligand. (Right) Schematic showing interactions between the ligand and the protein activator binding cleft. Dotted red line represents the hydrogen bonding.

Although the binding interaction between the pancuronium moiety to the activator binding cleft of PKCδ did not seem to have as many hydrogen bonds as in the case of the rolitetracycline interaction, its hydrophobic nature may also contribute to the binding. Around the wall of the activator binding cleft is lined with multiple hydrophobic residues (e.g. Met239, Pro241, Leu250, Trp252, Leu254) which could confer to the binding of the ligand with certain conformation. This could be the reason for the high predicted activation value reported from the PLS model. Therefore, the pancuronium moiety is another interesteing class of PKCδ activator candidates that is worth exploring further biochemically.

3. Mecillinam (predicted by SOMs)

Mecillinam (Figure 11) or (2S, 5R, 6R)-6-[(E/Z)-(azepan-1-ylmethylene)amino]-3,3 dimethyl-7-oxo-4-thia-1-azabicyclo[3.2.0]heptane-2-carboxylic acid, similarly to rolitetra-cycline, is one of the penicillin family antibiotics. SOMs model predicted its fold activation toward PKCδ to be 1.17, which is significantly lower than the values from the PLS model. This could be the result of an 'overfitting' nature of the SOMs model that generally weighted heavily on the training set, thus resulted in a less accurate values on the test ligands (training set RMSE = 0.0011, test set RMSE = 0.2319, in fold-activation unit from SOMs prediction). Nonetheless, docking study also revealed significant H-bond interactions between the ligand and the activator binding residues, which include H-bonds between the backbone amides of Ser240, Thr242 and the carbonyl oxygen on the ligand. H-bond between the backbone carbonyl of Leu251 and the carboxylic hydrogen is also found. Further biochemical

investigation and confirmation is necessary (as currently being undertaken in our laboratory) to validate and compare these results.

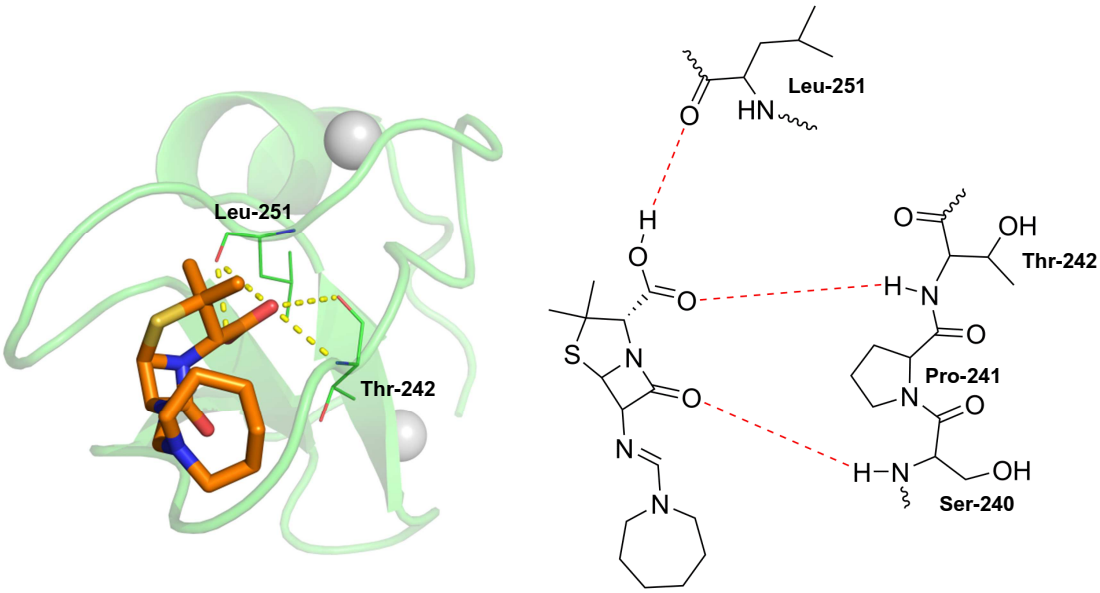

Figure 16. (Left) Best docked conformation of mecillinam in the activator binding cleft of PKCδ, highlighting the H-bonds between the backbone amides of Ser240, Thr242 and the carbonyl oxygen on the ligand. H-bond between the backbone carbonyl of Leu251 and the carboxylic hydrogen is also shown. (Right) Schematic showing interactions between the ligand and the protein activator binding cleft. Dotted red lines represent the hydrogen bonding.

4. Ketorolac (predicted by SOMs)

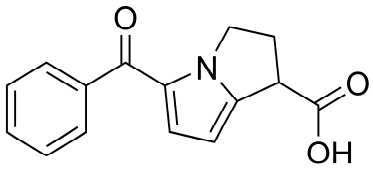

Figure 17. Ketorolac

Another interesting candidate predicted by the SOMs model (with a predicted fold activation of 1.17) is Ketorolac or (±)-5-benzoyl-2,3-dihydro-<brF />1H-pyrrolizine-1-carboxylic acid, 2-amino-2-(hydroxymethyl)-1,3-propanediol. Ketorolac or ketorolac tromethamine is a non-steroidal anti-inflammatory drug (NSAID) in the family of heterocyclic acetic acid derivatives, used as an analgesic. Docking of this coumpound into the the activator binding cleft of PKCδ (Figure 18) revealed H-bonds between the backbone carbonyls of Thr242, Leu251, Gln257 and the carboxylic hydrogen of the ligand. H-bond between the backbone amide of Thr252 and the the carboxylic oxygen is also found to contribute to the binding.

Moreover, a π-σ interaction is found between the phenyl group of ketorolac and the aliphatic chain of Leu254 as its hydrophobic interaction.

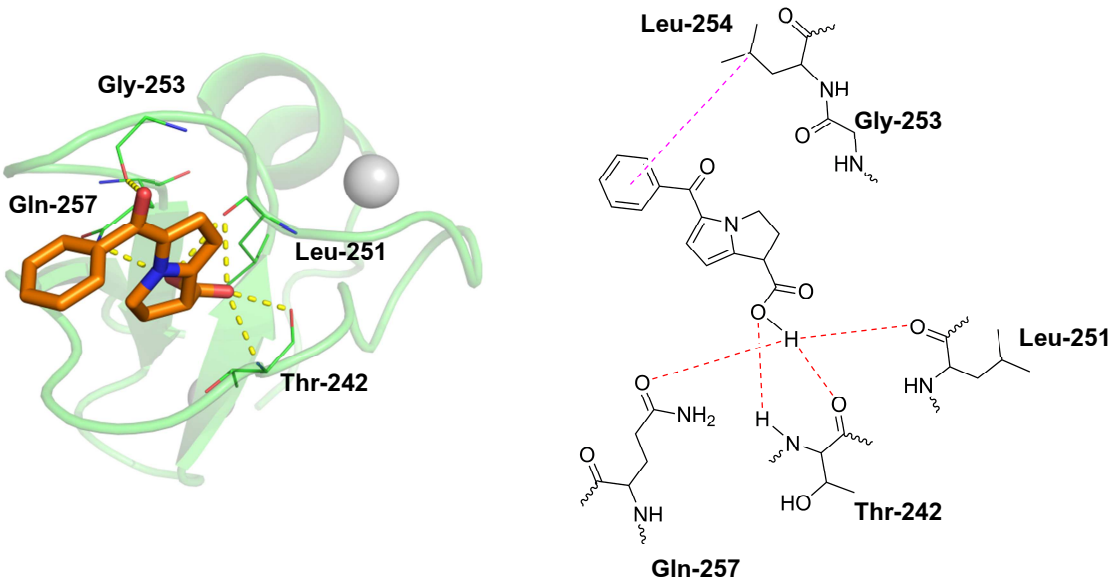

Figure 18. (Left) Best docked conformation of ketorolac in the activator binding cleft of PKCδ, highlighting the H-bonds between the backbone carbonyls of Thr242, Leu251, Gln257 and the carboxylic hydrogen of the ligand. H-bond between the backbone amide of Thr252 and the the carboxylic oxygen is also shown. A π-σ interaction is found between the phenyl group of ketorolac and the aliphatic chain of Leu254. (Right) Schematic showing interactions between the ligand and the protein activator binding cleft. Dotted red lines represent the hydrogen bondings and the dotted purple line represent the π-σ interaction.

Interactions between the Activator Binding Cleft of PKCδ and Candidate Ligands from the Virtual Screening

Virtual screening via AutoDock Vina was empoyed to select from 896 ligands within the US NIH Clinical Collection. This resulted in binding affinity (kcal/mol) that can be ranked, picked and further investigated either by a detailed molecular docking, molecular dynamics (MD) simulations, or biochemical assay conformation. The top 8 candidate compounds that were predicted as potent ligands for the activator binding cleft of PKCδ are shown in table 3.

From the confirmative re-docking, we have selected a total of 20 compounds to advance to the biochemical testing. However, in this report, we will show the potential interactions at the activator binding site for only the top 2 (with the highest ranking binding affinity), which are telmisartan and irinotecan.

Table 3 Compounds within the US NIH Clinical Collection with the best binding affinity (lowest energy) predicted by the AutoDock Vina virtual screening.

Virtual Screening	
Compound Name	**Binding Affinity (kcal/mol)**
Telmisartan	-8.6
Irinotecan	-8.2
Zafirlukast	-8.0
Montelukast	-7.9
Pirenperone	-7.7
MK-693	-7.6
Cyproheptadine hydrochloride	-7.5
Imatinib	-7.5

1. Telmisartan (predicted by AutoDock Vina virtual screening)

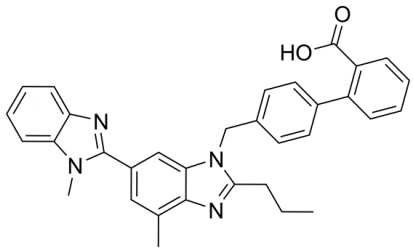

Figure 19. Telmisartan

Telmisartan (Figure 19) or 2-(4-{[4-Methyl-6-(1-methyl-1H-1,3-benzodiazol-2-yl)-2-propyl-1H-1,3-benzodiazol-1-yl]methyl}phenyl)benzoic acid is an angiotensin II receptor antagonist (angiotensin receptor blocker, ARB) that has high affinity for the angiotensin II receptor type 1 (AT1), and generally used in the management of hypertension. Virtual screening via AutoDock Vina predicted that this drug has the highest binding affinity toward the activator binding site of PKCδ, with an energy of binding of -8.6 kcal/mol. The confirmative re-docking (Figure 20) showed that the tight binding is mediated by an H-bond interaction between the side-chain hydroxyl of Ser240 and one of the nitrogens on the benzodiazol group of the ligand. Some other unreported hydrophobic interaction may also play an important role in this binding as the nature of the ligand and the lining of the activator binding cleft are generally hydrophobic.

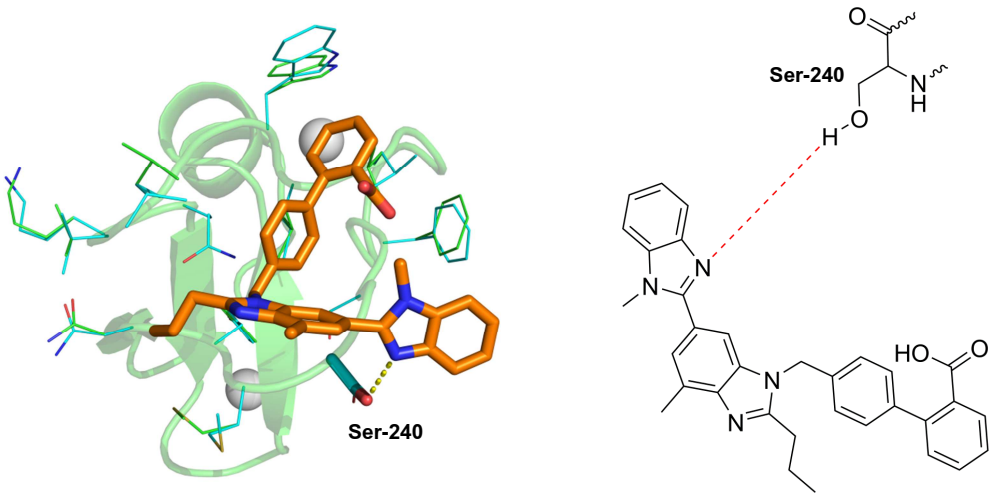

Figure 20. (Left) Best docked conformation of telmisartan in the activator binding cleft of PKCδ, highlighting the H-bonds between the side-chain hydroxyl of Ser240 and one of the nitrogens on the benzodiazol group of the ligand. (Right) Schematic showing interactions between the ligand and the protein activator binding cleft. Dotted red lines represent the hydrogen bonding.

2. Irinotecan (predicted by AutoDock Vina virtual screening)

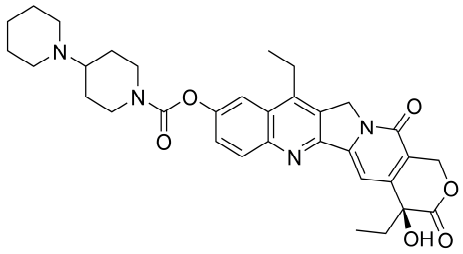

Figure 21. Irinotecan

Irinotecan or (S)-4,11-diethyl-3,4,12,14-tetrahydro-4-hydroxy- 3,14-dioxo1H-pyrano[3',4': 6,7]-indolizino[1,2-b]quinolin- 9-yl-[1,4'bipiperidine]-1'-carboxylate with a commecial name of Camptosar (Pfizer) Campto (Yakult Honsha) และ Irinotel (Atco Labs) is a drug used for the treatment of cancer. Irinotecan prevents DNA from unwinding by inhibition of topoisomerase 1, which eventually leads to inhibition of both DNA replication and transcription.

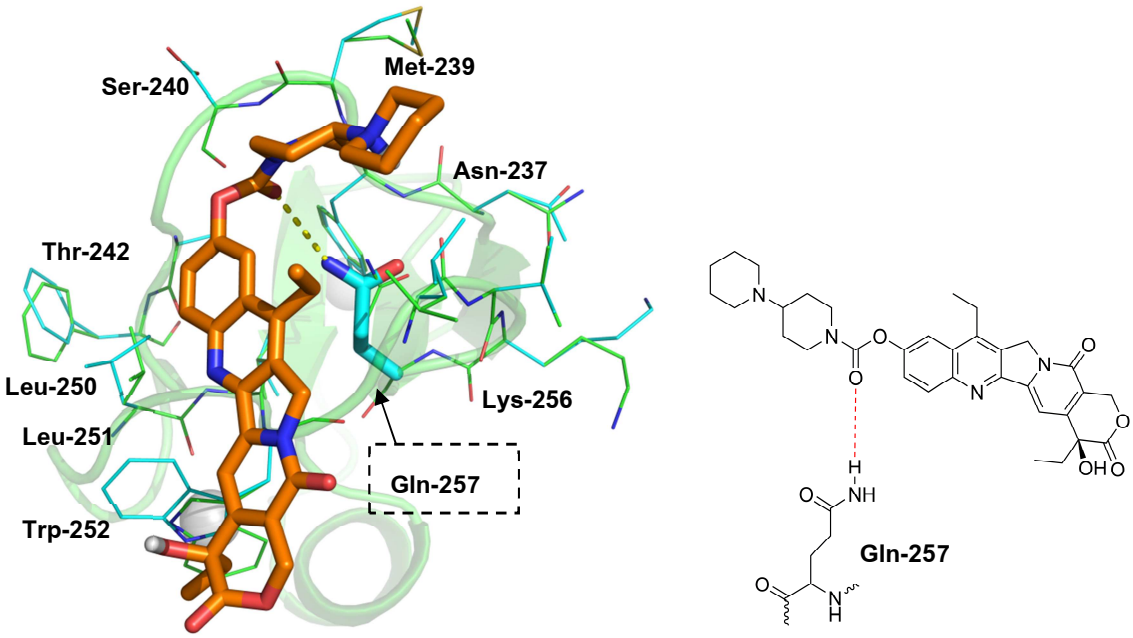

Figure 22. (Left) Best docked conformation of irinotecan in the activator binding cleft of PKCδ, highlighting the H-bonds between the side-chain amino group of Gln257 and the ester oxygen of the ligand. (Right) Schematic showing interactions between the ligand and the protein activator binding cleft. Dotted red lines represent the hydrogen bonding.

Virtual screening of this drug indicated a good binding affinity of -8.2 kcal/mol. When re-docked into the activator binding cleft of PKCδ, a hydrogen bonding between the side-chain amino group of Gln257 and the ester oxygen of the ligand can be identified. The ligand also have several hydrophobic regions that could potentially contribute to the tight binding to the activator binding site. Confirmative MD simulations and biochemical testing for actual affinity and efficacy of these compounds are also being conducted in our laboratory.

Cell-based Assay for Evaluating Anti-Latency Effects

Aside from the direct in vitro biochemical assay for evaluating modulatory effects of compounds on PKC (as seen in the building of PLS and SOMs model for 'actual fold activation'), a cell-based assay was also developed for evaluating the anti-latency effect. J-lat clone 10.6 cells (that were derived from Jurkat cell lines), harboring a full-length HIV-1 genome (with no *env* nor *nef* gene) and a green fluorescent protein (GFP) gene downstream from the *rev* gene (Figure 23), were used in this step. When these cells were incubated with PKC modulators (e.g. bryostatin or phorbol esters) or other anti-latency agents (e.g. histone deacetylase inhibitor), the HIV-1 proviral gene and the GFP gene can be expressed, yielding a production of incomplete set of HIV-1 proteins (for safety reason) and GFP. GFP expression can thus be monitored by flow cytometry and correlated to the anti-latency efficacy or dosage

of the modulator compounds (Figure 23). Furthermore, HIV-1 protein production can also be confirmed by a measurement of HIV-1 p24 Gag antigen in the supernatant of the cells.

At this stage, we have demonstrated that this assay can be performed in our laboratory. Specifically, we have employed this cell-based anti-latency assay to exemplify a monitoring of the efficacy of bryostatin, which is one of the most potent PKC modulators. Flow cytometric histograms from the cell-based assays evaluating anti-latency effects (Figure 24) showed that J-lat clone 10.6 cells harboring a green fluorescent protein (GFP) within the HIV-1 proviral genome, incubated with 1 μM of PKC activator bryostatin or with 1 μM of histone deacetylase inhibitor suberanilohydroxamic acid (SAHA), yielded 55.2% and 44.7% of GFP+ cell population, respectively. This level of expression is satisfactorily high and can also be further improved by using a combination of those two classes of anti-latency drugs. Nonetheless, this assay will be used in our future confirmation of those candidate ligands identified by PLS, SOMs or virtual screening models. The results from this cell-base assayed will also be compared with the direct in vitro biochemical assay for evaluating modulatory effects of compounds on PKC.

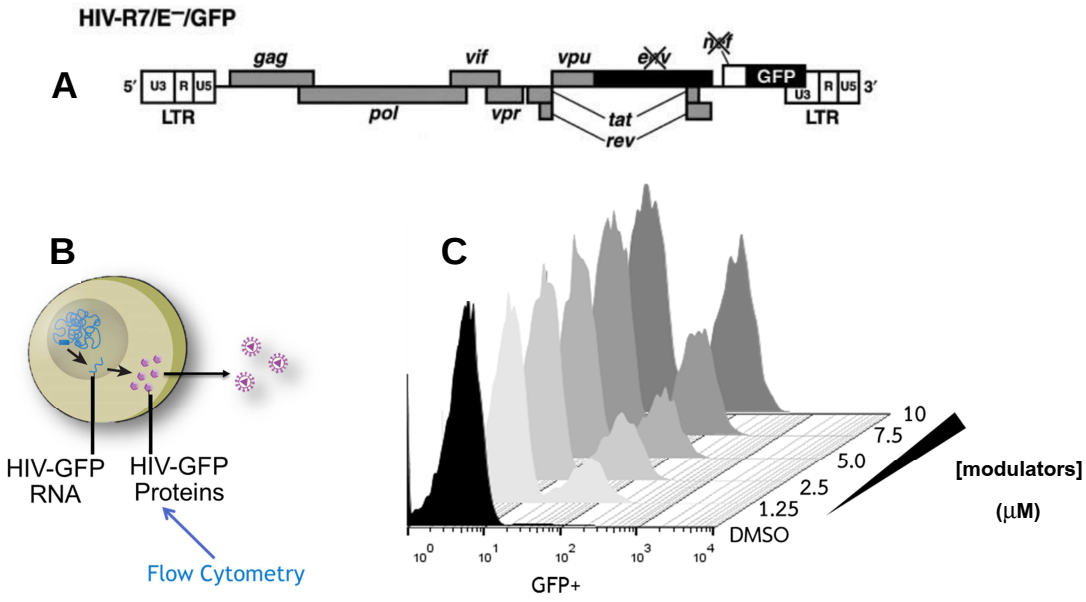

Figure 23. Cell-based Assays for Evaluating Anti-Latency Effects. J-lat clone 10.6 cells (that were derived from Jurkat cell lines) harbors a full-length HIV-1 genome (with no *env* nor *nef* gene) and a green fluorescent protein (GFP) gene downstream from the *rev* gene (A). When reactivated with PKC modulator compounds, transcription and translation of both proviral DNA and GFP occur, resulted in a detectable expression of GFP protein (B) that can be monitored by flow cytometry in a dose dependent manner to acquire half-maximal response/effectiveness concentration (EC_{50})(C).

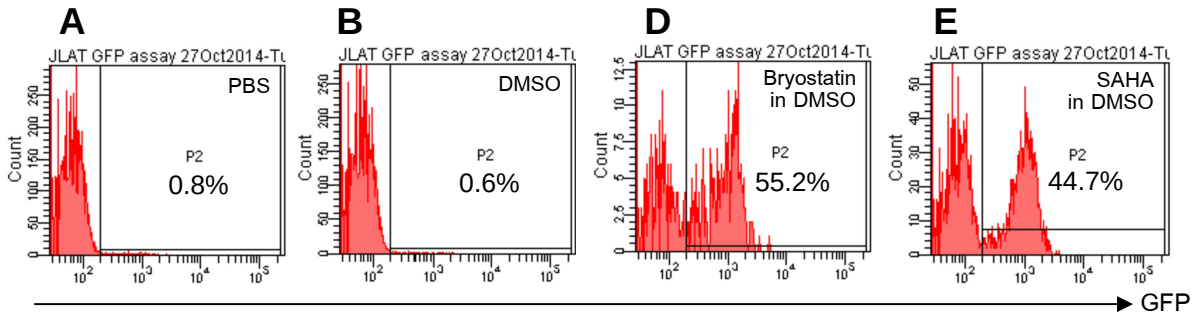

Figure 24. Flow cytometric histograms from the cell-based assays for evaluating anti-latency effects of selected compounds. J-lat clone 10.6 cells (10^5) harboring a green fluorescent protein (GFP) within the HIV-1 proviral genome (*env*-,*nef*-) were incubated with either PBS (A), DMSO (B) as negative controls, or with 1 µM of PKC activator bryostatin (C) in DMSO or with 1 µM of histone deacetylase inhibitor suberanilohydroxamic acid (SAHA)(D). Flow cytometric analysis was performed at 24 hours after the addition of the compounds on 4%- paraformaldehyde-fixed cells. Indicated percentages of GFP+ cell population (P2) were gated on live cells.

Conclusions

Protein kinase C is a family of serine/threonine kinase isozymes that has been widely recognized as targets for anticancer therapy, Alzheimer's disease, HIV/AIDS eradication and others, due to their important role in the signal transduction of various pathways. However, despite many efforts focused on describing accurate structural detail of the C1 domain of PKC, as well as the binding to its activators, that information has been lacking, thus hampering the development of potential therapies. The study presented herein demonstrates that MD simulation can be employed to gain insight into the differences in the binding of phorbol esters, the tumor-promoting activator of PKC, compared with bryostatin, a more potent activator that does not act as a tumor promoter. Hydrogen bonding data have provided the details of binding mechanisms observed in both ligands, and revealed a potential binding conformation of bryostatin that has never been described before. These H-bond networks, when combined with the deviations and fluctuations of the protein backbone, have led us to propose a model that describes the role of the highly conserved and highly homologous Trp252 in the ligand binding, as well as its potential involvement in the dynamic fluctuation modulation of the nearby Zn^{2+}-binding center. We have found that a toggling movement of the Trp252 side chain may cause the high backbone fluctuation observed in the Zn^{2+}-binding residues, which is mediated by the transient interaction between Trp252 and His269. When bryostatin is bound to the protein and the side chain of Trp252 samples toward a conformation that forms a hydrogen bond with the ligand, the transient interactions abrogate, and the dynamic fluctuations are dampened. This finding brings new insight into the design of new activators that favor the latter conformation.

The comparison of the dynamics properties observed in the activator-bound complexes also sheds light on how to explain the potency differences identified for both activators. Although many future experimental efforts are still needed in order to confirm our model and fully understand the binding mode of bryostatin, along with the mechanism by which it employs to activate PKC, this study sets the stage for investigating the structural detail of this important class of regulatory proteins. This information is inevitably required for the design of new analogues for future treatment of many related diseases.

Aside from the fundamental investigation on structural biology and dynamics of the protein function, we have also applied this knowledge onto the drug discovery aspect. Molecular docking and virtual screening were employed to search for new potential candidates

with novel scaffolds. However, initial molecular docking energy parameters did not correlate well with the direct in vitro biochemical assay for evaluating modulatory effects of compounds on PKC. Therefore, we have used advanced mathematical and statistical models, namely Partial Least Squares (PLS) and Self-Organizing Maps (SOMs) to perform a post-docking analysis. The resulted RMSE values from the test set and the training set of ligands were satisfactorily improved. This suggests that our post-docking analysis is reliable and rather necessary to accurately predict the fold activation of the PKC modulators.

Virtual screening using AutoDock Vina was also employed to help selecting the potential candidate ligands within the US NIH Clinical Collection. Combined with the results from PLS and SOMs, confirmative re-docking of the virtually screened candidates were inspected for their interactions with the activator binding cleft of PKCδ. Several hydrogen bonds and hydrophobic interactions were found to contribute to the predicted tight binding. The structural knowledge gained from the docking can also guide future chemical modifications of the compounds to further improve their efficacies. These candidates will also be further confirmed with the in vitro PKC protein assay, as well as tested in the modeled J-lat clone 10.6 cells that will help evaluating the anti-latency effect. The proven methods will unquestionably help advancing the science of drug development both domestically and internationally. If successful, the outcome from this ongoing study can also become a new alternative for treating HIV/AIDS.

References

1. Centers for Disease, C. (1982) A cluster of Kaposi's sarcoma and Pneumocystis carinii pneumonia among homosexual male residents of Los Angeles and Orange Counties, California. *MMWR Morb Mortal Wkly Rep* **31**, 305-307
2. สำนักนโยบายสำนักยุทธศาสตร์กระทรวงสาธารณสุข. (2554) กรอบยุทธศาสตร์งานสร้างเสริมสุขภาพและป้องกันโรคระดับชาติ ปี 2554-2558
3. Bodiwala, H. S., Sabde, S., Gupta, P., Mukherjee, R., Kumar, R., Garg, P., Bhutani, K. K., Mitra, D., and Singh, I. P. (2011) Design and synthesis of caffeoyl-anilides as portmanteau inhibitors of HIV-1 integrase and CCR5. *Bioorg Med Chem* **19**, 1256-1263
4. Flexner, C. (2007) HIV drug development: the next 25 years. *Nat Rev Drug Discov* **6**, 959-966
5. Siliciano, J. D., Kajdas, J., Finzi, D., Quinn, T. C., Chadwick, K., and Margolick, J. B. (2003) Long-term follow-up studies confirm the stability of the latent reservoir for HIV-1 in resting CD4+ T cells. *Nat Med* **9**, 727-728
6. Deeks, S. G. (2012) HIV: Shock and kill. *Nature* **487**, 439-440
7. Richman, D. D., Margolis, D. M., Delaney, M., Greene, W. C., Hazuda, D., and Pomerantz, R. J. (2009) The challenge of finding a cure for HIV infection. *Science* **323**, 1304-1307
8. Richman, D. D. (2011) Introduction: challenges to finding a cure for HIV infection. *Curr Opin HIV AIDS* **6**, 1-3
9. (2010) AIDS Epidemic Update 2010. UNAIDS: Geneva, Switzerland.
10. Greene, W. C., Debyser, Z., Ikeda, Y., Freed, E. O., Stephens, E., Yonemoto, W., Buckheit, R. W., Este, J. A., and Cihlar, T. (2008) Novel targets for HIV therapy. *Antiviral Res* **80**, 251-265
11. Brooks, D. G., Hamer, D. H., Arlen, P. A., Gao, L., Bristol, G., Kitchen, C. M., Berger, E. A., and Zack, J. A. (2003) Molecular characterization, reactivation, and depletion of latent HIV. in *Immunity*, United States. pp 413-423
12. Brooks, D. G., Kitchen, S. G., Kitchen, C. M., Scripture-Adams, D. D., and Zack, J. A. (2001) Generation of HIV latency during thymopoiesis. in *Nat Med*, United States. pp 459-464
13. Trono, D., Van Lint, C., Rouzioux, C., Verdin, E., Barré-Sinoussi, F., Chun, T. W., and Chomont, N. (2010) HIV persistence and the prospect of long-term drug-free remissions for HIV-infected individuals. *Science* **329**, 174-180
14. Blankson, J. N., Persaud, D., and Siliciano, R. F. (2002) The challenge of viral reservoirs in HIV-1 infection. *Annu Rev Med* **53**, 557-593
15. Archin, N. M., Liberty, A. L., Kashuba, A. D., Choudhary, S. K., Kuruc, J. D., Crooks, A. M., Parker, D. C., Anderson, E. M., Kearney, M. F., Strain, M. C., Richman, D. D., Hudgens, M. G., Bosch, R. J., Coffin, J. M., Eron, J. J., Hazuda, D. J., and Margolis, D. M. (2012) Administration of vorinostat disrupts HIV-1 latency in patients on antiretroviral therapy. *Nature* **487**, 482-485
16. Siliciano, J. D., Lai, J., Callender, M., Pitt, E., Zhang, H., Margolick, J. B., Gallant, J. E., Cofrancesco, J., Jr., Moore, R. D., Gange, S. J., and Siliciano, R. F. (2007) Stability of the latent reservoir for HIV-1 in patients receiving valproic acid. in *J Infect Dis*, United States. pp 833-836
17. Margolis, D. M. (2011) Histone deacetylase inhibitors and HIV latency. *Curr Opin HIV AIDS* **6**, 25-29

18. Marsden, M. D., Kovochich, M., Suree, N., Shimizu, S., Mehta, R., Cortado, R., Bristol, G., An, D. S., and Zack, J. A. (2012) HIV latency in the humanized BLT mouse. *J Virol* **86**, 339-347
19. Pace, M. J., Agosto, L., Graf, E. H., and O'Doherty, U. (2011) HIV reservoirs and latency models. *Virology* **411**, 344-354
20. Williams, S. A., Chen, L. F., Kwon, H., Fenard, D., Bisgrove, D., Verdin, E., and Greene, W. C. (2004) Prostratin antagonizes HIV latency by activating NF-kappaB. in *J Biol Chem*, United States. pp 42008-42017
21. Williams, S. A., and Greene, W. C. (2007) Regulation of HIV-1 latency by T-cell activation. *Cytokine* **39**, 63-74
22. Yang, H. C., Xing, S., Shan, L., O'Connell, K., Dinoso, J., Shen, A., Zhou, Y., Shrum, C. K., Han, Y., Liu, J. O., Zhang, H., Margolick, J. B., and Siliciano, R. F. (2009) Small-molecule screening using a human primary cell model of HIV latency identifies compounds that reverse latency without cellular activation. *J Clin Invest* **119**, 3473-3486
23. Mehellou, Y., and De Clercq, E. (2010) Twenty-six years of anti-HIV drug discovery: where do we stand and where do we go? *J Med Chem* **53**, 521-538
24. Carr, A. (2003) Toxicity of antiretroviral therapy and implications for drug development. *Nat Rev Drug Discov* **2**, 624-634
25. Martinez-Picado, J., DePasquale, M. P., Kartsonis, N., Hanna, G. J., Wong, J., Finzi, D., Rosenberg, E., Gunthard, H. F., Sutton, L., Savara, A., Petropoulos, C. J., Hellmann, N., Walker, B. D., Richman, D. D., Siliciano, R., and D'Aquila, R. T. (2000) Antiretroviral resistance during successful therapy of HIV type 1 infection. *Proc Natl Acad Sci U S A* **97**, 10948-10953
26. Little, S. J., Holte, S., Routy, J. P., Daar, E. S., Markowitz, M., Collier, A. C., Koup, R. A., Mellors, J. W., Connick, E., Conway, B., Kilby, M., Wang, L., Whitcomb, J. M., Hellmann, N. S., and Richman, D. D. (2002) Antiretroviral-drug resistance among patients recently infected with HIV. *N Engl J Med* **347**, 385-394
27. (2007) The DAD Study Group. Class of antiretroviral drugs and the risk of myocardial infarction. *N. Engl. J. Med.* **356**, 1723-1735
28. De Clercq, E. (2007) The design of drugs for HIV and HCV. *Nat Rev Drug Discov* **6**, 1001-1018
29. Pommier, Y., Johnson, A., and Marchand, C. (2005) Integrase inhibitors to treat HIV/AIDS. *Nat Rev Drug Discov* **4**, 236 - 248
30. Wightman, F., Ellenberg, P., Churchill, M., and Lewin, S. R. (2012) HDAC inhibitors in HIV. *Immunol Cell Biol* **90**, 47-54
31. Lewin, S. R., Murray, J. M., Solomon, A., Wightman, F., Cameron, P. U., and Purcell, D. J. (2008) Virologic determinants of success after structured treatment interruptions of antiretrovirals in acute HIV-1 infection. *J Acquir Immune Defic Syndr* **47**, 140-147
32. Kulkosky, J., and Pomerantz, R. J. (2002) Approaching eradication of highly active antiretroviral therapy-persistent human immunodeficiency virus type 1 reservoirs with immune activation therapy. in *Clin Infect Dis*, United States. pp 1520-1526

33. Emery, S., Capra, W. B., Cooper, D. A., Mitsuyasu, R. T., Kovacs, J. A., Vig, P., Smolskis, M., Saravolatz, L. D., Lane, H. C., Fyfe, G. A., and Curtin, P. T. (2000) Pooled analysis of 3 randomized, controlled trials of interleukin-2 therapy in adult human immunodeficiency virus type 1 disease. in *J Infect Dis*, United States. pp 428-434

34. Chun, T. W., Engel, D., Mizell, S. B., Hallahan, C. W., Fischette, M., Park, S., Davey, R. T., Jr., Dybul, M., Kovacs, J. A., Metcalf, J. A., Mican, J. M., Berrey, M. M., Corey, L., Lane, H. C., and Fauci, A. S. (1999) Effect of interleukin-2 on the pool of latently infected, resting CD4+ T cells in HIV-1-infected patients receiving highly active anti-retroviral therapy. *Nat Med* **5**, 651-655

35. Prins, J. M., Jurriaans, S., van Praag, R. M., Blaak, H., van Rij, R., Schellekens, P. T., ten Berge, I. J., Yong, S. L., Fox, C. H., Roos, M. T., de Wolf, F., Goudsmit, J., Schuitemaker, H., and Lange, J. M. (1999) Immuno-activation with anti-CD3 and recombinant human IL-2 in HIV-1-infected patients on potent antiretroviral therapy. *AIDS* **13**, 2405-2410

36. van Praag, R. M., Prins, J. M., Roos, M. T., Schellekens, P. T., Ten Berge, I. J., Yong, S. L., Schuitemaker, H., Eerenberg, A. J., Jurriaans, S., de Wolf, F., Fox, C. H., Goudsmit, J., Miedema, F., and Lange, J. M. (2001) OKT3 and IL-2 treatment for purging of the latent HIV-1 reservoir in vivo results in selective long-lasting CD4+ T cell depletion. *J Clin Immunol* **21**, 218-226

37. Fraser, C., Ferguson, N. M., Ghani, A. C., Prins, J. M., Lange, J. M., Goudsmit, J., Anderson, R. M., and de Wolf, F. (2000) Reduction of the HIV-1-infected T-cell reservoir by immune activation treatment is dose-dependent and restricted by the potency of antiretroviral drugs. *AIDS* **14**, 659-669

38. Kulkosky, J., Sullivan, J., Xu, Y., Souder, E., Hamer, D. H., and Pomerantz, R. J. (2004) Expression of latent HAART-persistent HIV type 1 induced by novel cellular activating agents. *AIDS Res Hum Retroviruses* **20**, 497-505

39. Mehla, R., Bivalkar-Mehla, S., Zhang, R., Handy, I., Albrecht, H., Giri, S., Nagarkatti, P., Nagarkatti, M., and Chauhan, A. (2010) Bryostatin modulates latent HIV-1 infection via PKC and AMPK signaling but inhibits acute infection in a receptor independent manner. *PLoS One* **5**, e11160

40. Nabel, G., and Baltimore, D. (1987) An inducible transcription factor activates expression of human immunodeficiency virus in T cells. *Nature* **326**, 711-713

41. Kagnoff, M. F., and Roebuck, K. A. (1999) Human immunodeficiency virus type 1 (HIV-1) infection and expression in intestinal epithelial cells: role of protein kinase A and C pathways in HIV-1 transcription. *J Infect Dis* **179**, S444-447

42. Roebuck, K. A., Gu, D. S., and Kagnoff, M. F. (1996) Activating protein-1 cooperates with phorbol ester activation signals to increase HIV-1 expression. *AIDS* **10**, 819-826

43. Yang, X., Chen, Y., and Gabuzda, D. (1999) ERK MAP kinase links cytokine signals to activation of latent HIV-1 infection by stimulating a cooperative interaction of AP-1 and NF-kappaB. *J Biol Chem* **274**, 27981-27988

44. Han, X. M., Laras, A., Rounseville, M. P., Kumar, A., and Shank, P. R. (1992) Human immunodeficiency virus type 1 Tat-mediated trans activation correlates with the phosphorylation state of a cellular TAR RNA stem-binding factor. *J Virol* **66**, 4065-4072

45. Jakobovits, A., Rosenthal, A., and Capon, D. J. (1990) Trans-activation of HIV-1 LTR-directed gene expression by tat requires protein kinase C. *EMBO J* **9**, 1165-1170

46. McKernan, L. N., Momjian, D., and Kulkosky, J. (2012) Protein Kinase C: One Pathway towards the Eradication of Latent HIV-1 Reservoirs. *Adv Virol* **2012**, 805347

47. Spitaler, M., and Cantrell, D. A. (2004) Protein kinase C and beyond. in *Nat Immunol*, United States. pp 785-790

48. Steinberg, S. F. (2008) Structural basis of protein kinase C isoform function. in *Physiol Rev*, United States. pp 1341-1378

49. Hamer, D. H., Bocklandt, S., McHugh, L., Chun, T. W., Blumberg, P. M., Sigano, D. M., and Marquez, V. E. (2003) Rational design of drugs that induce human immunodeficiency virus replication. *J Virol* **77**, 10227-10236

50. Marquez, V. E., Nacro, K., Benzaria, S., Lee, J., Sharma, R., Teng, K., Milne, G. W., Bienfait, B., Wang, S., Lewin, N. E., and Blumberg, P. M. (1999) The transition from a pharmacophore-guided approach to a receptor-guided approach in the design of potent protein kinase C ligands. *Pharmacol Ther* **82**, 251-261

51. Garcia-Bermejo, M. L., Leskow, F. C., Fujii, T., Wang, Q., Blumberg, P. M., Ohba, M., Kuroki, T., Han, K. C., Lee, J., Marquez, V. E., and Kazanietz, M. G. (2002) Diacylglycerol (DAG)-lactones, a new class of protein kinase C (PKC) agonists, induce apoptosis in LNCaP prostate cancer cells by selective activation of PKCalpha. *J Biol Chem* **277**, 645-655

52. Ashburn, T. T., and Thor, K. B. (2004) Drug repositioning: identifying and developing new uses for existing drugs. *Nat Rev Drug Discov* **3**, 673-683

53. Lombardino, J. G., and Lowe, J. A., 3rd. (2004) The role of the medicinal chemist in drug discovery--then and now. *Nat Rev Drug Discov* **3**, 853-862

54. Kitchen, D. B., Decornez, H., Furr, J. R., and Bajorath, J. (2004) Docking and scoring in virtual screening for drug discovery: methods and applications. *Nat Rev Drug Discov* **3**, 935-949

55. Schneider, G., and Fechner, U. (2005) Computer-based de novo design of drug-like molecules. *Nat Rev Drug Discov* **4**, 649-663

56. Bajorath, J. (2002) Integration of virtual and high-throughput screening. *Nat. Rev. Drug Discov.* **1**, 882-894

57. Langer, T., and Hoffmann, R. D. (2001) Virtual screening: an effective tool for lead structure discovery. *Curr. Pharm. Design* **7**, 509-527

58. Walters, W. P., Stahl, M. T., and Murcko, M. A. (1998) Virtual screening [mdash] an overview. *Drug Discov. Today* **3**, 160-178

59. Gohlke, H., and Klebe, G. (2002) Approaches to the description and prediction of the binding affinity of small-molecule ligands to macromolecular receptors. *Angew. Chem. Int. Ed.* **41**, 2644-2676

60. Zhang, G., Kazanietz, M. G., Blumberg, P. M., and Hurley, J. H. (1995) Crystal structure of the cys2 activator-binding domain of protein kinase C delta in complex with phorbol ester. *Cell* **81**, 917-924

61. Trott, O., and Olson, A. J. (2010) AutoDock Vina: improving the speed and accuracy of docking with a new scoring function, efficient optimization, and multithreading. *J. Comp. Chem.* **31**, 455-461

62. Hornak, V., Abel, R., Okur, A., Strockbine, B., Roitberg, A., and Simmerling, C. (2006) Comparison of multiple Amber force fields and development of improved protein backbone parameters. *Proteins* **65**, 712-725

63. Lange, O. F., van der Spoel, D., and de Groot, B. L. (2010) Scrutinizing molecular mechanics force fields on the submicrosecond timescale with NMR data. *Biophys. J* **99**, 647-655

64. Jorgensen, W. L., Chandrasekhar, J., Madura, J. D., Impey, R. W., and Klein, M. L. (1983) Comparison of simple potential functions for simulating liquid water. *J. Chem. Phys.* **79**, 926-935

65. Berendsen, H. J. C., Postma, J. P. M., van Gunsteren, W. F., DiNola, A., and Haak, J. R. (1984) Molecular dynamics with coupling to an external bath. *J. Chem. Phys.* **81**, 3684-3690

66. Hess, B., Bekker, H., Berendsen, H. J. C., and Fraaije, J. G. E. M. (1997) LINCS: A Linear Constraint Solver for Molecular Simulations. *J. Comp. Chem.* **18**, 1463-1472

67. Darden, T., York, D., and Pedersen, L. (1993) Particle mesh Ewald: An N·log(N) method for Ewald sums in large systems. *J. Chem. Phys.* **98**, 10089-10092

68. Essmann, U., Perera, L., Berkowitz, M. L., Darden, T., Lee, H., and Pedersen, L. G. (1995) A smooth particle mesh Ewald method. *J. Chem. Phys.* **103**, 8577-8593

69. Humphrey, W., Dalke, A., and Schulten, K. (1996) VMD: visual molecular dynamics. *Journal of Molecular Graphics* **14**, 33-38

70. Gallastegui, E., Marshall, B., Vidal, D., Sanchez-Duffhues, G., Collado, J. A., Alvarez-Fernandez, C., Luque, N., Terme, J. M., Gatell, J. M., Sanchez-Palomino, S., Munoz, E., Mestres, J., Verdin, E., and Jordan, A. (2012) Combination of biological screening in a cellular model of viral latency with virtual screening identifies novel compounds that reactivate HIV-1. *J Virol* **86**, 3795-3808

71. Perola, E., Xu, K., Kollmeyer, T. M., Kaufmann, S. H., Prendergast, F. G., and Pang, Y. P. (2000) Successful virtual screening of a chemical database for farnesyltransferase inhibitor leads. *J Med Chem* **43**, 401-408

72. Irwin, J. J., and Shoichet, B. K. (2005) ZINC--a free database of commercially available compounds for virtual screening. *J Chem Inf Model* **45**, 177-182

73. Irwin, J. J., Raushel, F. M., and Shoichet, B. K. (2005) Virtual screening against metalloenzymes for inhibitors and substrates. *Biochemistry* **44**, 12316-12328

74. Loy, B. A., Lesser, A. B., Staveness, D., Billingsley, K. L., Cegelski, L., and Wender, P. A. (2015) Toward a biorelevant structure of protein kinase C bound modulators: design, synthesis, and evaluation of labeled bryostatin analogues for analysis with rotational echo double resonance NMR spectroscopy. *J Am Chem Soc* **137**, 3678-3685

75. Das, J., and Rahman, G. M. (2014) C1 domains: structure and ligand-binding properties. *Chem Rev* **114**, 12108-12131

76. Das, J., Addona, G. H., Sandberg, W. S., Husain, S. S., Stehle, T., and Miller, K. W. (2004) Identification of a general anesthetic binding site in the diacylglycerol-binding domain of protein kinase Cdelta. in *J Biol Chem*, United States. pp 37964-37972

77. Keck, G. E., Poudel, Y. B., Welch, D. S., Kraft, M. B., Truong, A. P., Stephens, J. C., Kedei, N., Lewin, N. E., and Blumberg, P. M. (2009) Substitution on the A-ring confers to bryopyran analogues the unique biological activity characteristic of bryostatins and distinct from that of the phorbol esters. *Org. Lett.*, United States. pp 593-596

78. Keck, G. E., Li, W., Kraft, M. B., Kedei, N., Lewin, N. E., and Blumberg, P. M. (2009) The bryostatin 1 A-ring acetate is not the critical determinant for antagonism of phorbol ester-induced biological responses. *Org. Lett.* **11**, 2277-2280

79. DeChristopher, B. A., Loy, B. A., Marsden, M. D., Schrier, A. J., Zack, J. A., and Wender, P. A. (2012) Designed, synthetically accessible bryostatin analogues potently induce activation of latent HIV reservoirs in vitro. in *Nat Chem*, England. pp 705-710

80. Wender, P. A., Hinkle, K. W., Koehler, M. F., and Lippa, B. (1999) The rational design of potential chemotherapeutic agents: synthesis of bryostatin analogues. in *Med Res Rev*, 1999 John Wiley & Sons, Inc., United States. pp 388-407

81. Wender, P. A., and Baryza, J. L. (2005) Identification of a tunable site in bryostatin analogs: C20 Bryologs through late stage diversification. *Org Lett* **7**, 1177-1180

82. Wender, P. A., and Hinkle, K. W. (2000) Synthesis and biological evaluation of a new class of bryostatin analogues: the role of the C20 substituent in protein kinase C binding. *Tetrahedron Lett.* **41**, 6725-6729

83. Wender, P. A., Cribbs, C. M., Koehler, K. F., Sharkey, N. A., Herald, C. L., Kamano, Y., Pettit, G. R., and Blumberg, P. M. (1988) Modeling of the bryostatins to the phorbol ester pharmacophore on protein kinase C. *Proc Natl Acad Sci U S A* **85**, 7197-7201

84. Stewart, M. D., Morgan, B., Massi, F., & Igumenova, T. I. (2011). Probing the determinants of diacylglycerol binding affinity in the C1B domain of protein kinase C alpha. *J Mol Biol*, **408**, 949-970

85. Irie, K., Yanagita, R. C., and Nakagawa, Y. (2012) Challenges to the development of bryostatin-type anticancer drugs based on the activation mechanism of protein kinase Cdelta. *Med Res Rev* **32**, 518-535

86. Kazanietz, M. G., Wang, S., Milne, G. W., Lewin, N. E., Liu, H. L., and Blumberg, P. M. (1995) Residues in the second cysteine-rich region of protein kinase C delta relevant to phorbol ester binding as revealed by site-directed mutagenesis. *J Biol Chem* **270**, 21852-21859

87. Nacro, K., Sigano, D. M., Yan, S., Nicklaus, M. C., Pearce, L. L., Lewin, N. E., Garfield, S. H., Blumberg, P. M., and Marquez, V. E. (2001) An optimized protein kinase C activating diacylglycerol combining high binding affinity (Ki) with reduced lipophilicity (log P). *J Med Chem* **44**, 1892-1904

88. James, L. C., and Tawfik, D. S. (2003) Conformational diversity and protein evolution--a 60-year-old hypothesis revisited. *Trends Biochem Sci* **28**, 361-368

89. Shen, N., Guryev, O., and Rizo, J. (2005) Intramolecular occlusion of the diacylglycerol-binding site in the C1 domain of munc13-1. *Biochemistry* **44**, 1089-1096

90. Lin, W. Q., Jiang, J. H., Shen, Q., Wu, H. L., Shen, G. L., and Yu, R. Q. (2005) Piecewise hypersphere modeling by particle swarm optimization in QSAR studies of bioactivities of chemical compounds. *J Chem Inf Model* **45**, 535-541

91. Bogi, K., Lorenzo, P. S., Szallasi, Z., Acs, P., Wagner, G. S., and Blumberg, P. M. (1998) Differential selectivity of ligands for the C1a and C1b phorbol ester binding domains of protein kinase Cdelta: possible correlation with tumor-promoting activity. *Cancer Res* **58**, 1423-1428

92. Lorenzo, P. S., Bogi, K., Hughes, K. M., Beheshti, M., Bhattacharyya, D., Garfield, S. H., Pettit, G. R., and Blumberg, P. M. (1999) Differential roles of the tandem C1 domains of protein kinase C delta in the biphasic down-regulation induced by bryostatin 1. *Cancer Res* **59**, 6137-6144

93. Lorenzo, P. S., Bögi, K., Acs, P., Pettit, G. R., and Blumberg, P. M. (1997) The catalytic domain of protein kinase Cdelta confers protection from down-regulation induced by bryostatin 1. *J Biol Chem* **272**, 33338-33343

94. Wang, Q. J., Fang, T. W., Fenick, D., Garfield, S., Bienfait, B., Marquez, V. E., and Blumberg, P. M. (2000) The lipophilicity of phorbol esters as a critical factor in determining the pattern of translocation of protein kinase C delta fused to green fluorescent protein. *J Biol Chem* **275**, 12136-12146

Appendix

Output

Manuscript Submitted to Journal of Biomolecular Structure & Dynamics (on May 5, 2015)

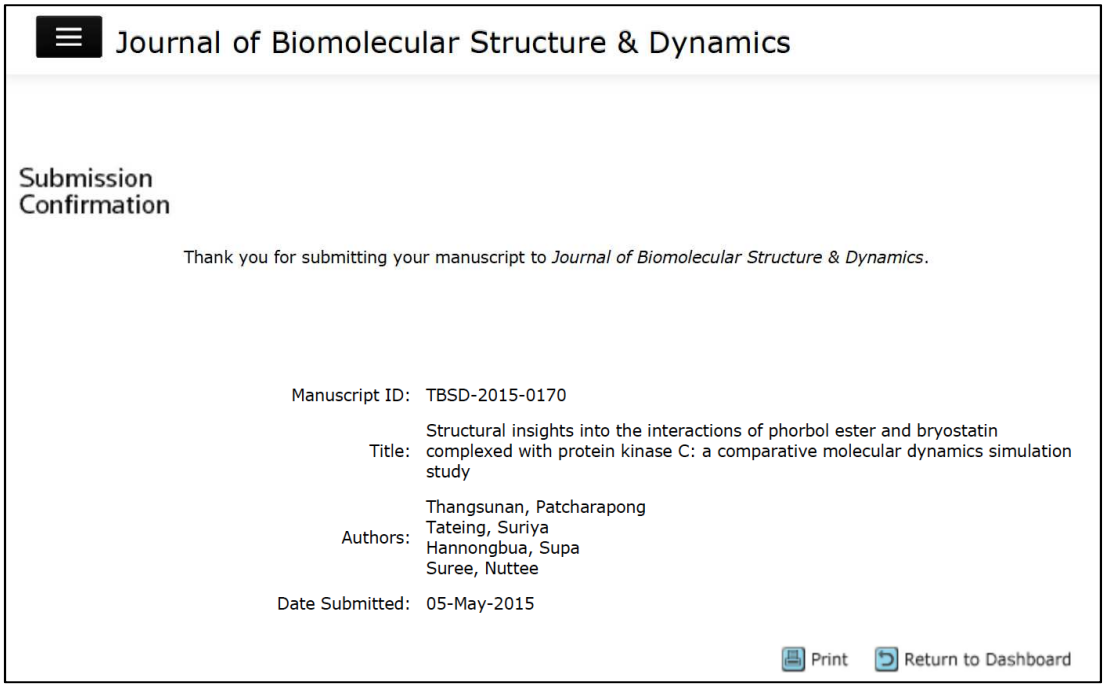

Journal of Biomolecular Structure & Dynamics

Submission Confirmation

Thank you for submitting your manuscript to *Journal of Biomolecular Structure & Dynamics*.

Manuscript ID:	TBSD-2015-0170
Title:	Structural insights into the interactions of phorbol ester and bryostatin complexed with protein kinase C: a comparative molecular dynamics simulation study
Authors:	Thangsunan, Patcharapong Tateing, Suriya Hannongbua, Supa Suree, Nuttee
Date Submitted:	05-May-2015

Print Return to Dashboard

Submission Status on May 18, 2015 : Under Review

Submitted Manuscripts

Manuscript ID	Manuscript Title	Date Created	Date Submitted	Status
TBSD-2015-0170	Structural insights into the interactions of phorbol ester and bryostatin complexed with protein kinase C: a comparative molecular dynamics simulation study [View Submission] (Cover Letter)	05-May-2015	05-May-2015	ADM: Sarma, Ramaswamy Under Review

top

Submitted Manuscript

Structural insights into the interactions of phorbol ester and bryostatin complexed with protein kinase C: a comparative molecular dynamics simulation study

Patcharapong Thangsunan[a,b], Suriya Tateing[a,b], Supa Hannongbua[c], and Nuttee Suree[b,*]

[a]Graduate Program in Biotechnology, The Graduate School, Chiang Mai University; [b]Division of Biochemistry and Biochemical Technology, Department of Chemistry, Faculty of Science, Chiang Mai University, 239 Huay Kaew Rd, Suthep, Muang, Chiang Mai 50200, Thailand; [c]Department of Chemistry, Faculty of Science, Kasetsart University, Bangkok 10900, Thailand

*Corresponding author. Email: nuttee.suree@cmu.ac.th

Abstract

Protein kinase C (PKC) isozymes are important regulatory enzymes that have been implicated in many diseases, including cancer, Alzheimer's disease, and in the eradication of HIV/AIDS. Given its potential clinical ramifications, PKC modulators, e.g. phorbol esters and bryostatin, are also of great interest in the drug development. However, structural detail on the binding between PKC and its modulators, especially bryostatin—the highly potent and non-tumor promoting activator for PKCs, is still lacking. Here we report the first comparative molecular dynamics (MD) study aimed at gaining structural insight into the mechanisms by which the PKC delta cys2 activator domain is used in its binding to phorbol ester and bryostatin-1. Potential energy analysis revealed that PKC-bryostatin complex is energetically more favorable than either free PKC protein or the PKC-phorbol ester complex. As anticipated in the phorbol ester binding, hydrogen bonds are formed through the backbone atoms of Thr242, Leu251 and Gly253 of PKC. However, the opposition of H-bond formation between Thr242 and Gly253 may cause the phorbol ester complex to become less stable. For bryostatin, hydrogen bonds are formed between its C30 carbomethoxy substituent and the Gly253 backbone carbonyl. Additionally, the indole Nε1 of the highly homologous Trp252 also forms an H-bond to the C20 ester group on bryostatin. Backbone fluctuations also suggest that this latter H-bond formation may abrogate the transient interaction between Trp252 and His269, thus dampening the fluctuations observed on the nearby Zn^{2+}-coordinating residues. This new dynamic fluctuation dampening model can potentially benefit future design of new PKC modulators.

Keywords: protein kinase C; molecular dynamics simulation; phorbol ester; bryostatin; binding mechanism

Introduction

The protein kinase C (PKC) family of serine/threonine kinase enzymes is involved in one of the major signal transduction pathways (Nishizuka, 1995; Takai, Kishimoto, Kikkawa, Mori, & Nishizuka, 1979). PKCs have also been implicated in a wide variety of cellular growth controls, which could become therapeutic target candidates for many diseases, such as cancer, cardiovascular diseases, diabetes, stroke, lung and kidney complications, Alzheimer's disease, Parkinson's disease, autoimmune conditions, and HIV/AIDS eradication (Battaini & Mochly-Rosen, 2007; Das & Rahman, 2014; DeChristopher et al., 2012; Irie, Nakagawa, & Ohigashi, 2005; Irie, Yanagita, & Nakagawa, 2012; Loy et al., 2015; Mochly-Rosen, Das, & Grimes, 2012; Nishizuka, 1984). Diacylglycerol (DAG) has been shown as the endogenous regulator for most of PKC isozymes (Blumberg, 1991; Nishizuka, 1992), though PKCs can also be activated by plant-derived phorbol esters (Nishizuka, 1984) or marine bryozoa-isolated bryostatin compounds (de Vries, Herald, Pettit, & Blumberg, 1988). PKCs are categorized into subclasses based on their domain composition and respective co-factor/activator sensitivity (Hurley & Grobler, 1997; Newton, 1995). The classical or conventional PKC isoforms (α, βI, βII, γ) are responsive to DAG, phospholipids and Ca^{2+}, while novel isoforms (δ, ε, η, θ) are responsive to only DAG and phospholipids. In contrast, atypical PKCs (ζ, λ/ι) are unresponsive to these activators (Akimoto et al., 1994; Kazanietz et al., 1993; Ono et al., 1989).

The structure of all PKCs comprises a pseudosubstrate (PS) domain, activator-responsive C1 domain, Ca^{2+}-sensitive C2 domain (which is absent in atypical PKCs), and a C-terminal catalytic kinase region that consists of the C3 (ATP-binding) and C4 (catalytic) domains (Figure 1A). In an inactive state, the PS domain occupies the substrate binding site in the kinase region. Once their regulatory domains are engaged with the appropriate combination of signals such as DAG, phospholipids, Ca^{2+}, phorbol esters or bryostatin derivatives, the C1 and C2 domains translocate to the membrane, causing the PS domain to be released from the active site of the kinase region, allowing the access of substrate and the subsequent phosphorylation (Hurley & Grobler, 1997; Newton, 1995). The structural information of how the signals trigger the kinase activation has been of wide interest for many research groups. Molecular structures have been solved for the activator-responsive C1 domains from PKCα (Hommel, Zurini, & Luyten, 1994), PKCγ (R. X. Xu, Pawelczyk, Xia, & Brown, 1997), and PKCδ (Zhang, Kazanietz, Blumberg, & Hurley, 1995), either alone or bound with phorbol ester. The Ca^{2+}-sensitive C2 domain of PKCs α, βII, δ, η, and ε has been described (Guerrero-Valero et al., 2009; Littler et al., 2006; Ochoa et al., 2001; Pappa, Murray-Rust, Dekker, Parker, & McDonald, 1998; Sutton & Sprang, 1998; Verdaguer, Corbalan-Garcia, Ochoa, Fita, & Gomez-Fernandez, 1999). The catalytic domains of PKCs βII, θ, and ι have also been reported (Grodsky et al., 2006; Messerschmidt et al., 2005; Takimura et al., 2010; Z. B. Xu et al., 2004). More recently, a crystal structure of full-length PKC βII was determined at 4.0 Å resolution, through which an allosteric activation mechanism, involving an interaction between the catalytic domain and the C1B domain, has been described (Leonard, Rozycki, Saidi, Hummer, & Hurley, 2011).

C1 domains in both conventional and novel PKCs are of particular interest mainly because they are responsive to the potent activators such as phorbol esters or bryostatin. High affinity binding to DAG, phorbol ester, or to bryostatin triggers a protein translocation to the membranes (Wang et al., 2000). Accurate structural understanding of how these activators bind to the protein, induce a translocation to the membrane and mediate the subsequent activation can help guide the design of improved PKC modulators. Structurally, each of the tandem cysteine-rich domains, C1A and C1B, contains only approximately 50 amino acids and binds to two Zn^{2+} ions. Crystal structures of the C1B domain in PKCδ

(PDB ID: 1PTR)(Zhang et al., 1995) revealed that the entire domain surface is generally hydrophilic. In the case of phorbol ester binding, however, the phorbol ester molecule caps the activator binding cleft, thereby creating a large continuous hydrophobic surface that is suitable for the membrane penetration and anchoring of the protein domain (Zhang et al., 1995). According to the crystal structure (Zhang et al., 1995), the binding is mediated by hydrogen bond formations involving the backbone carbonyls and amides of Thr242, Leu251 and Gly253 on the activator binding cleft of the protein, and the C3, C4 and C20 of phorbol ester. Moreover, no major conformational change was observed upon the binding.

However, the binding and activation mechanism of bryostatin, a highly potent and non-tumor promoting class of compounds, is less clear. To date, traditional X-ray crystallography and NMR spectroscopy have been utilized to determine the structures of protein-ligand complexes, but rather focused on the DAG or phorbol ester binding either with or without a membrane-like component (Hommel et al., 1994; Loy et al., 2015; Rahman & Das, 2015). Structure determination might have also been hampered by the fact that the activator binding may not occur in a normal buffered water environment, unless associated with the lipid bilayer (P. A. Wender, Irie, & Miller, 1995). The information of the C1-ligand interaction, which would be most beneficial to the design of preclinical drug candidates, and its correlation to prior biochemical (Dries, Gallegos, & Newton, 2007; Zhang et al., 1995) and mutagenesis (Kazanietz et al., 1995) studies, have been limited to only the case of DAG binding. Molecular dynamics studies have also been employed to gain insights into the exchanging conformers and the significance of particular residues in the DAG binding (Stewart, Morgan, Massi, & Igumenova, 2011), or on how the PKC C1 domains interact differently with various lipids (Li, Ziemba, Falke, & Voth, 2014). Hence, structural insights into the binding of bryostatin to the PKC C1 domain, in comparison to phorbol ester, is still lacking and greatly needed for developing a more complete understanding of the protein complex structure and dynamics.

Furthermore, the role of some potentially important residues on the C1 activator binding cleft has not yet been fully elucidated. For example, to date, the structural role and the exact side chain orientation of Trp252 are still unknown (Das & Rahman, 2014). Sequence alignment of the C1domains in the PKC proteins showed that it is highly conserved (Das & Rahman, 2014). Mutation from Trp to Gly at this position also resulted in a reduced binding affinity to [^{3}H] phorbol 12,13-dibutyrate (PDBu), worsening its K_d from 0.8 nM (wild-type) to 25 nM (Kazanietz et al., 1995). Moreover, previous molecular dynamic simulations (Nacro et al., 2001) also suggested that the aromatic ring of Trp252 in PKCδ may contribute to the binding of a potent diacylglycerol analogue via a favorable van der Waals (VDW) interaction with the branched *sn*-1 acyl group of the ligand, suggesting a sensible importance of this residue in the binding of activator. Intriguingly, in the PKCγ C1A, PKCδ C1A, PKCθ C1A, and PKCθ C1B domains, the aromatic rings of this tryptophan is oriented toward the binding pocket, while the orientation of the homologous tryptophan in β2-chimaerin is away from the pocket (Das & Rahman, 2014). In Munc13.1, the homologous Trp588 occludes the diacylglycerol binding site and thus partially inhibiting the binding activity (Shen, Guryev, & Rizo, 2005). Therefore, the conformation of this residue or the involvement of other residues within the activator binding cleft, as well as their biological relevance, are still generally unknown.

To this end, our efforts have focused on using MD simulation, which is suited for structural investigation of these particular protein-ligand systems. Reported herein are the results of comparative MD simulations of the complexes between phorbol ester or bryostatin and PKCδ cys2 activator-binding (C1B) domain. Potential energy, backbone dynamics and fluctuations have been compared between free PKC and the PKC-activator complexes. Hydrogen bonding networks and bond formation profiles within the phorbol ester or the

bryostatin complexes were analyzed. The combination of the protein dynamics, fluctuations and H-bond formation, have also led us to propose a model, for the first time, describing the roles of Trp252 in the binding to bryostatin, and in dampening the fluctuations observed in the proximal Zn^{2+}-binding center. The information presented here can help advance ongoing development of the drug design targeting protein kinase C.

Materials and methods

Molecular docking

Preparation of protein structure

The co-crystal structure of the cys2 activator binding domain of PKCδ with phorbol 13-acetate (PRB) (PDB ID: 1PTR)(Zhang et al., 1995) was retrieved from the RCSB Protein Data Bank. The PRB structure at the binding site of the complex was isolated from the protein structure using Accelrys Discovery Studio 4.0. The protein structure was then converted from 'pdb' into a 'pdbqt' format using AutoDockTools (ADT). Resolution of the three-dimensional grid box (x, y and z) was set as 30×30×30 with a grid spacing of 0.375 Å. The grid center, which is based on the original ligand, was set to 10.903 Å, 26.391 Å and 24.495 Å for x, y and z dimensions, respectively.

Preparation of ligand structures

The PKC activator, bryostatin 1, structure was sketched as a 'mol2' file using Accelrys Discover Studio 4.0. Phorbol 13-acetate (PRB) structure that was initially separated from the starting complex, and the bryostatin 1 structure were then assigned for atom type and energy minimized using Tripos force field in SYBYL 7.3 suite. The ligands were then converted from 'mol2' into a 'pdbqt' format using ADT.

Molecular docking for preparing ligand coordination in complexes

All docking calculations were performed using AutoDock Vina (Trott & Olson, 2010) on a Linux platform. From output files, the best docking conformation for each complex was chosen based on position and non-bonding interactions of the ester group of each ligand with the five key amino acid residues (Ser240, Pro241, Thr242, Leu251 and Gly253) at the binding site on the PKCδ structure. Partial atomic charges were optimized for their geometry and were calculated for ESP charges with Gaussian 09W software (G09) through the ground state using Restricted Hartree-Fock method with a split valence basis set 6−31G(d).

MD simulations

MD simulations for all experiments were performed using GROMACS 4.6.3 package, incorporated with Amber99SB force field (Hornak et al., 2006; Lange, van der Spoel, & de Groot, 2010). Three simulating systems, consisting of free PKCδ, PKCδ-phorbol 13-acetate and PKCδ-bryostatin 1, were neutralized by adding counter ions (sodium and chloride ions) and solvated by a cubic box with diameter of 2.0 Å with TIP3P water model (Jorgensen, Chandrasekhar, Madura, Impey, & Klein, 1983). Energy minimization was completed for three systems through steepest descent method for 5,000 steps, followed by 80-ps of MD simulations in all ensembles using the Berendsen coupling method (Berendsen, Postma, van Gunsteren, DiNola, & Haak, 1984) with a pressure (*P*) of 1 bar, at a reference temperature (*T*) of 300 K. The LINCS algorithm (Hess, Bekker, Berendsen, & Fraaije, 1997) was

performed to keep all the bonds containing rigid hydrogen atoms. The long range electrostatic interactions were investigated by using the particle-mesh Ewald (PME) algorithm (Darden, York, & Pedersen, 1993; Essmann et al., 1995) with a 2-fs time step. The MD production run for all of simulating system was set as 80 ns of constant-pressure and was carried out at 300 K. The atomic coordinates of the simulated structures were saved every 2 ps for the data analysis.

Data analysis

The data from all experiments were collected and analyzed by GROMACS analysis tools. GROMACS utilities such as g_energy (potential, kinetic, and total energy), g_rms (RMSD), g_rmsf (RMSF) and g_hbond (number of hydrogen bond), g_dist (hydrogen bond distance) were employed at various points in the process of performing molecular dynamics simulations. Trajectories and structures were visualized using Visual Molecular Dynamics (VMD) (Humphrey, Dalke, & Schulten, 1996), Accelrys Discovery Studio Visualizer 4.0 (Accelrys Software Inc.) and PyMol v.1.3 (Schrödinger, LLC.). GraphPad Prism 5 software was used for generating all the plots.

Results and discussion

Structure analysis of PKCδ protein

In the present study, comparative MD simulations were performed on the free cys2 activator binding domain of PKCδ (henceforth 'PKCδ'), phobol 13-acetate (henceforth 'phorbol ester') complexed with PKCδ, and bryostatin 1 (henceforth 'bryostatin') complexed with PKCδ, in order to gain insights into the binding mode as well as to explain differences in the activation mechanisms among the free and the activator-bound proteins. Focus was put also on the binding of bryostatin, which is one of the most potent activators for PKCs identified to date, in order to gain insight into how it functions. This is because, despite decades of effort focused on structural explanation of the mechanism, this information does not yet exist (Das & Rahman, 2014; Loy et al., 2015).

The free cys2 activator binding domain, as known as the C1 domain, is a part of five-domain conventional and novel PKCs (Figure 1A). It comprises three canonical long beta sheets (β1, β4, and β5), two short beta sheets (β2, and β3), and a C-terminal α-helix. The activator binding region is between the β1/β2 loop (Met239, Pro241, Thr242) and the β3/β4 loop (Leu251, Trp252, Gly253, and Leu254) (Figure 1B). The structure of this domain, as determined by X-ray crystallography (Zhang et al., 1995) (PBD ID's: 1PTQ for free protein, and 1PTR for phorbol ester-bound protein) revealed that its overall topology developed a global fold with two Zn^{2+} binding sites distal and proximal to the activator binding region. In good agreement with previous studies (Das et al., 2004; Zhang et al., 1995), the activator binding patch located at the tip of the molecule appears generally polar on the outer surface while a few hydrophobic residues covers parts of the inner wall of the binding pocket. However, most of the surface of the protein is hydrophilic, making this globular protein highly soluble in the cytosol (Zhang et al., 1995).

MD simulations

In order to gain insight into the modes of activator-binding mechanism, MD simulations were performed for free PKCδ and activator-bound PKCδ complexes. Initially, the crystal structure of phorbol ester-bound protein (PDB ID: 1PTR)(Zhang et al., 1995) was used as a template protein for this present study. The phorbol ester (phorbol 13-acetate) molecule was

removed manually from the protein structure to create a free PKCδ protein. Subsequently, the ligand molecule, either phorbol ester or bryostatin, was docked onto the activator binding region of PKCδ, and the MD simulations were performed for 80 ns. To confirm the validity of the docking and the MD simulations, an 80-ns snapshot of stable structure of PKCδ-phorbol ester complex was overlaid onto the original crystal structure complex of PKCδ-phorbol ester (Figure 1C). The comparison yielded a good alignment with an RMSD value between the two complexes (backbone and ligand) of 0.353 Å, indicating that the docking and the MD simulation are reliable.

When comparing the parameters resulting from the MD simulations of the free protein and the protein-activator complexes, several interesting discrepancies can be found. First, the potential energy plots (Figure 2A) showed a quick stabilization of all molecular systems and they remained stable for the entire 80 ns of the MD runs. However, the potential energy from the PKCδ-bryostatin complex stabilized at a significantly lower level (approximately -1.67×10^5 kcal/mol) than those of the free protein or the PKCδ-phorbol ester (approximately -1.51×10^5 kcal/mol). Second, during the MD simulations, the RMSDs of heavy atoms, side chains, and Cα-atoms of all molecular systems also showed different trends (Figure 2B). For both PKCδ-activator complexes, the monitored RMSDs fluctuated during the first 30 ns, and then became more stable afterwards. This is different in the case of the free protein where the RMSDs fluctuated throughout the 80 ns of MD. This indicated that, in the absence of activator, the PKCδ protein was constantly moving and was more away from the initial structure. On the other hand, when bound with either activator, the monitored structures initially moved slightly (within ca. 0.2 nm of backbone coordinates, or approximately an average of a single bond distance), and subsequently became stabilized after 30 ns and throughout the rest of the MD runs. Nonetheless, both the RMSD and potential energy trends of the complexes monitored during the MD simulations support the timeframe of 80 ns as adequate for analyzing the dynamics of both molecular systems.

Root mean-square fluctuations (RMSF) of backbone atoms (N, Cα and C atoms) during the molecular dynamics (MD) simulations are shown in Figure 2C. It is apparent that the PKCδ-bryostatin complex has the lowest values throughout the entire protein sequence, suggesting that lower average atomic mobility can be observed when the protein is bound to bryostatin. Free PKCδ protein had the highest fluctuation, and, as expected, showed the most prominent fluctuation towards the C-terminal loop. Interestingly, the areas with the fluctuation are also located in the activator binding regions (Met239–Thr242 and Trp252–Leu254), and on the two sets of Zn^{2+}-binding residues (His231, Cys261, Cys264, Cys280; and Cys244, Cys247, His269, and Cys272). However, when comparing the trends among all three molecular systems, it can be observed that three particular regions showed a dramatic drop in atomic mobility when a free protein is bound to bryostatin (Figure 2C, gradient columns). These include Trp252 and one set of the Zn^{2+}-binding residues (Cys244, Cys247, His269, Cys272). Notably, these two regions are in close proximity in the three-dimensional space, as the distances between His269 imidazole ring and the Trp252 benzene and indole rings are approximately 3.7 Å and 5.4 Å, respectively. This could imply a plausible π-π interaction or cation-π interaction between His269 and Trp252, as previously suggested (Das & Rahman, 2014), and possibly a role of Trp252 in the binding mechanism of bryostatin (*vide infra*). Taken together, it can be concluded from all the MD simulation throughout the monitored period, especially from the potential energy and the RMSFs, that the PKCδ-bryostatin complex is the most stable and shows the least fluctuation among the three molecular systems.

Hydrogen bonding networks in the PKCδ-activator complexes

Figure 3 summarizes the hydrogen bonding networks that can be observed during the 80-ns simulations. Phorbol ester forms four distinct hydrogen bonds with the activator binding groove of PKCδ (Figure 3A) while bryostatin forms only two (Figure 3B). As shown in Figures 3C and 3E, phorbol ester forms one hydrogen bond with the backbone amide of Thr242, one bond with the backbone carbonyl of Leu251, and two bonds with the backbone carbonyl and amide of Gly253. Bryostatin forms one hydrogen bond with Nε1 of the Trp252 indole ring and one bond with the backbone amide of Gly253. The evolution of bond formation between these two complexes is rather different. In the case of the phorbol ester binding, the numbers of H-bond varied greatly throughout the MD run. For bryostatin binding, on the other hand, the bond formation becomes much more consistent after the 30 ns time point, possibly when the H-bond to the Trp252 has been formed (*vide infra*).

When considering the H-bond formations, as indicated in Figures 3A–B, together with the bond distance of each (Figure 4), the identity of each H-bond could be specified roughly which key partner atom on the protein activator binding site is contributing to the H-bond formation (Figures 3A–B, side labels). Interestingly, in the case of PKCδ-phorbol ester complex, H-bonds of Gly253(-NH) and Thr242(-NH) exhibited almost exactly opposite bond formation behaviors over time (i.e. when one is present, the other is absent, and vice versa). The location of these two H-bonds are also on the opposite sides of the phorbol ester molecule (Figure 3C, dotted elliptical lines). This could imply that these two bonds are pulling against each other by having the phorbol ester molecule in the middle. This 'tug-of-war' H-bond network may potentially cause the binding to phorbol ester to become less energetically favorable when compared to the bryostatin binding (Figure 2), even though it has more H-bonds.

H-bond formation profile in the PKCδ-bryostatin complex (Figure 3B) can also be correlated with the H-bond distance (Figure 4). The evolution of H-bond formation on Gly253(-NH) appears more gradual than that of the one on Trp252(-Nε1). Moreover, when comparing all the H-bond formations in the PKCδ-phorbol ester complex, the bond formation on Gly253(-NH) to bryostatin exhibited much more consistent stability after 30-ns time period. The H-bond on Trp252(-Nε1), on the other hand, was not present before this time point. This may suggest a cooperative behavior of these two H-bond formations to bryostatin. It is possible that the *Z*-enoate of the B-ring on bryostatin (C13) may thread into the binding pocket first. Once the Gly253(-NH) of the protein starts to form a hydrogen bond to it, the side chain of Trp252 swings its indole ring coincidentally towards the binding pocket and forms a hydrogen bond to the ester group on the C-ring, thus helping to stabilize the ligand in place. The movement of this Trp252 side chain and its possible relevance to the structural fluctuation will be discussed further in the next section.

Notably, it is possible that in both complexes, Gly253(-NH) may form a hydrogen bond to the activator molecule first, leading to the other H-bond formations to the ligand. If this initial bond is not then stabilized by the other bonds (as in phorbol ester binding) the complex may not be as energetically favorable as the one that helps stabilizing this initial bond (as in bryostatin binding).

The validity of these two H-bond formations on the PKCδ-bryostatin complex is bolstered by previous structure-activity relationship studies of bryostatin derivatives (DeChristopher et al., 2012; Gary. E. Keck et al., 2009; Gary E. Keck et al., 2009; P. A. Wender & Baryza, 2005; Paul A. Wender & Hinkle, 2000; P. A. Wender, Hinkle, Koehler, & Lippa, 1999). For example, when the ester group on the C-ring C20, which potentially binds to Trp252, is absent in bryostatin 10 or in bryostatin 18, the K_i with the isozyme mixed

PKCs increased from ca. 1 nM to 3.4-4.8 nM (P. A. Wender et al., 1988; P. A. Wender et al., 1999). Attempts by the Wender group (P. A. Wender & Baryza, 2005; Paul A. Wender & Hinkle, 2000) to replace the aliphatic chains after the ester group at C20 with multiple substituents also resulted in two-to-sixty-fold decreases in the binding affinity for the rat brain PKCs. However, on the bryopyran analogues (pyran scaffolds on the A and B rings), it has been discovered that various modifications after this ester group on the C20 of the C ring still yielded very high affinity for PKC (K_i with PKCα = 0.70–1.05 nM, when compared to 1.35 nM for bryostatin 1). Nonetheless, when the functional effect of these bryopyran analogues was considered, they are more similar to that of the phorbol-12-myristate-13-acetate (PMA) as they are promoting proliferation of U937 leukemia cells, the effect that bryostatin 1 antagonizes and thus distinguishes itself from the phorbol ester activity (Gary E. Keck et al., 2009). Therefore, it can be deduced that the ester group on the C20 may be important for the binding to PKC. On the other hand, the long aliphatic chain beyond this ester group may neither be critical for the binding nor for retaining the unique biological characteristic of bryostatin. The biological characteristic may, rather, depend on the original substituents on the A and B rings. Taken together, these lines of experimental evidence are consistent with the MD structure of the PKCδ-bryostatin complex presented in this study that the ester group at C20 is important, but the aliphatic chain beyond this ester group may be dispensable. For the binding of Gly(-NH) to the C30 carbomethoxy substituent on the B-ring of bryostatin, it has been reported that the *Z*-enoate analogues (as found in the bryostatin 1 structure) were slightly more potent in the binding than their corresponding *des*-enoate forms (DeChristopher et al., 2012). Similar to the results from the PKC binding, *Z*-enoate analogues were also found to be more potent than the pyran form of the B-ring in their ability to reactivate latent HIV-1 expression in the model cell line J-Lat 10.6 (DeChristopher et al., 2012). These results confirmed that the substitution on the C13 of bryostatin may be critical in the activation function of PKC.

Furthermore, the Keck group (Gary. E. Keck et al., 2009) also reported a poor contribution of the A-ring C7 acetate to the binding and the biological function of bryostatin. Biological evaluation of several bryopyran analogues revealed that any modifications of this location did not result in an enhanced binding affinity for PKC. Thus, it can be concluded that the A-ring acetate is not the important structural determinant for antagonizing phorbol ester-induced biological responses (Gary. E. Keck et al., 2009). These lines of experimental evidence also coincide with the MD structure of PKCδ-bryostatin complex reported in this study that bryostatin may initially binds to the activator binding pocket via its C20 and C30 groups, while orienting the C7 substituents away from the binding site.

The role of Trp252 in the activator binding

The highly homologous Trp252 is also of particular interest in this study, largely due to its close proximity to one of the Zn^{2+} binding centers and to the activator site, and especially due to its vast side-chain movement during the MD simulations of both free protein and the protein-activator complexes (Figures 5A-C). Therefore, we have focused on delineating the role of this movement by correlating our MD structures to the backbone fluctuation data, in order to derive a possible model describing its relevance in the binding and activity.

Although the motions of this Trp252 side chain, observed by our 80-ns MD simulations, appear to be similar between the free protein and phorbol ester complex (Figures 5A, B), the motion in the bryostatin complex revealed a distinctive behavior (Figure 5C). It is apparent that, in the case of the free protein, Trp252 side chain samples various conformations, toggling randomly in and out of the activator binding site. When the phorbol ester molecule is bound, no apparent H-bond is formed between this residue and the

ligand (Figures 3C, E), and the side chain is still rotating randomly, though orienting away from the binding pocket, suggesting its non-involvement in the recognition. In contrast, bryostatin binding causes the toggling behavior of the Trp252 side chain to become much more restricted, largely due to the H-bond formation between the indole Nε1 and the ester group on C20 of the ligand (Figures 3D, 3F, and 5C). Notably, during the MD run, the aromatic rings of Trp252 starts to flip at approximately 30 ns (Figure 5C), which coincides with the beginning of the H-bond formation observed (Figures 3B and 4E).

At the farthest position away from the activator binding pocket, the Trp252 aromatic ring becomes in close contact and in parallel with the His269 imidazole ring (Figure 5D). Based solely upon this close proximity, it has also been proposed previously that these two side chains may interact with one another via cation-π or π-stacking interactions (Das & Rahman, 2014). As mentioned above, His269 also coordinates to a Zn^{2+} ion, along with Cys244, Cys247 and Cys272. Interestingly, Trp252 and these Zn^{2+}-binding residues are the only areas that have spiked backbone fluctuations observed in the free protein and in the phorbol ester complex, yet these fluctuations are quenched when bryostatin is bound (Figure 2C, gradient columns). Hence, although more complex models are possible, the available MD data from the free protein and from the bryostatin complex in this study, along with the previous combined NMR perturbation and relaxation study (Stewart et al., 2011) on the homologous Y123W mutation of PKCα C1B domain, are consistent with the following dynamic fluctuation dampening model. Portions of the loops harboring the Zn^{2+}-binding residues are vibrationally influenced by the toggling movement (in a nanosecond timescale) of the Trp252 aromatic ring, which is mediated by the transient interaction between Trp252 and His269. Once the bryostatin molecule is bound and the Trp252 Nε1 H-bond has been formed, the Trp252-His269 interaction no longer exists, thus resulting in lower fluctuations among the Zn^{2+}-binding residues (Figure 5E). We assume that these conformers may be further stabilized once the PKC-bryostatin complex tethers into the cell membrane lipid bilayer, where His269 becomes in close contact with the acidic phospholipid surface. It is possible that the previous interaction between His269 and Trp252 may not be easily reconstituted at this stage, thereby creating a more pronounced effect than that from the binding to phorbol ester, which does not require Trp252. The confirmation of this latter hypothesis is being investigated in detail in our laboratory by both MD simulation and quantum mechanical studies of the PKC-bryostatin complex in the context of its membrane tethering process.

The role of bryostatin binding in PKC activation is still largely unknown and the structural information of the PKC-bryostatin-membrane still does not yet exist (Das & Rahman, 2014; Irie et al., 2012; Loy et al., 2015). Previous mutation and molecular dynamics studies indicated that Trp252 may have some importance in the binding of the activators (Kazanietz et al., 1995; Nacro et al., 2001). Recently, a combined mutagenesis, MD and NMR perturbation and relaxation study (Stewart et al., 2011) also discovered that the homologous Y123W mutation of PKCα C1B domain (that resulted in a profound >100-fold increase in DAG binding affinity) did not alter the dynamics of the protein in the sub-nanosecond timescale, but rather caused a dramatic change in microsecond-timescale conformational dynamics. This change in lower timescale dynamics generally suggests a "preequilibrium sampling" or "selected fit" behavior, that the ligand selects a high-affinity conformer among others (James & Tawfik, 2003). Some variations of the orientation of the Trp252 side chain and its analogues are also observed in multiple homologous C1 domain structures, either positioning toward or away from the activator binding pocket (Lin et al., 2005; Shen et al., 2005).

When considering our PKCδ-bryostatin complex structure, there still are several hydrophilic parts of the ligand being exposed to the solvent. This indicates that the binding

mechanism might not be the same as the one proposed for the phorbol ester binding by which the ligand simply caps the activator cleft and switches the hydrophobicity of the protein head and making it suitable for the membrane penetration (Zhang et al., 1995). It is possible that the PKCδ C1B-bryostatin may require another binding partner (or partners) to fulfill a complete activation. This hypothesis can be bolstered by the fact that the C1A and C1B domains both contribute to the PKC translocation induced by bryostatin (Bögi et al., 1998; Lorenzo et al., 1999), and the C1A and the catalytic (C4) domains may be involved in a protection from downregulation of PKCδ induced by bryostatin (Das & Rahman, 2014; Lorenzo et al., 1999; Lorenzo, Bögi, Acs, Pettit, & Blumberg, 1997).

The mechanism by which the bryostatin-bound PKC triggers cellular localization is also unclear. It has been known that, in the case of hydrophobic ligands such as phorbol ester or 12-*O*-tetradecanoylphorbol-13-acetate (TPA), they tend to translocate PKCs to the cell membrane, while hydrophilic ligands such as bryostatin (at 10-1,000 nM concentration) translocate them to the nuclear membrane (Wang et al., 2000). Therefore, structural biology studies on the C1B domain and other potentially involved domains of the PKC protein, both in the presence and absence of bryostatin or phospholipid bilayer, are greatly needed. Though the analyses of the conformational activation pathway is more complex than anticipated, our MD data presented here has provided structural insight into the activator binding, as well as one of the possible models leading to a more complete description of the mechanism and to their function.

Conclusions

Protein kinase C is a family of serine/threonine kinase isozymes that has been widely recognized as targets for anticancer therapy, Alzheimer's disease, HIV/AIDS eradication and others, due to their important role in the signal transduction of various pathways. However, despite many efforts focused on describing accurate structural detail of the C1 domain of PKC, as well as the binding to its activators, that information has been lacking, thus hampering the development of potential therapies. The study presented herein demonstrates that MD simulation can be employed to gain insight into the differences in the binding of phorbol esters, the tumor-promoting activator of PKC, compared with bryostatin, a more potent activator that does not act as a tumor promoter. Hydrogen bonding data have provided the details of binding mechanisms observed in both ligands, and revealed a potential binding conformation of bryostatin that has never been described before. These H-bond networks, when combined with the deviations and fluctuations of the protein backbone, have led us to propose a model that describes the role of the highly conserved and highly homologous Trp252 in the ligand binding, as well as its potential involvement in the dynamic fluctuation modulation of the nearby Zn^{2+}-binding center. We have found that a toggling movement of the Trp252 side chain may cause the high backbone fluctuation observed in the Zn^{2+}-binding residues, which is mediated by the transient interaction between Trp252 and His269. When bryostatin is bound to the protein and the side chain of Trp252 samples toward a conformation that forms a hydrogen bond with the ligand, the transient interactions abrogate, and the dynamic fluctuations are dampened. This finding brings new insight into the design of new activators that favor the latter conformation.

The comparison of the dynamics properties observed in the activator-bound complexes also sheds light on how to explain the potency differences identified for both activators. Although many future experimental efforts are still needed in order to confirm our model and fully understand the binding mode of bryostatin, along with the mechanism by which it employs to activate PKC, this study sets the stage for investigating the structural

detail of this important class of regulatory proteins. This information is inevitably required for the design of new analogues for future treatment of many related diseases.

Acknowledgment

This work was supported by the Grant for New Researcher (Grant: MRG5680003) from the Thailand Research Fund, Thailand's Office of the Higher Education Commission, and Chiang Mai University; N.S. was supported by the Chiang Mai University Young Faculty Research Grant; the National Research Council of Thailand (Grant: 2556NRCT51390); the National Research University Project under Thailand's Office of the Higher Education Commission; and the Research Fund for DPST Graduate with First Placement (Grant: 037/2555). P.T. was supported by the JSTP-NSTDA research grant for graduate study (Grant: JSTP-06-55-35E). We would like to thank the Computer Technology Center of NECTEC for the SYBYL software, the Drug Discovery Research Laboratory and the Department of Chemistry, Faculty of Science, Chiang Mai University for research facilities. We also thank Prof. Richard Deming (CSU Fullerton) for helpful suggestions.

References

Akimoto, K., Mizuno, K., Osada, S., Hirai, S., Tanuma, S., Suzuki, K., & Ohno, S. (1994). A new member of the third class in the protein kinase C family, PKC lambda, expressed dominantly in an undifferentiated mouse embryonal carcinoma cell line and also in many tissues and cells. *Journal of Biological Chemisty, 269*, 12677−12683.

Battaini, F., & Mochly-Rosen, D. (2007). Happy birthday protein kinase C: past, present and future of a superfamily. *Pharmacological Research, 55*, 461−466.

Berendsen, H. J. C., Postma, J. P. M., van Gunsteren, W. F., DiNola, A., & Haak, J. R. (1984). Molecular dynamics with coupling to an external bath. *Journal of Chemical Physics, 81*, 3684−3690.

Blumberg, P. M. (1991). Complexities of the protein kinase C pathway. *Molecular Carcinogenesis, 4*, 339−344.

Bögi, K., Lorenzo, P. S., Szallasi, Z., Acs, P., Wagner, G. S., & Blumberg, P. M. (1998). Differential selectivity of ligands for the C1a and C1b phorbol ester binding domains of protein kinase C delta: possible correlation with tumor-promoting activity. *Cancer Research, 58*, 1423−1428.

Darden, T., York, D., & Pedersen, L. (1993). Particle mesh Ewald: An N·log(N) method for Ewald sums in large systems. *Journal of Chemical Physics, 98*, 10089−10092.

Das, J., & Rahman, G. M. (2014). C1 domains: structure and ligand-binding properties. *Chemical Reviews, 114*, 12108−12131.

Das, J., Addona, G. H., Sandberg, W. S., Husain, S. S., Stehle, T., & Miller, K. W. (2004). Identification of a general anesthetic binding site in the diacylglycerol-binding domain of protein kinase C delta. *Journal of Biological Chemistry, 279*, 37964−37972.

de Vries, D. J., Herald, C. L., Pettit, G. R., & Blumberg, P. M. (1988). Demonstration of sub-nanomolar affinity of bryostatin 1 for the phorbol ester receptor in rat brain. *Biochemical Pharmacology, 37*, 4069−4073.

DeChristopher, B. A., Loy, B. A., Marsden, M. D., Schrier, A. J., Zack, J. A., & Wender, P. A. (2012). Designed, synthetically accessible bryostatin analogues potently induce activation of latent HIV reservoirs in vitro. *Nature Chemistry, 4*, 705−710.

Dries, D. R., Gallegos, L. L., & Newton, A. C. (2007). A single residue in the C1 domain sensitizes novel protein kinase C isoforms to cellular diacylglycerol production. *Journal of Biological Chemistry, 282*, 826−830.

Essmann, U., Perera, L., Berkowitz, M. L., Darden, T., Lee, H., & Pedersen, L. G. (1995). A smooth particle mesh Ewald method. *Journal of Chemical Physics, 103*, 8577−8593.
Grodsky, N., Li, Y., Bouzida, D., Love, R., Jensen, J., Nodes, B., Nonomiya, J., & Grant, S. (2006). Structure of the catalytic domain of human protein kinase C beta II complexed with a bisindolylmaleimide inhibitor. *Biochemistry, 45*, 13970−13981.
Guerrero-Valero, M., Ferrer-Orta, C., Querol-Audí, J., Marin-Vicente, C., Fita, I., Gómez-Fernández, J. C., Verdaguer, N., & Corbalán-García, S. (2009). Structural and mechanistic insights into the association of PKC alpha-C2 domain to PtdIns(4,5)P2. *Proceedings of the National Academy of Sciences, 106*, 6603−6607.
Hess, B., Bekker, H., Berendsen, H. J. C., & Fraaije, J. G. E. M. (1997). LINCS: A Linear Constraint Solver for Molecular Simulations. *Journal of Computational Chemistry, 18*, 1463−1472.
Hommel, U., Zurini, M., & Luyten, M. (1994). Solution structure of a cysteine rich domain of rat protein kinase C. *Nature Structural Biology, 1*, 383−387.
Hornak, V., Abel, R., Okur, A., Strockbine, B., Roitberg, A., & Simmerling, C. (2006). Comparison of multiple Amber force fields and development of improved protein backbone parameters. *Proteins, 65*, 712−725.
Humphrey, W., Dalke, A., & Schulten, K. (1996). VMD: visual molecular dynamics. *Journal of Molecular Graphics, 14*, 33−38.
Hurley, J. H., & Grobler, J. A. (1997). Protein kinase C and phospholipase C: bilayer interactions and regulation. *Current Opinion Structural Biology, 7*, 557−565.
Irie, K., Nakagawa, Y., & Ohigashi, H. (2005). Toward the development of new medicinal leads with selectivity for protein kinase C isozymes. *Chemical Record, 5*, 185−195.
Irie, K., Yanagita, R. C., & Nakagawa, Y. (2012). Challenges to the development of bryostatin-type anticancer drugs based on the activation mechanism of protein kinase C delta. *Medicinal Research Reviews, 32*, 518−535.
James, L. C., & Tawfik, D. S. (2003). Conformational diversity and protein evolution−a 60-year-old hypothesis revisited. *Trends in Biochemical Sciences, 28*, 361−368.
Jorgensen, W. L., Chandrasekhar, J., Madura, J. D., Impey, R. W., & Klein, M. L. (1983). Comparison of simple potential functions for simulating liquid water. *Journal of Chemical Physics, 79*, 926−935.
Kazanietz, M. G., Areces, L. B., Bahador, A., Mischak, H., Goodnight, J., Mushinski, J. F., & Blumberg, P. M. (1993). Characterization of ligand and substrate specificity for the calcium-dependent and calcium-independent protein kinase C isozymes. *Molecular Pharmacology, 44*, 298−307.
Kazanietz, M. G., Wang, S., Milne, G. W., Lewin, N. E., Liu, H. L., & Blumberg, P. M. (1995). Residues in the second cysteine-rich region of protein kinase C delta relevant to phorbol ester binding as revealed by site-directed mutagenesis. *Journal of Biological Chemistry, 270*, 21852−21859.
Keck, G. E., Li, W., Kraft, M. B., Kedei, N., Lewin, N. E., & Blumberg, P. M. (2009). The bryostatin 1 A-ring acetate is not the critical determinant for antagonism of phorbol ester-induced biological responses. *Organic Letters, 11*, 2277−2280.
Keck, G. E., Poudel, Y. B., Welch, D. S., Kraft, M. B., Truong, A. P., Stephens, J. C., Kedei, N., Lewin, N. E., & Blumberg, P. M. (2009). Substitution on the A-ring confers to bryopyran analogues the unique biological activity characteristic of bryostatins and distinct from that of the phorbol esters. *Organic Letters, 11*, 593−596.
Lange, O. F., van der Spoel, D., & de Groot, B. L. (2010). Scrutinizing molecular mechanics force fields on the submicrosecond timescale with NMR data. *Biophysical Journal, 99*, 647−655.

Leonard, T. A., Rozycki, B., Saidi, L. F., Hummer, G., & Hurley, J. H. (2011). Crystal structure and allosteric activation of protein kinase C beta II. *Cell, 144*, 55−66.

Li, J., Ziemba, B. P., Falke, J. J., & Voth, G. A. (2014). Interactions of protein kinase C-alpha C1A and C1B domains with membranes: a combined computational and experimental study. *Journal of the American Chemical Society, 136*, 11757−11766.

Lin, W. Q., Jiang, J. H., Shen, Q., Wu, H. L., Shen, G. L., & Yu, R. Q. (2005). Piecewise hypersphere modeling by particle swarm optimization in QSAR studies of bioactivities of chemical compounds. *Journal of Chemical Information and Modeling, 45*, 535−541.

Littler, D. R., Walker, J. R., She, Y. M., Finerty, P. J., Jr., Newman, E. M., & Dhe-Paganon, S. (2006). Structure of human protein kinase C eta (PKC eta) C2 domain and identification of phosphorylation sites. *Biochemical and Biophysical Research Communications, 349*, 1182−1189.

Lorenzo, P. S., Bögi, K., Acs, P., Pettit, G. R., & Blumberg, P. M. (1997). The catalytic domain of protein kinase Cdelta confers protection from down-regulation induced by bryostatin 1. *Journal of Biological Chemistry, 272*, 33338−33343.

Lorenzo, P. S., Bögi, K., Hughes, K. M., Beheshti, M., Bhattacharyya, D., Garfield, S. H., Pettit, G. R., & Blumberg, P. M. (1999). Differential roles of the tandem C1 domains of protein kinase C delta in the biphasic down-regulation induced by bryostatin 1. *Cancer Research, 59*, 6137−6144.

Loy, B. A., Lesser, A. B., Staveness, D., Billingsley, K. L., Cegelski, L., & Wender, P. A. (2015). Toward a biorelevant structure of protein kinase C bound modulators: design, synthesis, and evaluation of labeled bryostatin analogues for analysis with rotational echo double resonance NMR spectroscopy. *Journal of the American Chemical Society, 137*, 3678−3685.

Messerschmidt, A., Macieira, S., Velarde, M., Badeker, M., Benda, C., Jestel, A., Brandstetter, H., Neuefeind, T., & Blaesse, M. (2005). Crystal structure of the catalytic domain of human atypical protein kinase C-iota reveals interaction mode of phosphorylation site in turn motif. *Journal of Molecular Biology, 352*, 918−931.

Mochly-Rosen, D., Das, K., & Grimes, K. V. (2012). Protein kinase C, an elusive therapeutic target? *Nature Review Drug Discovery, 11*, 937−957.

Nacro, K., Sigano, D. M., Yan, S., Nicklaus, M. C., Pearce, L. L., Lewin, N. E., Garfield, S. H., Blumberg, P. M., & Marquez, V. E. (2001). An optimized protein kinase C activating diacylglycerol combining high binding affinity (Ki) with reduced lipophilicity (log P). *Journal of Medicinal Chemistry, 44*, 1892−1904.

Newton, A. C. (1995). Protein kinase C: structure, function, and regulation. *Journal of Biological Chemistry, 270*, 28495−28498.

Nishizuka, Y. (1984). The role of protein kinase C in cell surface signal transduction and tumour promotion. *Nature, 308*, 693−698.

Nishizuka, Y. (1992). Intracellular signaling by hydrolysis of phospholipids and activation of protein kinase C. *Science, 258*, 607−614.

Nishizuka, Y. (1995). Protein kinase C and lipid signaling for sustained cellular responses. *FASEB Journal, 9*, 484−496.

Ochoa, W. F., Garcia-Garcia, J., Fita, I., Corbalan-Garcia, S., Verdaguer, N., & Gomez-Fernandez, J. C. (2001). Structure of the C2 domain from novel protein kinase C epsilon. A membrane binding model for Ca^{2+}-independent C2 domains. *Journal of Molecular Biology, 311*, 837−849.

Ono, Y., Fujii, T., Igarashi, K., Kuno, T., Tanaka, C., Kikkawa, U., & Nishizuka, Y. (1989). Phorbol ester binding to protein kinase C requires a cysteine-rich zinc-finger-like sequence. *Proceedings of the National Academy of Sciences, 86*, 4868−4871.

Pappa, H., Murray-Rust, J., Dekker, L. V., Parker, P. J., & McDonald, N. Q. (1998). Crystal structure of the C2 domain from protein kinase C-delta. *Structure, 6*, 885−894.

Rahman, G. M., & Das, J. (2015). Modeling studies on the structural determinants for the DAG/phorbol ester binding to C1 domain. *Journal of Biomolecular Structures and Dynamics, 33*, 219−232.

Shen, N., Guryev, O., & Rizo, J. (2005). Intramolecular occlusion of the diacylglycerol-binding site in the C1 domain of munc13-1. *Biochemistry, 44*, 1089−1096.

Stewart, M. D., Morgan, B., Massi, F., & Igumenova, T. I. (2011). Probing the determinants of diacylglycerol binding affinity in the C1B domain of protein kinase C alpha. *Journal of Molecular Biology, 408*, 949−970.

Sutton, R. B., & Sprang, S. R. (1998). Structure of the protein kinase C beta phospholipid-binding C2 domain complexed with Ca^{2+}. *Structure, 6*, 1395−1405.

Takai, Y., Kishimoto, A., Kikkawa, U., Mori, T., & Nishizuka, Y. (1979). Unsaturated diacylglycerol as a possible messenger for the activation of calcium-activated, phospholipid-dependent protein kinase system. *Biochemical and Biophysical Research Communications, 91*, 1218−1224.

Takimura, T., Kamata, K., Fukasawa, K., Ohsawa, H., Komatani, H., Yoshizumi, T., Takahashi, I., Kotani, H., & Iwasawa, Y. (2010). Structures of the PKC-iota kinase domain in its ATP-bound and apo forms reveal defined structures of residues 533-551 in the C-terminal tail and their roles in ATP binding. *Acta Crystallographica D: Biological Crystallography, 66*, 577−583.

Trott, O., & Olson, A. J. (2010). AutoDock Vina: improving the speed and accuracy of docking with a new scoring function, efficient optimization, and multithreading. *Journal of Computational Chemistry, 31*, 455−461.

Verdaguer, N., Corbalan-Garcia, S., Ochoa, W. F., Fita, I., & Gomez-Fernandez, J. C. (1999). Ca(2+) bridges the C2 membrane-binding domain of protein kinase C alpha directly to phosphatidylserine. *EMBO Journal, 18*, 6329−6338.

Wang, Q. J., Fang, T. W., Fenick, D., Garfield, S., Bienfait, B., Marquez, V. E., & Blumberg, P. M. (2000). The lipophilicity of phorbol esters as a critical factor in determining the pattern of translocation of protein kinase C delta fused to green fluorescent protein. *Journal of Biological Chemistry, 275*, 12136−12146.

Wender, P. A., & Baryza, J. L. (2005). Identification of a tunable site in bryostatin analogs: C20 Bryologs through late stage diversification. *Organic Letters, 7*, 1177−1180.

Wender, P. A., & Hinkle, K. W. (2000). Synthesis and biological evaluation of a new class of bryostatin analogues: the role of the C20 substituent in protein kinase C binding. *Tetrahedron Letters, 41*, 6725−6729.

Wender, P. A., Cribbs, C. M., Koehler, K. F., Sharkey, N. A., Herald, C. L., Kamano, Y., Pettit, G. R., & Blumberg, P. M. (1988). Modeling of the bryostatins to the phorbol ester pharmacophore on protein kinase C. *Proceedings of the National Academy of Sciences, 85*, 7197−7201.

Wender, P. A., Hinkle, K. W., Koehler, M. F., & Lippa, B. (1999). The rational design of potential chemotherapeutic agents: synthesis of bryostatin analogues. *Medicinal Research Reviews, 19*, 388−407.

Wender, P. A., Irie, K., & Miller, B. L. (1995). Identification, activity, and structural studies of peptides incorporating the phorbol ester-binding domain of protein kinase C. *Proceedings of the National Academy of Sciences, 92*, 239−243.

Xu, R. X., Pawelczyk, T., Xia, T. H., & Brown, S. C. (1997). NMR structure of a protein kinase C-gamma phorbol-binding domain and study of protein-lipid micelle interactions. *Biochemistry, 36*, 10709−10717.

Xu, Z. B., Chaudhary, D., Olland, S., Wolfrom, S., Czerwinski, R., Malakian, K., Lin, L., Stahl, M. L., Joseph-McCarthy, D., Benander, C., Fitz, L., Greco, R., Somers, W. S., & Mosyak, L. (2004). Catalytic domain crystal structure of protein kinase C-theta (PKCtheta). *Journal of Biological Chemistry, 279*, 50401−50409.

Zhang, G., Kazanietz, M. G., Blumberg, P. M., & Hurley, J. H. (1995). Crystal structure of the cys2 activator-binding domain of protein kinase C delta in complex with phorbol ester. *Cell, 81*, 917−924.

Figure Captions

Figure 1. Structure of the cys2 activator-binding domain of protein kinase C. (A) Schematic representation of C1 (cys2) domain located within PKC proteins. For both conventional (α, βI, βII, γ) and novel (δ, θ, ε, η) PKCs, four distinct domains (C1–C4) and five variable regions (V1–V5) are present, along with the amino-terminal pseudosubstrate (PS) domain. The secondary structure topology of the C1A or cys2 domain is highlighted, showing the activator binding site located between the β1-β2 and the β3-β4 loops. (B) Crystal structure of the cys2 activator-binding domain of PKCδ (PDB ID: 1PTR)(Zhang et al., 1995) with the activator binding site (residues 239–242 and 250–254) highlighted in stick representation. Phorbol ester molecule was removed from the original crystal structure. (C) Comparison between the crystal structure of PKCδ (PDB ID: 1PTR, shown in yellow and pale yellow) and the 80-ns MD simulated complex of phorbol ester molecule docked onto the original activator binding site of PKC (this study, shown in cyan and purple). Backbone and ligand RMSD between the two structures is 0.353 Å.

Figure 2. Comparison of parameters resulted from the MD simulations of free PKCδ protein (black), PKC-phorbol ester complex (red), and PKC-bryostatin complex (blue). (A) Plot of the potential energy (kcal/mol) during 80 ns MD of the free protein and complexes. (B) The backbone RMSD vs. MD simulation time. (C) RMSF of the free protein and complexes during 80 ns MD showing fluctuations among the protein amino acids. Activator binding regions are highlighted in the dotted lines with some key binding residues indicated. Downward arrows on the topology schematic line indicate the locations of two sets (red or blue) of Zn^{2+}-coordinating residues. The three gradient columns highlighted the regions that have the most prominent differences of the RMSF values from all molecular systems, which coincide with Trp252 and one set of the Zn^{2+}-binding residues.

Figure 3. Hydrogen bond formations found in the complexes between the PKC protein and phorbol ester (A, C, E) or bryostatin (B, D, F). (A, B) Number of H-bonds between PKC and the ligands during total course of 80 ns of MD simulations. (C, D) Three dimensional structures of the binding site of the protein focusing on the H-bond formations (dotted yellow lines). Key binding residues are indicated. The dotted elliptical lines highlight H-bond formations to Gly253(-NH) and Thr242(-NH) as color-coded in figure 3A. (E, F) Schematics summarizing hydrogen-bonding interactions (dotted lines) in the phorbol ester binding or in the bryostatin binding.

Figure 4. Hydrogen bond distances between PKC protein residues and phorbol ester (A-D) or bryostatin (E, F) molecules as a function of time. For the PKC-phorbol ester complex, H-bonds on Leu251 backbone -CO (A), Gly253 backbone -NH (B) and -CO (C), and Thr242 backbone -NH (D) are shown. For the PKC-bryostatin, H-bonds on Trp252-Nε1 (E) and Gly253 backbone -NH (F) are shown.

Figure 5. The role of Trp252 in activator binding. Cartoon views of the activator binding site of PKC highlighting the movements of the Trp252 side chain in the free PKC protein (A), PKC-phorbol ester complex (B), and the PKC-bryostatin complex (C) are shown. The vibrational motions on residues of PKC structures are represented by superimposing seven snapshots at different time points during the MD simulations. In the complexes (B, C), 10 ns: light green, 20 ns: cyan, 30 ns: magenta, 40 ns: yellow, 50 ns: pink, 60 ns: light gray, and 70 ns: purple. For (C), the ligand conformation and the H-bond of only the 70-ns structure is represented. (D) Cartoon representation of free PKC structure showing a close proximity (3.7–5.4 Å) between the side chain of Trp252 and the Zn^{2+}-coordinating His269. (E) Dynamic fluctuation dampening model describing how the binding of bryostatin may influence a reduction of the backbone fluctuation of Trp252 and the proximal Zn^{2+}-binding center. In the free protein, interaction between Trp252 and His269 modulates the fluctuation of this area due to the toggling movement of Trp252 side chain. Once bound with bryostatin, this interaction diminishes and may result in the evident reduction in fluctuation of all involved residues.

Figures

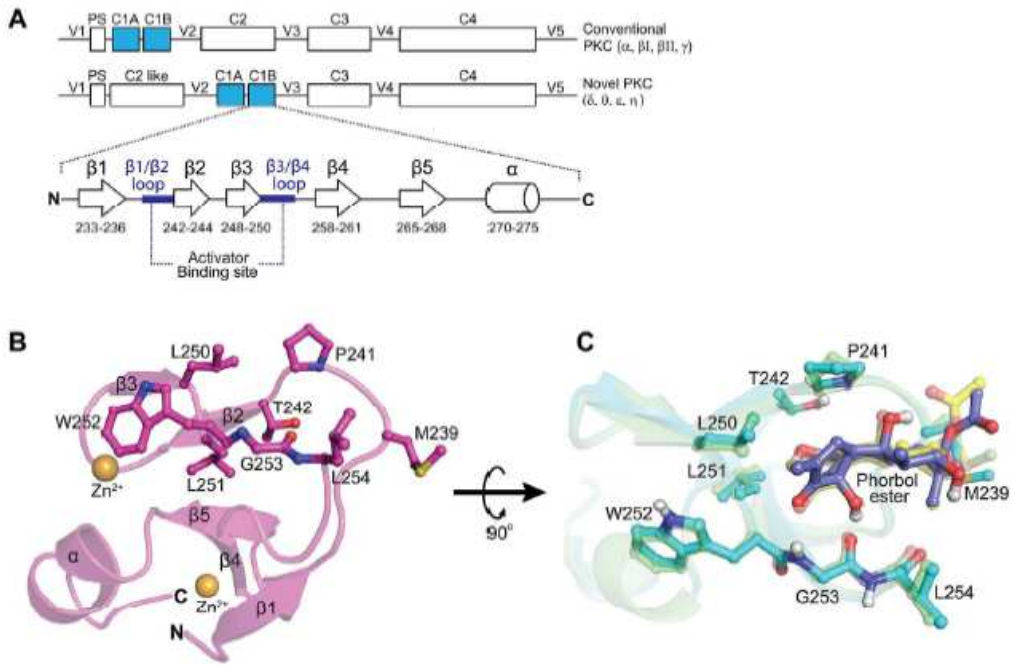

Figure 1 Thangsunan, et al.

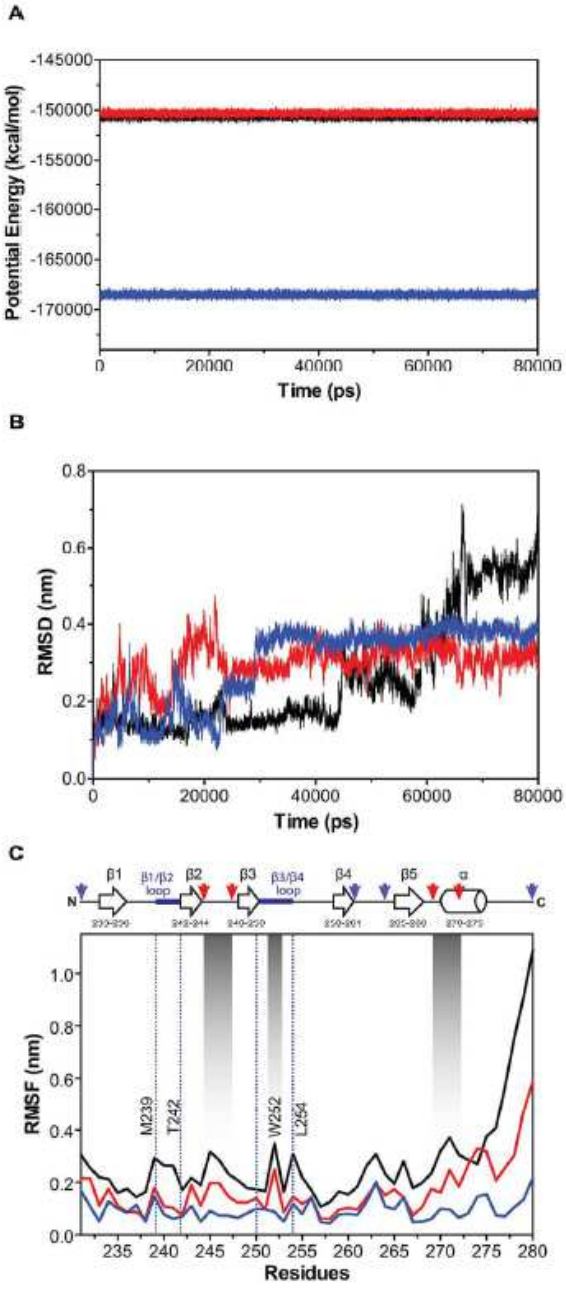

Figure 2 Thangsunan, et al.

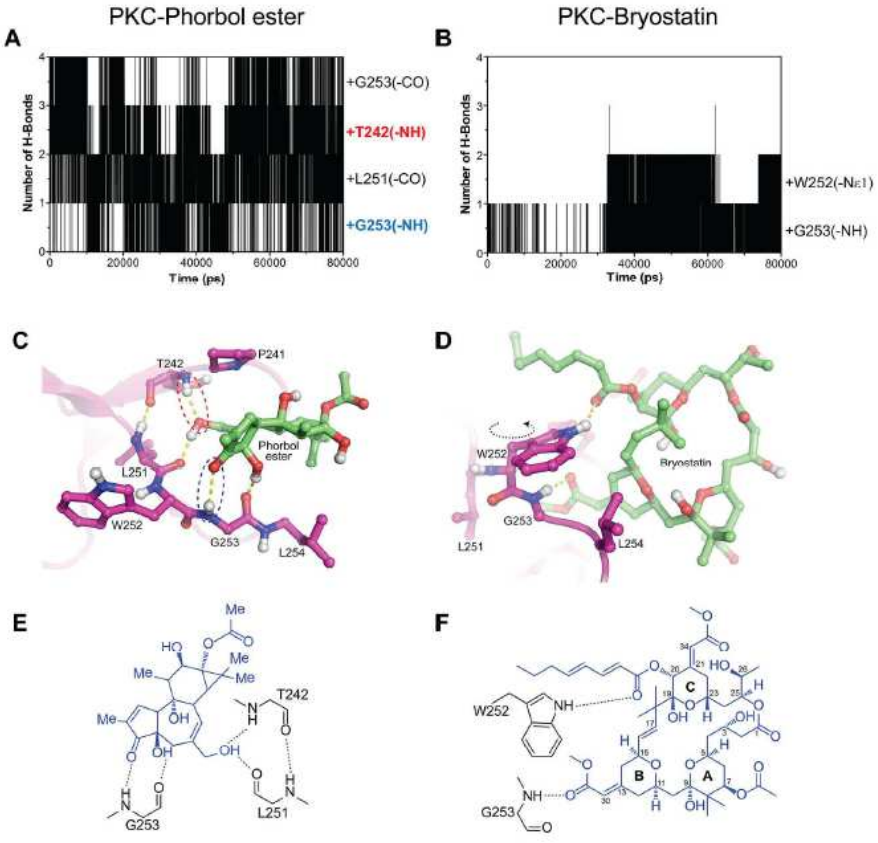

Figure 3 Thangsunan, et al.

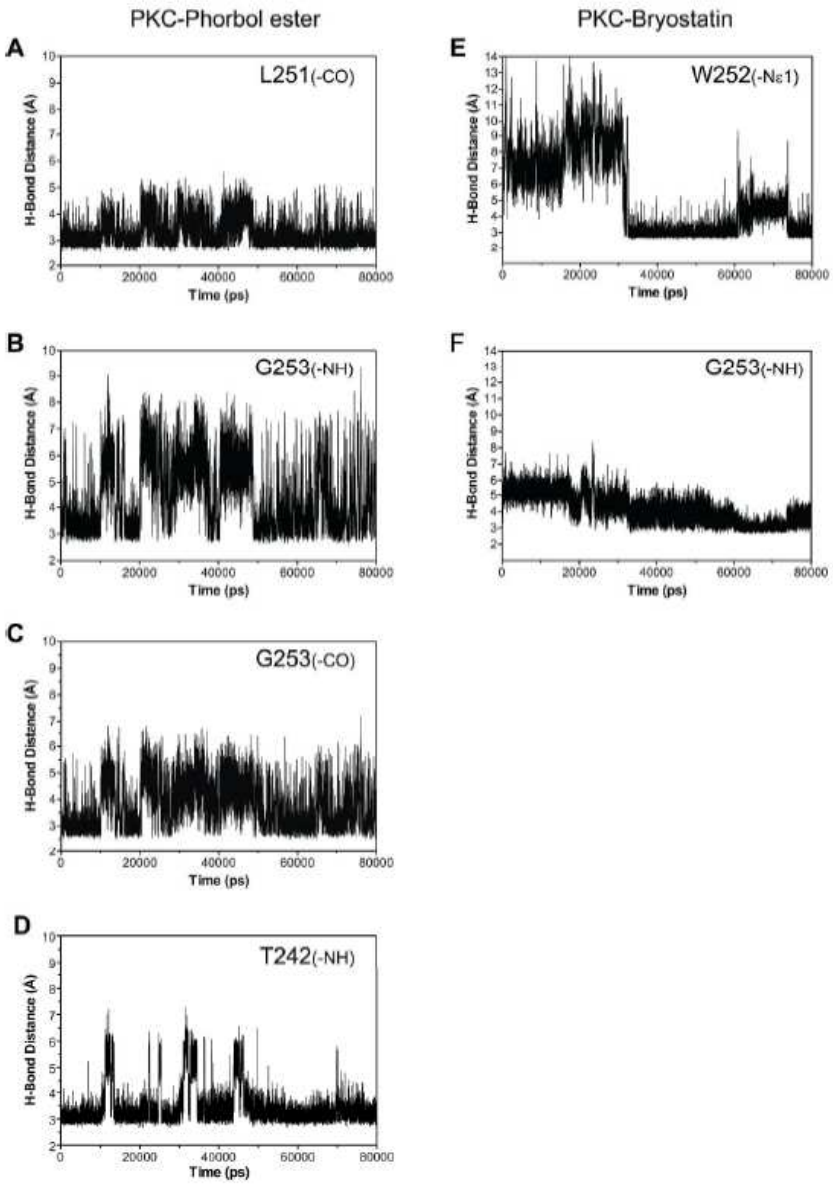

Figure 4 Thangsunan, et al.

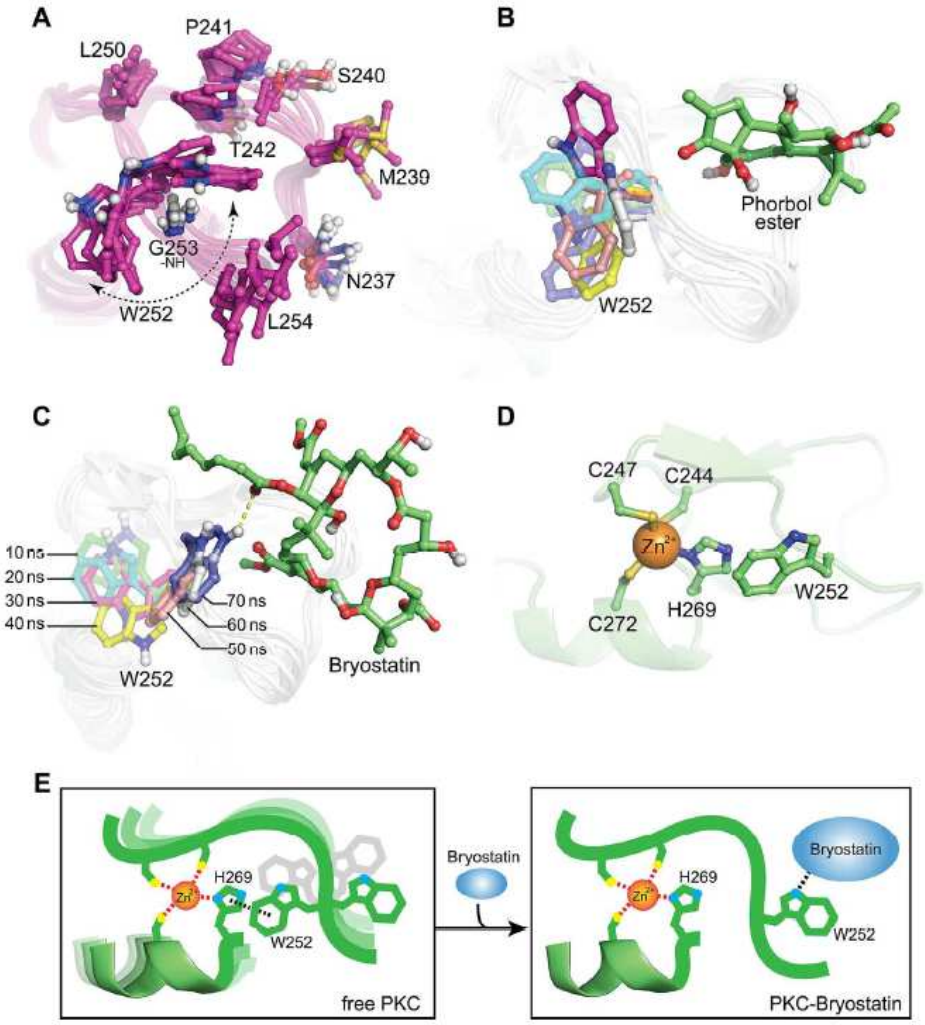

Figure 5 Thangsunan, et al.